DEVELOPMENT OF HIGHLY STABLE MULTI-BANDGAP AMORPHOUS SILICON ALLOY STACKED SOLAR CELLS

Yukihiko NAKATA

Energy Conversion Laboratories

SHARP CORPORATION

January, 1992

DEVELOPMENT OF HIGHLY STABLE MULTI-BANDGAP AMORPHOUS SILICON ALLOY STACKED SOLAR CELLS

Yukihiko NAKATA

Energy Conversion Laboratories

SHARP CORPORATION

January, 1992

ABSTRACT

A series of systematic studies has been carried out on multi-bandgap amorphous silicon (a-Si) alloy stacked solar cells to increase stability. An important key issue for practical power uses of a-Si solar cells is improvement of stability for light-induced degradation as well as conversion efficiency This key issue has been approached from three directions of material, analytical, and device technologies.

As the material technologies, improvement of amorphous silicon alloy materials, namely amorphous silicon carbon (a-SiC), amorphous silicon (a-Si) and amorphous silicon germanium (a-SiGe), and their applications to solar cells have been investigated. The a-SiC films with high quality have been applied to p/i interface layers and photovoltaic active layers of a-Si alloy solar cells, so that the solar cell performances have been improved. The dependence of a-SiGe optical bandgap on preparation condition has been clarified. As a result, the a-Si alloy materials having a photo-conductivity of more than 10^{-5} S/cm have been obtained for a wide range of optical bandgap, from 1.39 eV to 2.0 eV.

As the analytical technologies, a new method for measuring current - voltage characteristics of each component cell in a-Si alloy solar cells has been developed on a basis of investigation of method for measuring spectral photo-response of each component cell. Using this new method, light-induced degradation of each component cell in a-Si alloy stacked solar cells has been clarified. Moreover, dependence of light-induced degradation in a-Si alloy solar cells on exposure light intensity and bias voltage has been quantitatively clarified. On the basis of this dependence, a new accelerated test method of light-induced degradation has been proposed. Using this accelerated test method, light-induced degradation under outdoor exposure for one year can be estimated in a short time from experimental data under simulated light.

As the device technologies, bandgap profiling and optical confinement have been investigated. Effect of the bandgap profiling on solar cell performances has been clarified. On the basis of the effects of the bandgap profiling, bandgap profiles of a-SiC and a-SiGe solar cells have been designed. And the optical confinement has been developed at the front and rear sides of solar cells.

By applying these technologies as mentioned above, highly stable multi-bandgap a-Si alloy stacked solar cells have been investigated. As a result, an a-Si/a-Si/a-SiGe stacked solar cell with an initial efficiency of 10.0 % and a degradation ratio of 10 % in the first year has been obtained. An a-SiC/a-Si/a-SiGe multi-bandgap stacked solar cell with an initial efficiency of 11.0 % has been also obtained. Moreover, an a-SiC/a-Si/a-SiGe multi-bandgap stacked solar cell with an initial efficiency of 10.7 % and a degradation ratio of 14 % in the first year has been obtained by designing the bandgap profile to obtain high stability.

ACKNOWLEDGMENT

The author would like to express his sincere thanks to Professor Yoshihiro Hamakawa of Osaka University for his kind advice, encouragement through the course of this thesis work and critical reading of this thesis. The author wishes to give his appreciation to Associate professor Hiroaki Okamoto of Osaka University. The author wishes to make his deep acknowledgment to Professors Kenji Gamou, Sadahiko Yamamoto, Takeshi Kobayashi, Tadashi Sueta, Tetsuro Kobayashi and Masanori Okuyama of Osaka University.

This work has been done at Energy Conversion Laboratories, Corporate Research and Development Group, SHARP Corporation, Kitakatsuragi-gun Nara. The author wishes give his highest appreciation to Mr. I. Fujimoto, Dr. S. Kataoka and Mr. K. Matsuki for their recognition, encouragement and advice of this thesis work. The author wishes to make his greatest thanks to T. Izumi, T. Inoguchi, H. Itoh and T. Tsuji for their encouragement, advice and useful discussions. The author wishes to thank to Mr. E. Kinoshita for his correction of this manuscript.

The author wishes to express his gratitude to his co-workers in the Energy Conversion Laboratories, Dr. Y. Yamamoto, Messrs. T. Kobe, M. Itoh, Y. Yokota, T. Okuno, M. Kaneiwa, K. Nomoto, T. Machida, Y. Inoue, H. Sannomiya, S. Moriuchi, Y. Takeda, Y. Yamamoto, S. Higasizaki and A. Chida for their useful discussions and advice in this thesis work. In particular, the author takes pleasure in acknowledging the important part played by Messrs. M. Itho, Y. Yokota, K. Nomoto, Y. Inoue, H. Sannomiya and S. Moriuchi for their considerable assistance.

Finally, the author wishes to thank his parents and all his family for their endless encouragement and support. In particular, the author wishes to thank Mrs. M. Nakata for her typewriting and Mr. T. Nakata for his correction of this manuscript.

This work was supported by the New Energy and Industrial Technology and Development Organization (NEDO) as a part of the Sunshine Project under the Ministry of International Trade and Industry.

TABLE OF CONTENTS

I. INTRODUCTION

1-1. Historical Background

1-1-1. Social background

The first "Oil Crisis" struck all countries on a global scale in 1973. It revealed both limited availability of fossil fuels and frailty of Japanese energy demand and supply structure. It is estimated that the worldwide energy demand will increase and especially electric energy demand in 2000 will increase to about ten times as much as that in 1970 though energy-saving technologies will be introduced. New energy sources, therefore, which substitute for energy sources using oil, are expected. The "Sunshine Project" which develops technologies relating to oil-substituting new energy sources was initiated in 1974 by the Japanese government. [1,2] Photovoltaic system was one of the most expected new energy sources. The price of the solar cell was ¥ 20,000 - ¥ 30,000/W_p at that time. In view of the price of the peripheral equipment, however, it is necessary to reduce this price to ¥100 - ¥200/W_p as the ultimate target in order to use photovoltaic power generation system as a new energy source. The Sunshine Project Headquarters was established in the Agency of Industrial Science and Technology (AIST), under the Ministry of International Trade and Industry (MITI). To pursue the Sunshine Project, the New Energy Development Organization (NEDO) and Photovoltaic Power Generation Technology Research Association (PVTEC) were established at 1980 and 1990, respectively.

On the other hand, a tremendous amount of oil consumption has generated air pollution and acid rain, then it has destroyed ecological recycle balance and induced a greenhouse warming effect by increase of carbon dioxide (CO_2) content. [3,4] The interim report of Inter-governmental Panel on Climate Change (IPCC) was approved in August 1990. The CO_2 content increased sharply in the middle of

1960s, which corresponds to the increased number of vehicles, and it has been steadily increasing. It is estimated elsewhere that the increase of CO_2 content will induce global warming of 1.5 to 2.5 ℃ by the year 2030. So clean energy sources that do not generate CO_2 are expected.

Because of such social backgrounds as described above, expectation of photovoltaic system is becoming larger as an inexhaustible and clean energy source which solves both of energy and environmental problems.

1-1-2. Technical background.

The first solar cell was made in 1954 by D. M. Chapin et al. [5] They demonstrated that sunlight could be converted directly into electrical power with a conversion efficiency of about 6 % by using a p-n junction in single-crystalline silicon. In Japan, mass production of single-crystalline silicon solar cells was introduced in 1963 by SHARP corporation.

From a viewpoint of amorphous silicon (a-Si), Professor W. E. Spear and P. G. LeComber achieved the initial success of p-n control in a-Si by a glow discharge in silane in 1975. [6] This success impacted on many researchers of amorphous materials and devices. Then, in 1976, D. E. Carlson and C. R. Wronski demonstrated the first a-Si solar cell with a conversion efficiency of 2.4 %, [7] and a Schottky barrier type a-Si solar cell with a conversion efficiency of 5.5 % was introduced in 1977. [8] These results encouraged the researchers of a-Si solar cells because of the advantages such as low production energy, simple production process, and productivity of large area thin film.

On the other hand, in 1977, D. Staebler and C. Wronski discover that photo- and dark-conductivities of a-Si films are changed by light exposure and they return to initial values by thermal annealing. [9] These light-induced changes are

called Staebler-Wronski (S-W) effect. A conversion efficiency of a-Si solar cell is also decreased by light exposure and the degradation is assumed to be caused by the S-W effect.

Three other important key technologies were developed by Professor Y. Hamakawa's group of Osaka University to improve the conversion efficiency furthermore, and those technologies have been applied widely to a-Si solar cells up to the present time. The first one is a p-i-n junction structure of a-Si solar cells. The p-i-n type a-Si solar cell with an efficiency of 4.5% was demonstrated in 1978. [10] In this cell structure, most of the carriers are photo-generated in the i-layer with high electric field and they drift out efficiently as electric power. The second one is a stacked solar cell structure. An effect of heterostructure stacked junction using internal carrier exchange through localized states was first discovered in 1979. [11] This effect was applied to the high voltage solar cell called "HOMLAC (Horizontally Multi-Layered Photovoltaic Cell)", which has stacked solar cell structure. [12,13] The third one is a wide bandgap p-type amorphous silicon carbon (a-SiC). [14-16] A good p-n control was obtained in a-SiC:H prepared by plasma decomposition of silane and methane as mixture. This material has excellent optical transparency and good photo-conductivity. This a-SiC:H material applied to p-layer at light incident side, so that the conversion efficiency was improved more than 8%. Research and development of a-Si solar cells were incorporated into the Sunshine Project in 1980 with the background of these and other achievements. Moreover, to obtain higher conversion efficiency, various technologies, for example a textured transparent conductive oxide (TCO) [17], "buffer layer" [18], and "delta-doping" [19], have been developed.

On the other hand, some technologies were developed to industrialize a-Si solar cells. A submodule structure, called an integrated type a-Si solar cell, was

developed. [20] Elementary solar cells in the submodule are connected in a series on an insulated substrate. This submodule structure reduces the cost of connection in a series as compared with crystalline solar cells. A consecutive, separated reaction chamber method was developed in 1979 to prevent intermixing of impurities such as boron and phosphorus, [21] and a-Si single-junction solar cells for electric calculators were industrialized by SANYO [22] and other companies in 1980. In 1983, a-Si tandem type solar cells by a roll-to-roll process were put into mass production by SHARP corporation.[23]

As material technologies, a guiding principle of improvement of film quality in a-Si alloy materials, namely amorphous silicon germanium (a-SiGe) and a-SiC, was given by Dr. A. Matsuda. [24] Many investigations, recently, which improve the light-induced degradation in a-Si materials such as deuterated a-Si [25,26], a-Si from xenon diluted SiH_4 plasma [27], " Chemical Annealing " [28], have been conducted and a clue to stabilize materials is becoming clear.

Using these materials, structures, and methods as mentioned above, initial conversion efficiencies of 13.3 % for a 1 cm^2 cell [29], 10.2 % for a 10 cm $\times$ 10 cm submodule [24], 9.1 % for a 30 cm $\times$ 40 cm submodule [30], 8.5 % for a 40 cm $\times$ 120 cm tandem submodule [31] have been achieved respectively so far.

But stability of the a-Si solar cells is not sufficient enough for outdoor uses although many studies of light-induced degradation have been done, and it is necessary to improve the stability. Therefore, a-Si solar cells with high stability as well as high conversion efficiency were greatly expected.

Such social and technical backgrounds of this work, including the results of this work, are summarized chronologically in Table 1-1.

Table 1-1 Social and Technical backgrounds of this work

	Social background	Technical background
1954		· First c-Si solar cell (Chapin et al.)
1963		· Mass-production of c-Si solar cell (SHARP)
1973	· Oil Crisis	
1974	· Sunshine Project	
1975		· p-n control of a-Si (Spear et al.)
1976		· First a-Si solar cell (Carlson et al.)
1977		· Staebler and Wronski Effect
1978		· p-i-n cell structure (Hamakawa et al.)
1979		· Integrated type cell (Kuwano et al.) · Separated reaction chamber (Kuwano et al.)
1980	· R&D of a-Si solar cells were incorporated into Sunshine Project. · NEDO[1] was established.	· Stacked cell structure (Hamakawa et al.) · a-Si solar cells for electric calculators put on the market.
1981		· p-type a-SiC at light incident side of solar cell (Hamakawa et al.)
1983		· Textured TCO (Hayashi et al.)
1987		· Guiding principle of a-Si alloy (Matsuda et al.) · Buffer layer (Konagai et al.)
1989		· a-Si/a-Si/a-SiGe stacked cell with 10.0 % and 10 %/year (Nakata et al.) · Delta-doping (Konagai et al.)
1990	· PVTEC[2] was established. · Interim report of IPCC[3]	· Deuterated a-Si (Matsuda et al.) · Chemical annealing (Shimizu et al.)
1991		· a-SiC/a-Si/a-SiGe stacked cell with 10.7 % and 14 %/year (Nakata et al) · a-Si from Xe diluted plasma (Matsuda et al.)

1) NEDO: New Energy Development Organization

2) PVTEC: Photovoltaic Power Generation Technology Research Association

3) IPCC: Inter-governmental Panel on Climate Change

1-2 Objective of This Work

Solar cells for outdoor power uses are almost single- or poly-crystalline solar cells today. Many photovoltaic systems using single- or poly-crystalline solar cells have been established. [32-35] In 1989 the production of crystalline solar cells in Japan was about 2.5 MWp/year. There will be, however, a limit in the price of the crystalline solar cells, because it is difficult to reduce the price of Si wafer greatly. The limit in the price will obstruct the abundant outdoor power uses of the crystalline solar cells as a future new energy source. On the other hand, a-Si solar cells have an advantage of low cost, because the thicknesses of the photovoltaic active layers are able to be less than 1 μm and they are directly made on large area substrates from gases by simple processes. Therefore, a-Si solar cells are produced for consumer uses, for example electric calculators and watches, and their production in Japan reached about 7.2 MWp/year in 1989. They have great probability of breaking through the price limit of the crystalline solar cells and reducing the price to about ¥100 - ¥200/Wp as the ultimate target as a new energy source. Therefore, a-Si solar cells would be greatly expected for a future new energy source. But the conversion efficiencies of a-Si solar cells are decreased under intense light, and a-Si solar cells are hardly used for outdoor uses so far. Therefore, to use as future new energy source, the most important key issue is the improvement of the stability for light-induced degradation as well as the conversion efficiency. The objective of this work is to improve the stability of a-Si solar cells. This objective has been approached from three directions of material, analytical and device technologies, as shown in Fig. 1-1. The details of these technologies are described in the following chapter.

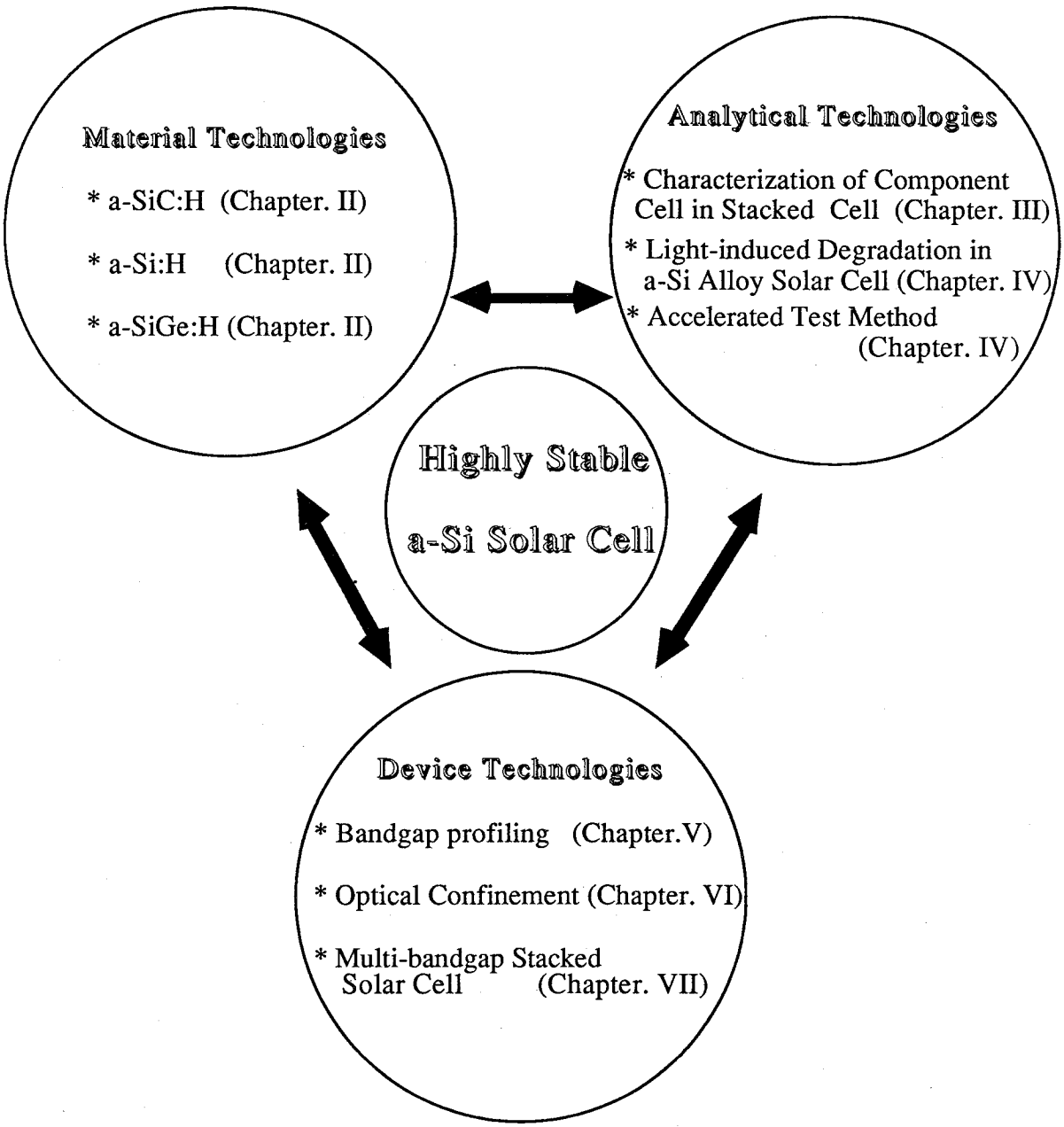

Fig. 1-1 Approach to highly stable a-Si solar cells from three directions of material, analytical, and device technologies.

In chapter II, the improvement of amorphous silicon alloy materials, namely amorphous silicon carbon (a-SiC), amorphous silicon (a-Si) and amorphous silicon germanium (a-SiGe), and its applications to solar cells are described. The dependence of a-SiC film properties on hydrogen dilution ratio is investigated to improve the film quality. [36] The a-SiC film with high quality is applied to p/i interface layers and photovoltaic active layers of a-Si alloy solar cells. The dependence of a-SiGe optical bandgap on preparation condition is clarified. As a result, the a-Si alloy materials having a photo-conductivity of more than 10^{-5} S/cm are demonstrated for a wide range of optical bandgap, from 1.39 eV to 2.0 eV.

Chapter III presents investigation of method for measuring spectral photo-response and characterization of component cells in a-Si alloy stacked solar cells. The methods for measuring the spectral photo-response of a-Si alloy single-junction solar cells [37] and each component cell in a-Si alloy stacked solar cells [38,39] are investigated. On the basis of the method for measuring the spectral photo-response of each component cell, a new method for measuring current - voltage characteristics of each component cell in a-Si alloy stacked solar cells are proposed. [40] Using this new method, the light-induced degradation of each component cell in a-Si alloy solar stacked cells has been clarified.

In chapter IV, analysis of light-induced degradation in a-Si alloy solar cells and its application to accelerated test method are described. Dependence of light-induced degradation in a-Si alloy solar cells on exposure light intensity and bias voltage is quantitatively investigated and discussed theoretically. [41-44] On the basis of this dependence, a new accelerated test method of light-induced degradation has been proposed. Using this accelerated test method, the light-induced degradation under the outdoor exposure for one year can be estimated in a short time from the experimental data under the simulated light. The

validity of the new accelerated test method is experimentally confirmed.

Chapter V describes bandgap profiling in a-Si alloy solar cells. The improvement of the performances in a-SiGe and a-SiC solar cells by the bandgap profiling is investigated and the effects of the bandgap profiling on the solar cell performances are clarified. [45-47] On the basis of the effects of the bandgap profiling, the bandgap profiles of a-SiGe and a-SiC solar cells are designed.

In chapter VI, the technologies of optical confinement at the front and rear sides of the solar cells are described. Texturing of rear silver reflector, inserting of ZnO film, glass / textured SnO_2 substrates and MgF_2 / In_2O_3 double anti-reflection coating are investigated. [46,48] Using these technologies of the optical confinement, the solar cells with high conversion efficiency are demonstrated.

Chapter VII covers the development of highly stable multi-bandgap a-Si alloy stacked solar cells. By applying the technologies as mentioned above, an a-Si/a-Si/a-SiGe stacked solar cell with an initial efficiency of 10.0 % and a degradation ratio of 10 % in the first year has been obtained. [40] An a-SiC/a-Si/a-SiGe multi-bandgap stacked solar cell with an initial efficiency of 11.0 % has been obtained. [46-48] Moreover, an a-SiC/a-Si/a-SiGe multi-bandgap stacked solar cell with an initial efficiency of 10.7 % and a degradation ratio of 14 % in the first year has been obtained by designing the bandgap profile to obtain the high stability. [47]

In the final chapter, some conclusions obtained through this thesis work are summarized.

REFERENCES

1) T. Mukai: Tech. Digest of 1st Int. Photovol. Sci. Engi. Conf., Kobe (1984) 13.

2) T. Goto: Tech. Digest of 5th Int. Photovol. Sci. Engi. Conf., Kyoto (1990) 13.

3) Y. Hamakawa: OPTOELECTRONICS - Devices and Technologies, Vol. 5, No. 2 (1990) 113.

4) Y. Kaya: Tech. Digest of 5th Int. Photovol. Sci. Engi. Conf., Kyoto (1990) 3.

5) D. M. Chapin, C. S. Fuller, G. L. Pearson: J. Appl. Phys. 25 (1954) 676.

6) W. E. Spear, and P. G. LeComber: Solid State Commun., 17 (1975) 1198.

7) D. E. Carlson and C. R. Wronski: Appl. Phys. Lett., 28 (1976) 671.

8) D. E. Carlson: IEEE Trans. on Electron Devices, ED-24 (1977) 449.

9) D. Staebler and C. Wronski: Appl. Phys. Lett., 31 (1977) 292; J. Appl. Phys., 51 (1980) 3262.

10) H. Okamoto, Y. Nitta, T. Adachi, and Y. Hamakawa: Int. Conf. on Solid Films and Surfaces, Tokyo (1978) S1-6, B52.

11) Y. Hamakawa, H. Okamoto, and Y. Nitta: Appl. Phys. Lett. 35 (1979) 15.

12) Y. Hamakawa, H. Okamoto, and Y. Nitta: Proc. 14th Photovol. Special Conf. San Diego (1980) 1074.

13) H. Okamoto, Y. Nitta, and Y. Hamakawa: Jpn. J. Appl. Phys., 19 (1980) 545.

14) Y. Tawada, H. Okamoto, and Y. Hamakawa: Appl. Phys. Lett. 39 (1981) 273.

15) Y. Tawada, M. Kondo, H. Okamoto, and Y. Hamakawa: Solar Energy Mat., 6 (1982) 299.

16) Y. Hamakawa and Y. Tawada: Int. J. Solar Energy 1 (1982) 125.

17) H. Iida, N. Shiba, T. Mishuku, H. Karasawa, A. Ito, M. Yamanaka, Y. Hayashi: IEEE Electron Device Lett., EDL-4 (1983) 157.

18) W. Y. Kim, H. Tasaki, M. Konagai and K. Takahashi: J. Appl. Phy. 61 (1987) 3071.

19) Y. Kazama, K. Seki, W. Y. Kim, S. Yamanaka, M. Konagai and K. Takahashi: Jpn. J. Appl. Phys. 28 (1989) 1160.

20) Y. Kuwano, T. Imai, M. Ohnishi, and S. Nakano: Proc. 14th IEEE Photovol. Spec. Conf. (1980) 1408.

21) Y. Kuwano, M. Ohnishi, H. Nishiwaki, S. Tsuda, H. Shibuya, and S. Nakano: Proc. 15th IEEE Photovol. Spec. Conf. (1981) 689.

22) Y. Kuwano and M. Ohnishi: 9th Int. Conf. on Amorphous and Liquid Semiconductors, Grenoble (1981) 1155.

23) H. Morimoto and M. Izu: Japan Annual Reviews in Electronics, Computers & Telecominucations (Amorphous Semiconductor Technologies & Devices) (OHM · North-Holland, Tokyo, 1984), Vol. 16, 212.

24) A. Matsuda and K. Tanaka: J. Non-Cryst. Solids 97&98 (1987) 1367.

25) G. Ganguly, A. Suzuki, S. Yamasaki, K. Nomoto and A. Matsuda: J. Appl. Phys. 68 (1990) 3738.

26) G. Ganguly, S. Yamasaki and A. Matsuda: Philos. Mag. B63 (1991) 28.

27) A. Matsuda, S. Mashima, K. Hasezaki, A. Suzuki, S. Yamasaki and P. J. McElheny: Appl. Phys. Lett. (to be published)

28) H. Shirai, D. Das, J. Hanna and I. Shimizu: Tech. Digest of 5th Int. Photovol. Sci. Eng. Conf. Kyoto (1990) 59.

29) J. Yang, R. Ross, T. Glatfelter, R. Mohr, G. Hammond, C. Bernotaitis, E. Chen, J. Burdick, M. Hopson and S. Guha: Proc. 20th Photovol. Spec. Conf., Las Vegas (1988) 241.

30) Y. Hishikawa, M. Ohnishi and Y. Kuwano: Proc. Mat. Res. Soc. Symp. Vol. 192 (1990) 3.

31) Y. Ichikawa and H. Sakai: OPTOELECTRONICS - Devices and Technologies, Vol. 5, No. 2 (1990) 189.

32) Y. Nakata, N. Shibuya, T. Kobe, K. Okamoto, A. Suzuki and T. Tsuji: Jpn. J. Appl. Phys. Vol. 19. Supplement 19-2 (1980) 75.

33) Y. Nakata, T. Kobe, N. Shibuya, T. Machida, T. Takemoto and T. Tsuji: Proc. 16th IEEE Photovol. Spec. Conf., San Diego (1982) 993.

34) N. Shibuya, T. Maruyama, H. Yoshida, Y. Nakata and T. Tsuji: Tech. Digest of 1st Int. Photovol. Sci. Engi. Conf., Kobe (1984) 623.

35) N. Shibuya, T. Maruyama, H. Yoshida, Y. Nakata and T. Tsuji: Proc. Int. Conf. Solar and Wind Energy Application, Beijing, China (1985) 41.

36) K. Nomoto, Y. Takeda, S. Moriuchi, H. Sannomiya, T. Okuno, A. Yokota, M. Kaneiwa, M. Itoh, Y. Yamamoto, Y. Nakata and T. Inoguchi: Tech. Digest of 4th Int. Photovol. Sci. Engi. Conf., Sydney (1989) 85.

37) Y. Nakata, Y. Inoue, H. Sannomiya, K. Nomoto, A. Yokota, M. Itoh and T. Tsuji: OPTOELECTRONICS - Devices and Technologies , Vol. 6, No.1, (1991) 141.

38) M. Kaneiwa, K. Nomoto, M. Itoh, Y. Yamamoto, Y. Nakata and T. Inoguchi: Tech. Digest of 4th Int. Photovol. Sci. Engi. Conf., Sydney (1989) 673.

39) Y. Nakata and T. Inoguchi: OPTOELECTRONICS - Devices and Technologies,Vol. 4, No. 1, (1989) 75.

40) S. Moriuchi, Y. Inoue, H. Sannomiya, A. Yokota, M. Itoh, Y. Nakata and H. Itoh: Proc. 21st IEEE Photovol. Spec. Conf., Florida (1990) 1449.

41) T. Kobe, Y. Nakata, T. Machida, Y. Yamamoto and T. Tsuji: Proc. 18th IEEE Photovol. Spec. Conf., Las Vegas (1985) 1594.

42) A. Yokota, H. Sannomiya, S. Moriuchi, Y. Inoue, M. Itoh, Y. Nakata and T. Tsuji: Tech. Digest of 5th Int. Photovol. Sci. Engi. Conf., Kyoto (1990) 637.

43) Y. Nakata, A. Yokota, H. Sannomiya, S. Moriuchi, Y. Inoue, K. Nomoto, M. Itoh and T. Tsuji: Mat. Res. Soc. Symp. Proc., Vol. 219 (1991) 433.

44) Y. Nakata, A. Yokota, H. Sannomiya, S. Moriuchi, Y. Inoue, K. Nomoto, M. Itoh and T. Tsuji: Jpn. J. Appl. Phys., Vol. 31, Part 1, No. 2 (1992) (in press)

45) Y. Nakata, H. Sannomiya, S. Moriuchi, A. Yokota, Y. Inoue, M. Itoh and H. Itoh: Mat. Res. Soc. Symp. Proc., Vol. 192 (1990) 15.

46) Y. Nakata, H. Sannomiya, S. Moriuchi, Y. Inoue, K. Nomoto, A. Yokota, M. Itoh and T. Tsuji: OPTOELECTRONICS - Devices and Technologies , Vol. 5, No. 2, (1990) 209.

47) Y. Nakata (Editors: Y. Sakurai, K. Suzuki, T. Masumoto, K. Shirae, Y. Hamakawa): PROGRESS IN AMORPHOUS MATERIALS - Science and Technology - (Elsevier Science Publishers B. V., Amsterdam, to be published in 1992) sub-section 4.5.4.

48) H. Sannomiya, S. Moriuchi, Y. Inoue, K. Nomoto, A. Yokota, M. Itoh, Y. Nakata and T. Tsuji: Tech. Digest of 5th Int. Photovol. Sci. Engi. Conf., Kyoto (1990) 387.

II. IMPROVEMENT OF FILM QUALITY IN AMORPHOUS SILICON ALLOY AND ITS APPLICATION TO SOLAR CELLS

2-1. Introduction

An important key issue to use a-Si solar cells as one of future new energy sources is improvement of the stability for the light-induced degradation as well as the conversion efficiency. This key issue has to be approached from three directions of material, analytical, [1-8] and device technologies. In this chapter, the material technologies are described.

Electric properties, for example mobility and life time, of a-Si alloy materials are worse than those of crystal silicon (c-Si), but light absorption coefficients of a-Si alloy materials are larger than that of c-Si. In addition, one of the big advantages of a-Si alloy materials is that their optical bandgap can be continuously controlled by changing the compositional ratio of the alloy, even though bandgap of c-Si is constant. There are some device technologies that are making use of advantage of the optical bandgap controllability. The first one is a p/i interface layer where carbon composition is graded. [9-11] The second one is a multi-bandgap stacked solar cell where component solar cells with different bandgap materials are stacked in the order of decreasing bandgap from the light incident side. [4,12-14] The third one is a bandgap profiling where bandgap of photovoltaic active layer is changed. [12-14] To make use of these technologies and improve the solar cell characteristics, it is necessary to improve the film quality of a-Si alloy materials for a wide range of bandgap.

A guiding principle of improvement of film quality in a-Si alloy materials, namely hydrogenated amorphous silicon germanium (a-SiGe:H) and hydrogenated amorphous silicon carbon (a-SiC:H), was given by A. Matsuda. [15,16] According to

the guiding principle, a-Si alloy materials with high quality are expected to grow when the surface diffusion coefficient of adsorbed precursors is large, and a hydrogen dilution method is very effective.

In this chapter, the improvement of the film quality in a-Si alloy materials, for example a-SiC:H and a-SiGe:H, and its application to the p/i interface layer and the photovoltaic active layer of a-Si solar cell are described.[17)]

2-2. Improvement of Film Quality in a-SiC:H and its Application to Solar Cells

2-2-1. Experimental

a-SiC:H films were prepared by using a conventional capacitance-coupled RF plasma Chemical Vapor Deposition (CVD) system. Various hydrogen dilution ratios: $H_2/(SiH_4+CH_4)$ were controlled by H_2 gas flow rate under a constant flow rate and a constant total pressure of the source gases (SiH_4, CH_4). Substrate temperature was held at 200 ℃ throughout these experiments.

Photo-conductivity (σ_{ph}) under AM 1 light of 100 mW/cm^2, and dark-conductivity (σ_d) were measured using samples with coplanar type electrode. Optical bandgap (Egopt) was determined by Tauc's plot. Electron and hole mobility were measured by Time-of-Flight method using samples structure of Glass / Transparent Conductive Oxide (TCO) / n$^+$(a-Si:H) / i (a-SiC:H, $\sim 1\mu$ m)/ Pt. Carbon content in the films was determined by Auger electron spectroscopy. Integrated absorption intensity of Si-H bond ($\sim$ 650 cm^{-1}), Si-C bond ($\sim$ 770cm^{-1}) was calculated from infrared rays (IR) spectra. Refractive index was obtained from the interference fringes in the near IR transmission spectra.

Basic solar cell structure is S.S./n$^+$ (a-Si:H) i(a-Si:H or a-SiC:H) b(a-SiC:H) p$^+$(a-SiC:H)/TCO, where b represents p/i interface layer and S.S. is stainless steel substrate.

2-2-2. Dependence of a-SiC:H film properties on hydrogen dilution ratio

Recently, A. Matsuda et al. reported that a-SiC:H films with high quality were obtained by a hydrogen dilution method. [15,16] Since hydrogen dilution ratio : $H_2/(SiH_4+CH_4)$ is regarded as a key parameter of preparation conditions, the dependence of the optical and electrical properties of a-SiC:H film on the hydrogen dilution ratio is investigated systematically.

Figure 2-2-1 shows the dependence of optical bandgap (Egopt), photo-conductivity (σ_{ph}), and dark-conductivity (σ_{d}) of a-SiC:H films on the hydrogen dilution ratio under various preparation conditions. As the hydrogen dilution ratio increases, Egopt decreases, while Egopt increases again in the further hydrogen dilution ratios. On the other hand, σ_{ph} increases as the hydrogen dilution ratio increases, but further hydrogen dilution causes σ_{ph} to begin to decrease. Such behavior of Egopt and σ_{ph} against the hydrogen dilution ratio is almost same in the various preparation conditions, as shown in Fig. 2-2-1.

To clarify the origin of such phenomena, carbon content, Si-H bond and Si-C bond content, and refractive index were investigated by using the samples prepared under SiH_4+CH_4= 4 sccm, RF power = 40 W, that are included in Fig. 2-2-1. These data are shown in Figs. 2-2-2 (a), (b) and (c), respectively. As shown in Figs. 2-2-2 (a) and (b), as the hydrogen dilution ratio increases, the carbon content and the Si-C content in the films decrease while the Si-H bond content increases. It is understood from these results that the decrease of Egopt with the hydrogen dilution is caused by the decrease of the carbon content and the increase of Egopt in the region of the further hydrogen dilution ratio is caused by the increase of the Si-H bond content. On the other hand, as shown in Fig. 2-2-2 (c), refractive index increases at first as the hydrogen dilution ratio increases. It is considered that this is caused not only by the decrease of the

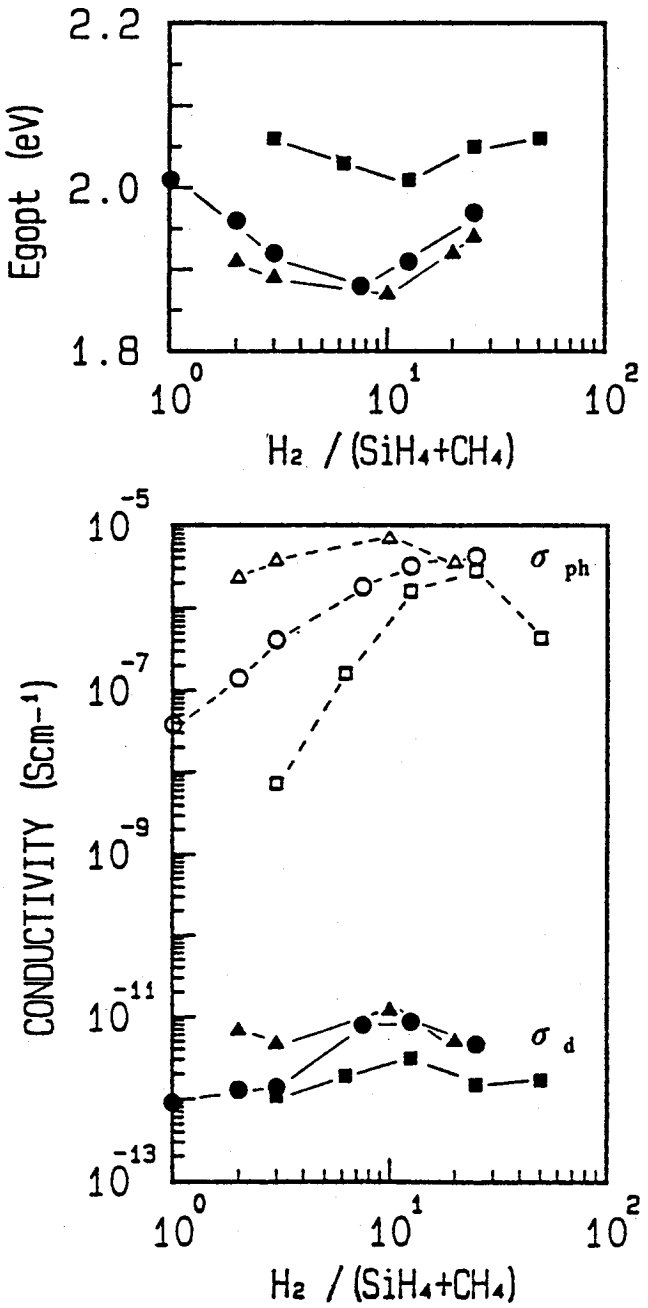

Fig. 2-2-1. Dependence of optical bandgap (Egopt), photo-conductivity (σ_{ph}), and dark-conductivity (σ_{d}) of a-SiC:H films on hydrogen dilution ratio: $H_2/(SiH_4+CH_4)$.

□,■: $SiH_4 + CH_4$ = 4 sccm, RF power=40 W

△,▲: $SiH_4 + CH_4$ = 4 sccm, RF power=20 W

○,●: $SiH_4 + CH_4$ = 15 sccm, RF power=20 W

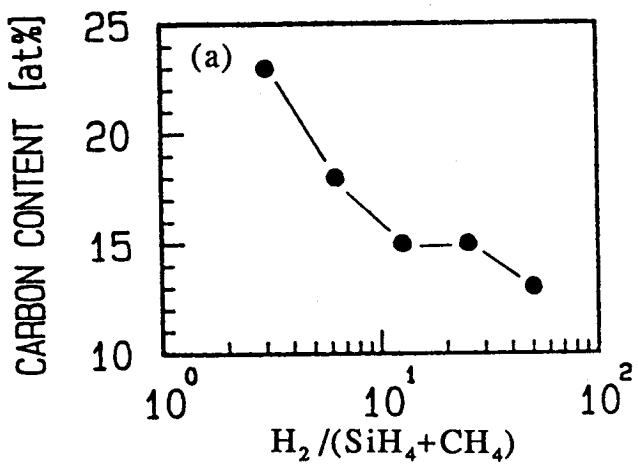

(a) Carbon content (C/(Si+C) at%)

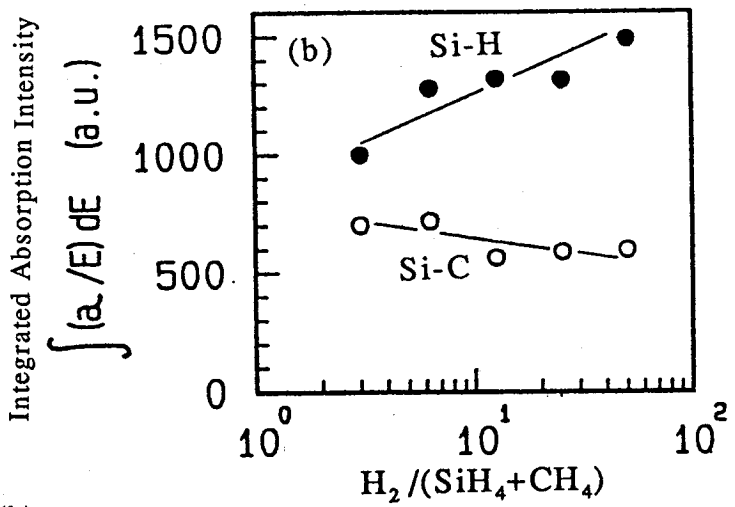

(b) IR integrated absorption intensity of Si-H bond, Si-C bond

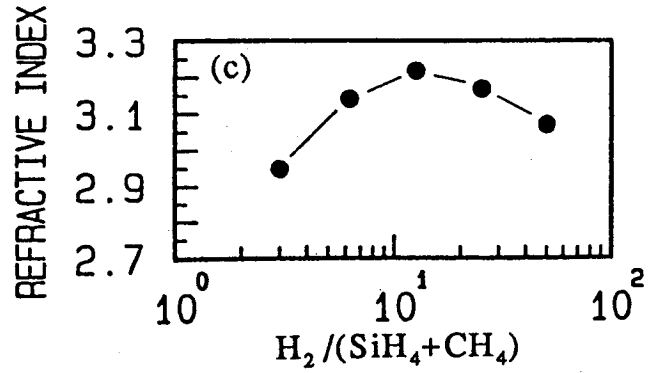

(c) Refractive index

Fig. 2-2-2. Dependence of Carbon content (C/(Si+C) at%) (a), IR integrated absorption intensity of Si-H bond and Si-C bond (b), and Refractive index (c) of a-SiC:H films on hydrogen dilution ratio: $H_2/(SiH_4+CH_4)$.

carbon content in the films but also by the higher density of films with hydrogen dilution, because of the rapid increase of σ_{ph} shown in Fig. 2-2-1. But, under the further hydrogen dilution ratio the refractive index again decreases, which indicates that the density of the films becomes lower. It is, therefore, inferred that the further hydrogen dilution causes the density of the film to become lower due to the excessive higher Si-H bond content in the films, which results in the decrease of σ_{ph}.

It was also confirmed that electron mobility (μ_e), hole mobility (μ_h), electron lifetime (τ_e), and hole lifetime (τ_h) show their maximum values at the hydrogen dilution ratio where σ_{ph} shows maximum, as shown in Fig. 2-2-3 .

Therefore, it has been clarified that there is the optimum hydrogen dilution ratio and this phenomenon is caused by the decrease of the carbon content and the increase of the Si-H bond content as the hydrogen dilution ratio increases. As a result, wide band gap a-SiC:H films with higher photo-conductivity and higher electron and hole mobility are obtained under the hydrogen dilution ratio of 10 $\sim$ 30 .

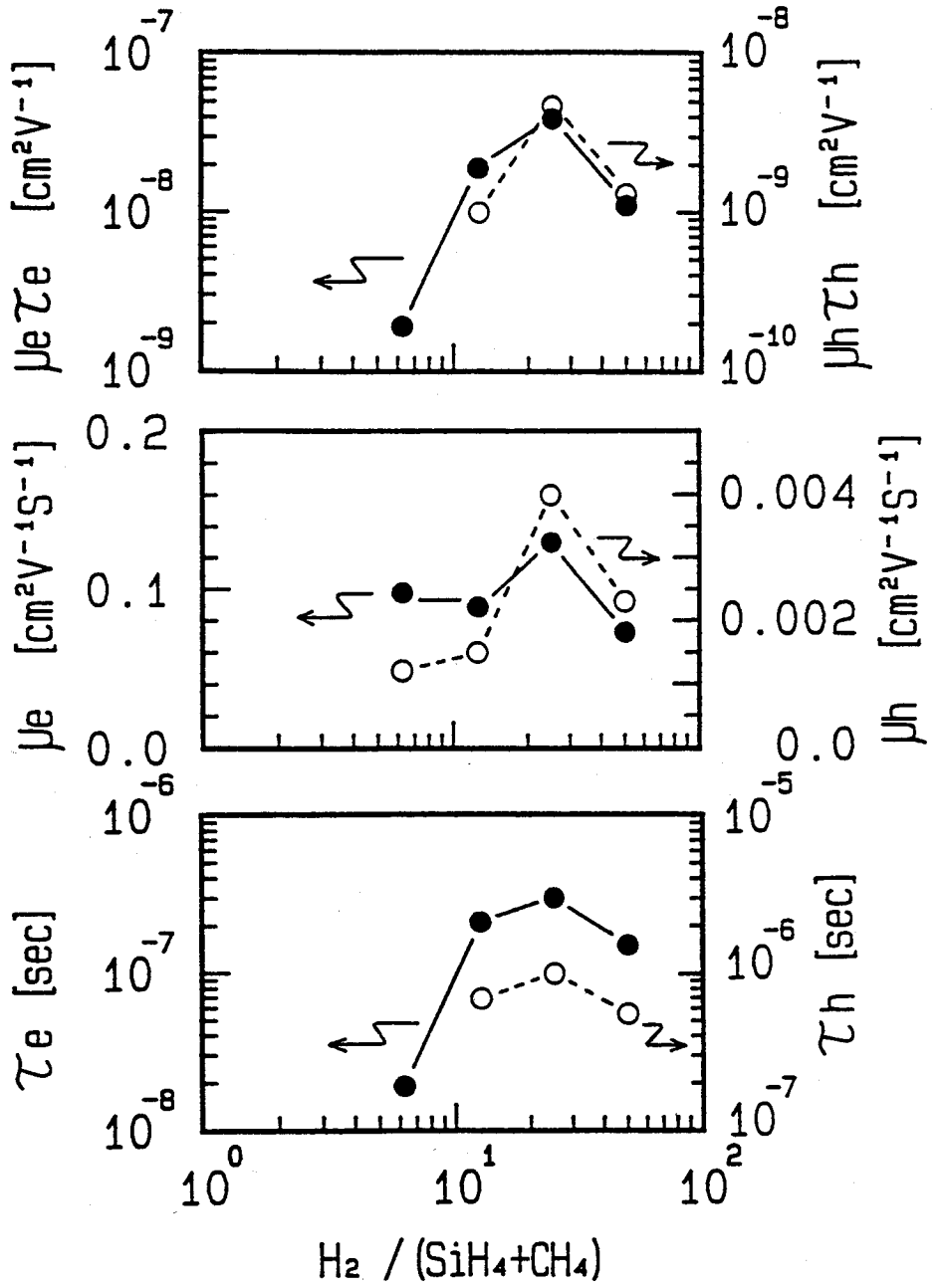

Fig. 2-2-3. Dependence of electron mobility (μ_e), hole mobility (μ_h), electron lifetime (τ_e), and hole lifetime (τ_h) of a-SiC:H films on hydrogen dilution ratio: $H_2/(SiH_4+CH_4)$.

2-2-3. Application of a-SiC:H films to p/i interface layers

In the next, a-SiC:H films prepared at various hydrogen dilution ratios were applied to p/i interface layers in a-Si:H single-junction cells and evaluated the solar cell characteristics. The other preparation conditions of the p/i interface layers were SiH_4+CH_4=15 sccm, RF power=20 W. The thickness of the p/i interface layer is 15 nm. Figure 2-2-4 shows the dependence of the cell characteristics on the hydrogen dilution ratio. The cell parameters shown in Fig. 2-2-4 are normalized to those of the cell without the p/i interface layer. It was already reported that introducing the p/i interface layer especially results in increase of open circuit voltage (V_{oc}) due to effective increase of built-in potential. [11] As shown in Fig. 2-2-4, V_{oc} increases by introducing p/i interface layer due to such effect. Moreover, both short circuit current (I_{sc}) and fill factor (F.F.) increase by applying a-SiC:H prepared under the optimum hydrogen dilution ratio to the p/i interface layer. The ordinary spectral response and the spectral response under bias voltage of +0.6 V normalized by that under bias voltage of 0 V are shown in Fig. 2-2-5. It is understood from the spectral response that the increase of I_{sc} is due to the increase of the spectral response at short wavelengths and the improvement of F.F. is caused by the reduction of the bias voltage dependence of spectral response at longer wavelengths. Under the further hydrogen dilution, V_{oc} drops and the conversion efficiency decreases. It is inferred that the drop of V_{oc} is caused by the change of the film properties under the further hydrogen dilution condition, as mentioned in section 2-2-2.

It can be concluded that the p/i interface layer becomes more active and the photo-generated carriers are collected effectively in the forward bias voltage and the conversion efficiency shows a maximum by applying the a-SiC:H films prepared under the optimum hydrogen dilution condition to the p/i interface layers.

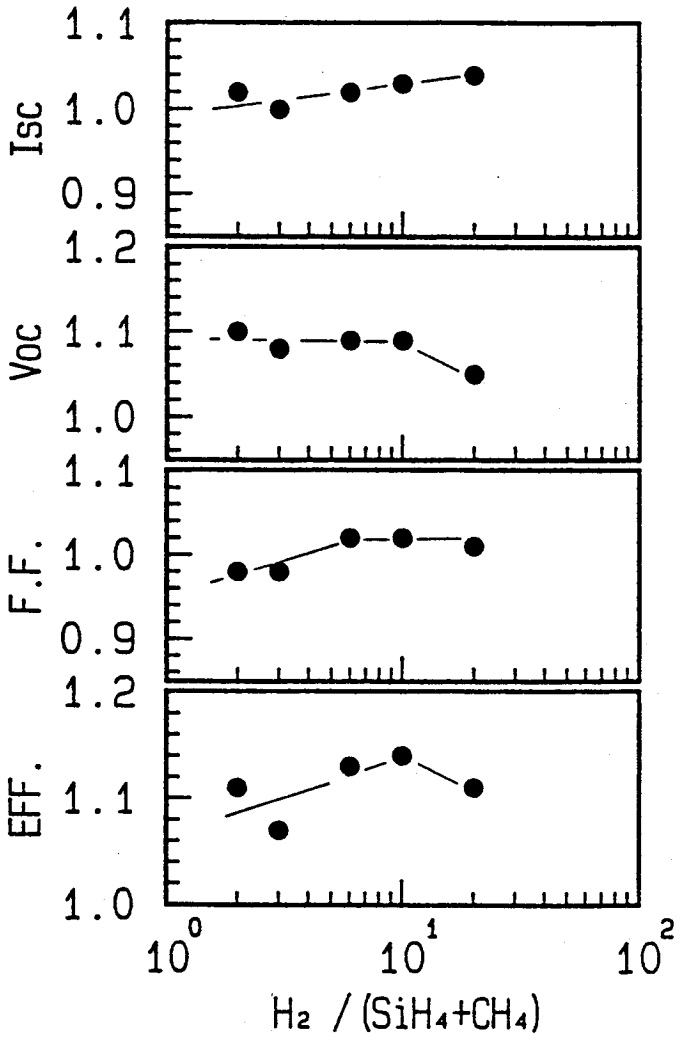

Fig. 2-2-4. Dependence of a-Si:H cell characteristics on hydrogen dilution ratio: $H_2/(SiH_4+CH_4)$ where a-SiC:H p/i interface layer was prepared. Each parameter is normalized to those of the cell without p/i interface layer. ($SiH_4 + CH_4$ = 15 sccm, RF power=20 W)

[I_{sc}: short circuit current V_{oc}: open circuit voltage
F.F.: fill factor EFF.: conversion efficiency]

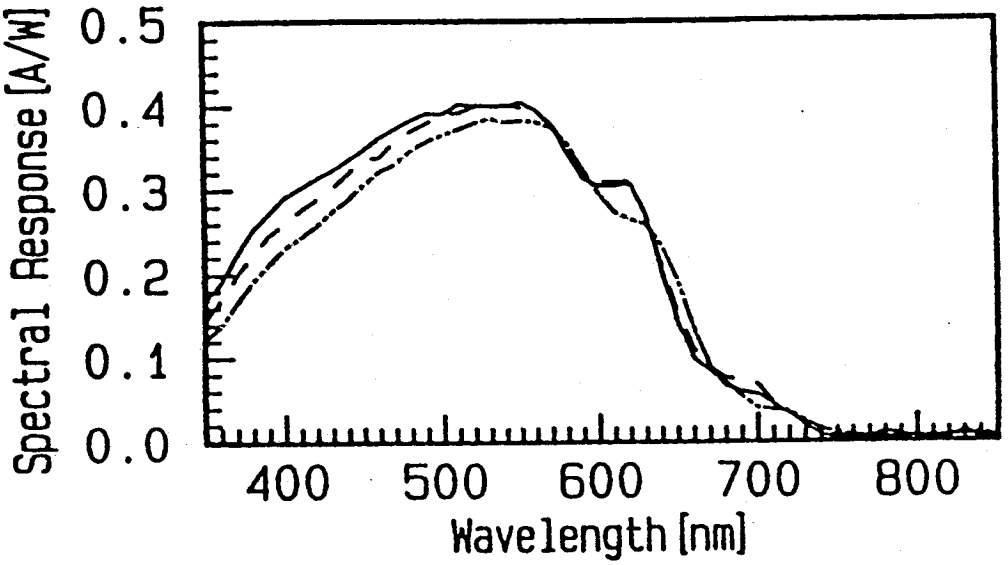

(a) Spectral photo-response

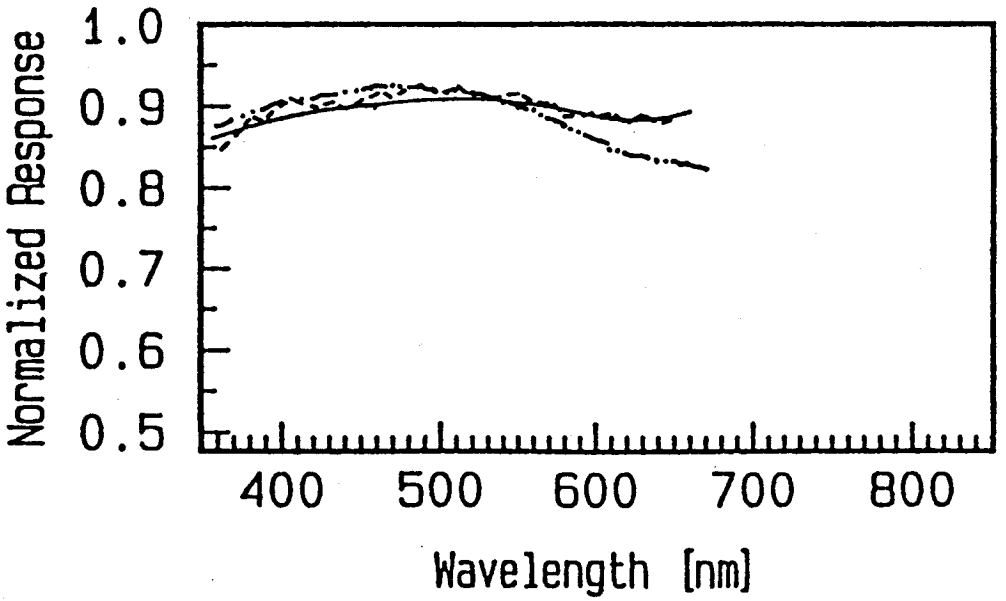

(b) Normalized spectral photo-response

Fig. 2-2-5. Spectral photo-response of the a-Si:H cells with a-SiC:H p/i interface layer in Fig. 2-2-4. ((a) Spectral photo-response under 0 V, (b) Spectral photo-response under +0.6 V normalized by taht under 0V, $H_2/(SH_4+CH_4)$= 2 (—··—), =10 (– – – –), =20 (——)).

2-2-4. Application of a-SiC:H films to photovoltaic active layers

It was reported that multi-bandgap stacked solar cells should obtain higher efficiency. [12-15] Therefore, a-SiC:H films with the high quality were applied to the photovoltaic active layer of the single-junction solar cells in order to use them as a component solar cell at the light incident side in the multi-bandgap stacked solar cell. The dependence of the a-SiC:H (Egopt ~ 1.97 eV) solar cell characteristics on the thickness of the i-layers are shown in Fig. 2-2-6 compared with the characteristics of a-Si:H (Egopt ~ 1.75 eV) solar cell. The conversion efficiency of a-SiC:H cell is almost the same value as that of a-Si:H cell due to the decrease of F.F.. However, a-SiC:H cells have higher V_{oc} than a-Si:H cell, and the purpose of applying the a-Si:H films to the photovoltaic active layers has been attained.

2-3. Improvement of Film Quality in a-SiGe:H

2-3-1. Experimental

a-SiGe:H films were prepared by using a conventional capacitance-coupled RF plasma CVD system. Hydrogen dilution ratios: $H_2/(SiH_4+GeH_4)$ was kept about 16. GeH_4 gas ratio: $GeH_4/(SiH_4+GeH_4)$ changed in the range of 12~25 %. Total gas flow rate is about 100 sccm, total gas pressure is 0.35 torr, and RF power is 10 W.

Photo-conductivity (σ_{ph}) under AM 1 light of 100 mW/cm^2, and dark-conductivity (σ_d) were measured by using samples with coplanar type electrode. Optical bandgap (Egopt) was determined by Tauc's plot. Germanium content in the films was determined by Auger electron spectroscopy. Integrated absorption intensity of Ge-H bond (~ 1880 cm^{-1}), Si-H bond (~ 2000 cm^{-1}), Si-H_2 bond (~2090 cm^{-1}) was calculated from infrared rays (IR) spectra.

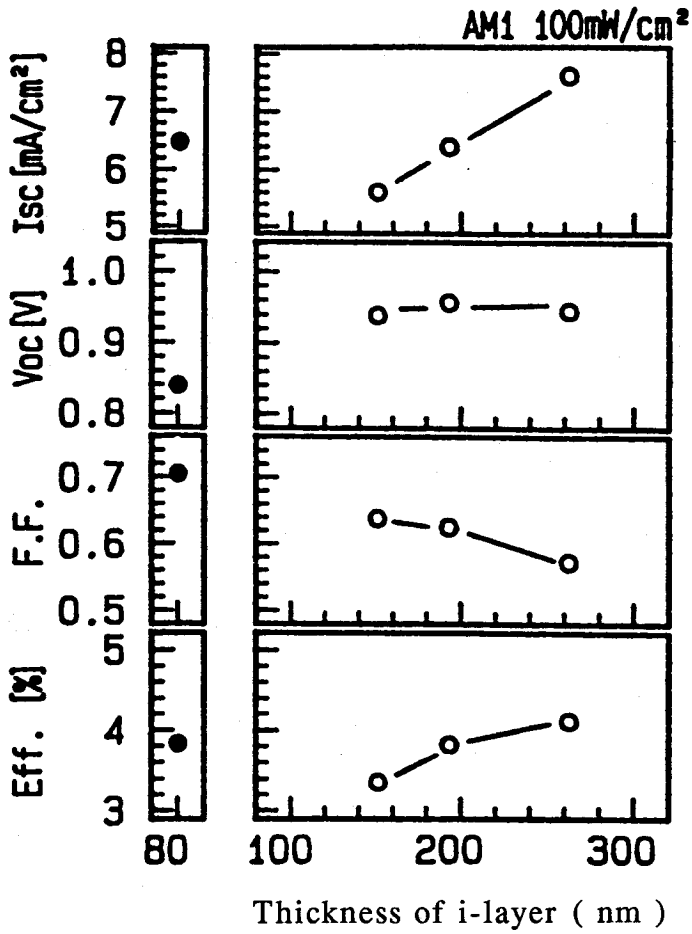

Fig. 2-2-6. Dependence of a-SiC:H cell characteristics (○) on i-layer thickness with data of a-Si:H cell (●). (Preparation conditions of a-SiC:H i-layer: RF power = 40W, $H_2/(SiH_4+CH_4)=30$)

[I_{sc}: short circuit current V_{oc}: open circuit voltage
F.F.: fill factor Eff.: conversion efficiency]

2-3-2 Dependence of a-SiGe:H film properties on preparation condition.

A guiding principle of improvement of film quality in a-Si alloy materials was given by A. Matsuda. [16,17] According to the guiding principle, larger surface diffusion coefficient (Ds) of the adsorbed precursors is necessary to obtain a-SiGe:H films with high quality. In order to obtain a larger Ds, hydrogen (H)-coverage of the growing surface and substrate temperature should be raised. In the case of a-Si:H, a growing surface is considered to be totally covered with hydrogen below the substrate temperature (Ts) of 300 ℃. However, in the case of a-SiGe:H, the H-coverage is decreased as the substrate temperature raises, because Ge-H bond is weaker than Si-H bond. Therefore, the dependence of a-SiGe:H film properties on the Ts was investigated to improve the film quality.

Figure 2-3-1 shows the dependence of optical bandgap (Egopt), photo-conductivity (σ_{ph}), and dark-conductivity (σ_{d}) of a-SiGe:H films on the Ts under GeH_4 gas ratios: GeH_4 /(SiH_4+GeH_4) of 14% and 20%. As the Ts increases, the Egopt decreases. On the other hand, the σ_{ph} increases as the Ts increases. Si-H bond, Si-H_2 bond, Ge-H bond content, and total hydrogen content, are shown in Figs. 2-3-2 (a), (b), (c) and (d), as a function of the Ts, respectively. As the Ts increases, Si-H bond, Si-H_2 bond content and total hydrogen content decrease, but Ge-H bond content does not change.

Figure 2-3-3 shows the σ_{ph} and the σ_{d} of the films that mentioned above, plotted against their optical bandgap.

As a result, it is concluded that the film quality in a-SiGe:H can be improved under high hydrogen dilution ratio by the increases of Ts, because of the decreases of Si-H_2 bond content and so on.

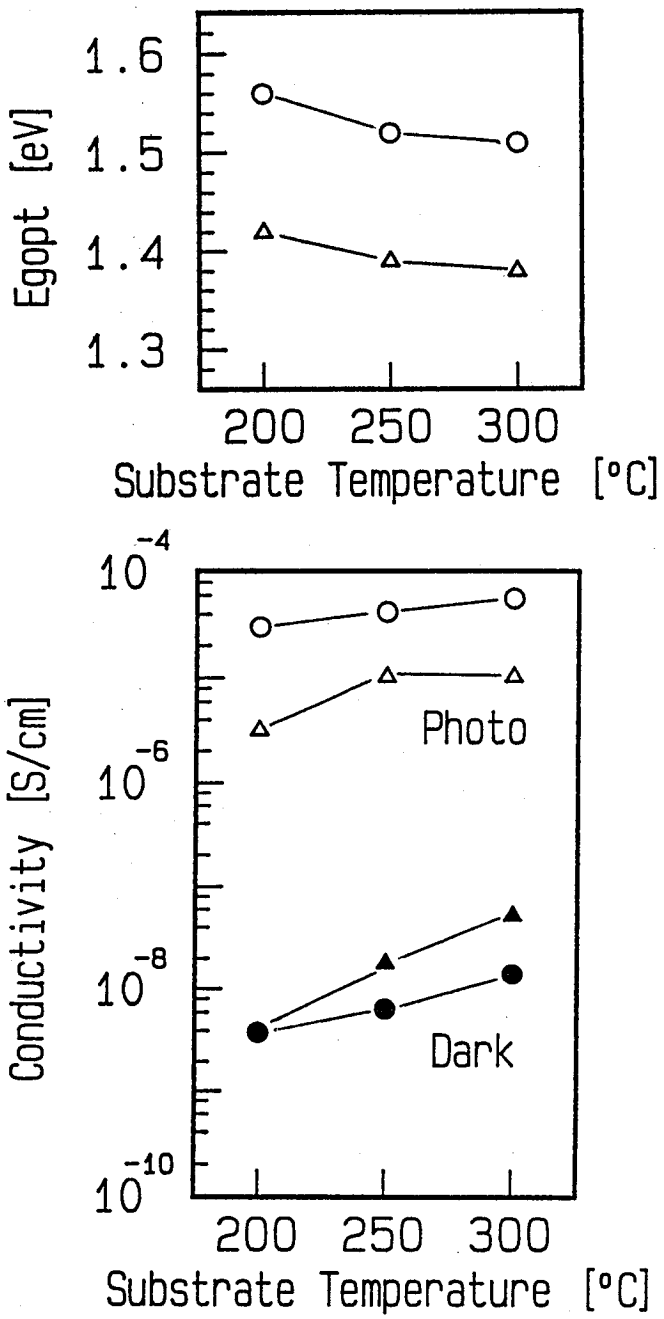

Fig. 2-3-1. Dependence of optical bandgap (Egopt), photo- and dark-conductivity of a-SiGe:H films on substrate temperature. (GeH_4 gas ratios: GeH_4 /(SiH_4+GeH_4) of 14% (○,●) and 20% (△,▲))

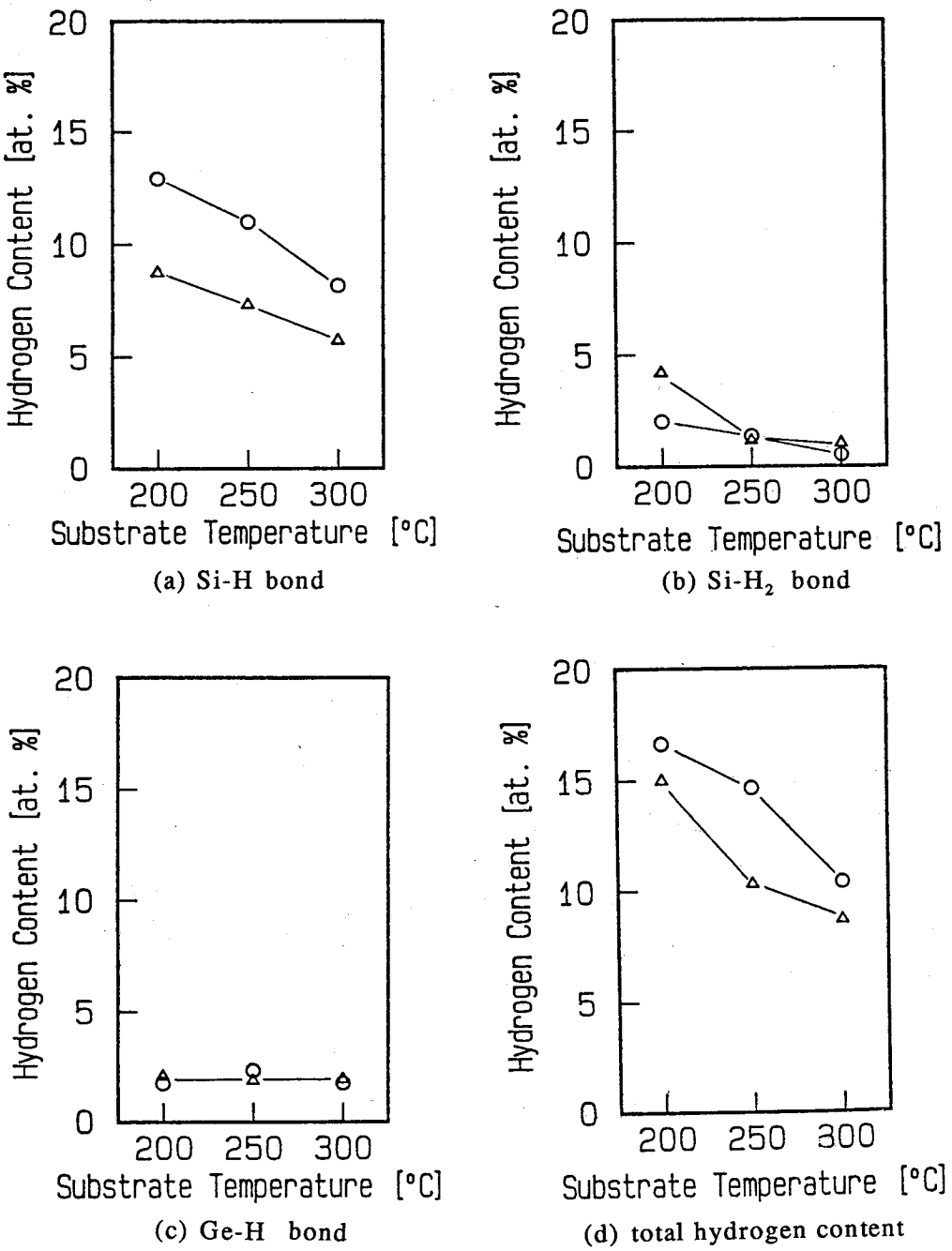

Fig. 2-3-2. Dependence of Si-H bond (a), $Si-H_2$ bond (b), Ge-H bond content (c), and total hydrogen content (d) of a-SiGe:H films on substrate temperature. (GeH_4 gas ratios: $GeH_4/(SiH_4+GeH_4)$ of 14% (○) and 20% (△))

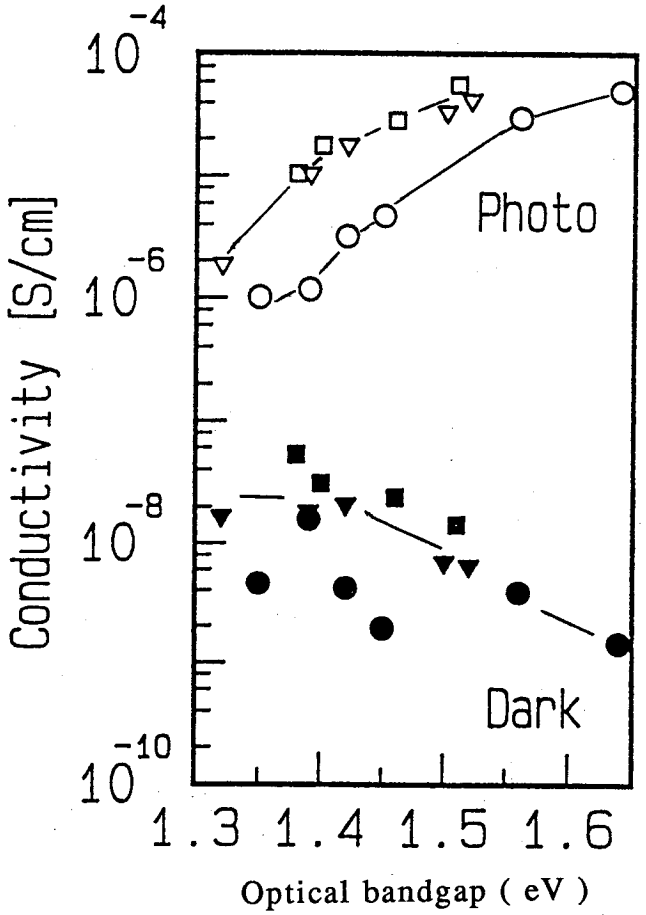

Fig. 2-3-3. Photo- and dark-conductivity of a-SiGe:H films against their optical bandgap.

(Substrate temperature: 200 ℃(○,●), 250 ℃(▽,▼) and 300 ℃(□,■))

2-3-3. Optical bandgap of a-SiGe:H films

One of the big advantages of a-Si alloy materials to be applied to the solar cell is that their optical bandgap (Egopt) can be continuously controlled. The Egopt is mainly determined by the compositional ratio and the total hydrogen content. In other words, very wide combinations of the compositional ratio and the total hydrogen content can be applied to obtain the same Egopt. Therefore, it is important to clarify the relationship among Egopt, Ge content, and total hydrogen content.

Figures 2-3-4 (a), (b) and (c) show the dependence of the Egopt, the Ge content, and the total hydrogen content of a-SiGe:H films on the GeH_4 gas ratio, respectively. The a-SiGe:H films were prepared under various GeH_4 gas ratios and substrate temperature (Ts). As the GeH_4 gas ratio increase, the Egopt decrease. But, under the certain GeH_4 gas ratio, the higher the Ts, the narrower the Egopt. This phenomenon was caused by the decrease of the hydrogen content because the Ge contents are same under the same GeH_4 gas ratio in spite of the different Ts, as shown in Figs. 2-3-4 (b) and (c).

As a result, based on the data of a-SiGe:H films, it is clarified the relationship among the optical bandgap, the Ge content and the total hydrogen content in the a-SiGe:H films, as shown in Fig. 2-3-5. Therefore, it becomes possible to choose the combinations of the Ge content and the total hydrogen content in order to improve the stability when the film with the certain Egopt is applied to solar cell.

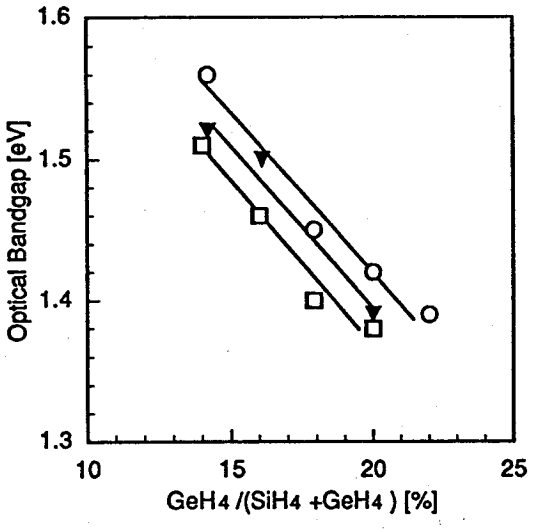

(a) Optical bandgap

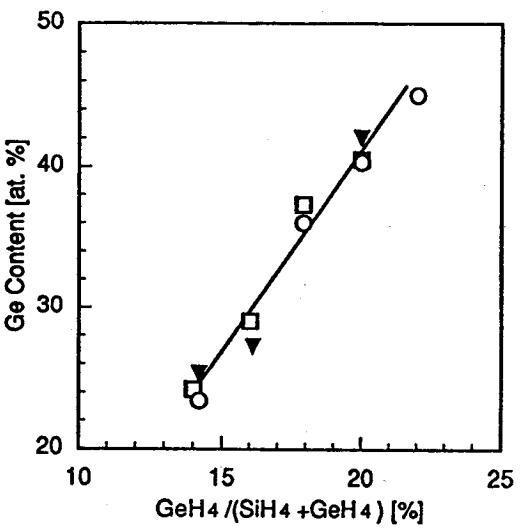

(b) Ge content

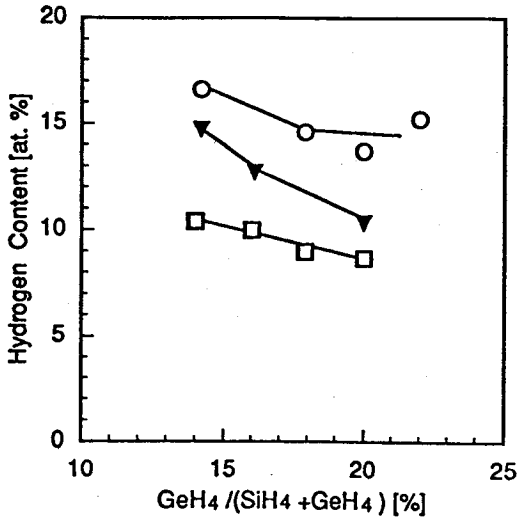

(c) Total hydrogen content

Fig. 2-3-4. Dependence of optical bandgap (a), Ge content (b), and total hydrogen content (c) of a-SiGe:H films on GeH_4 gas ratio: $GeH_4/(SiH_4+GeH_4)$. (Substrate temperature: 200 ℃ (○), 250 ℃(▼) and 300 ℃(□))

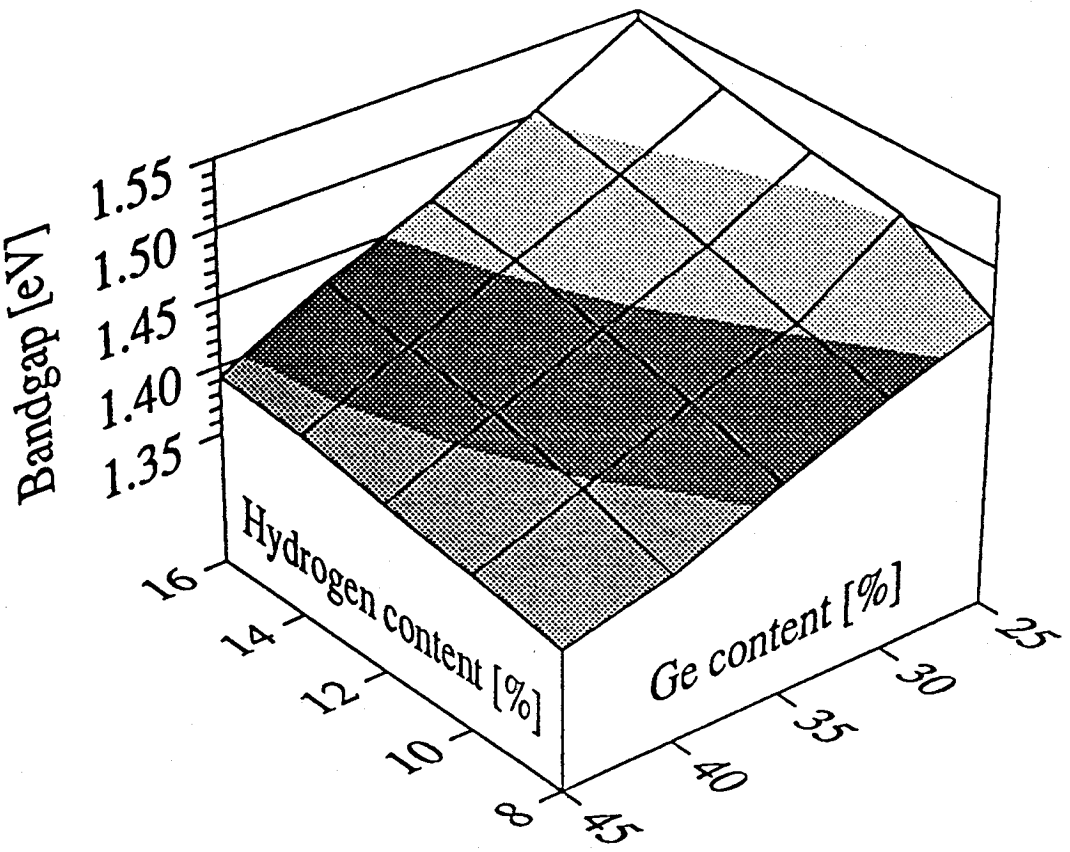

Fig. 2-3-5. Relationship among optical bandgap, Ge content and total hydrogen content in a-SiGe:H films.

2-4. Properties of a-Si Alloy Materials

The film quality in a-SiC:H and a-SiGe:H has been improved by the hydrogen dilution method, as mentioned in sections 2-2 and 2-3. The photo- and dark-conductivities of these a-Si alloy materials with high quality are shown in Fig. 2-3-6, against their optical bandgaps. The a-Si alloy materials having a photo-conductivity of more than 10^{-5} S/cm were obtained for a wide range of optical bandgap, from 1.39 eV to 2.0 eV. Therefore, these materials with high quality allow us to apply the bandgap control technologies, which is one of the big advantages of a-Si alloy materials, to the multi-bandgap stacked solar cell, the bandgap profiling and so on in order to improve the solar cell characteristics.

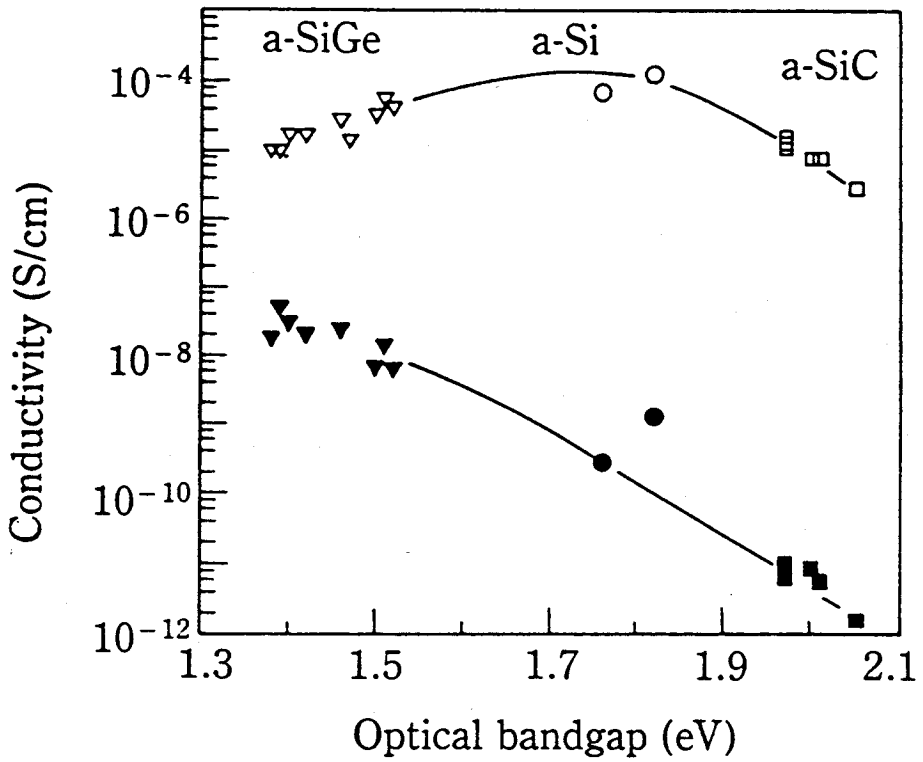

Fig. 2-3-6. Photo- and dark-conductivity of high quality a-Si alloy materials, namely a-SiGe:H (▽,▼), a-Si:H (○,●), a-SiC:H (□,■), against their optical bandgap.

2-5. Summary

The improvement of film quality in a-Si alloy materials and its application to solar cells were investigated and following results were obtained:

(1) It has been clarified that there is the optimum hydrogen dilution ratio of 10 ~ 30 to obtain a-SiC:H films with higher photo-conductivity and higher electron and hole mobilities. Such phenomenon is caused by the decrease of the carbon content and the increase of the Si-H bond content as the hydrogen dilution ratio increases.

(2) The conversion efficiencies of a-Si:H solar cells are improved by applying the high quality a-SiC:H films to p/i interface layers and the conversion efficiency shows a maximum at the optimum hydrogen dilution ratio as mentioned above.

(3) The high quality a-SiC:H films were applied to the photovoltaic active layer in order to use them as a component solar cell at the light incident side in the multi-bandgap solar cell. The a-SiC:H cells have higher open circuit voltage than a-Si:H cell.

(4) The film quality in a-SiGe:H can be improved under high hydrogen dilution ratio by the increase of substrate temperature. It is clarified the relationship between the optical bandgap, the Ge content and the total hydrogen content in the a-SiGe:H films.

(5) The a-Si alloy materials, namely a-SiGe:H, a-Si:H and a-SiC:H, having a photo-conductivity of more than 10^{-5} S/cm were obtained for a wide range of optical bandgap, from 1.39 eV to 2.0 eV. Therefore, these materials with high quality allow us to apply the bandgap control technologies to the multi-bandgap stacked solar cell, the bandgap profiling and so on in order to improve the solar cell characteristics.

REFERENCES

1) Y. Nakata, Y. Inoue, H. Sannomiya, K. Nomoto, A. Yokota, M. Itoh and T. Tsuji: OPTOELECTRONICS - Devices and Technologies, Vol. 6, No.1, (1991) 141.

2) M. Kaneiwa, K. Nomoto, M. Itoh, Y. Yamamoto, Y. Nakata and T. Inoguchi: Tech. Digest of 4th Int. Photovol. Sci. Engi. Conf., Sydney (1989) 673.

3) Y. Nakata and T. Inoguchi: OPTOELECTRONICS - Devices and Technologies,Vol. 4, No. 1, (1989) 75.

4) S. Moriuchi, Y. Inoue, H. Sannomiya, A. Yokota, M. Itoh, Y. Nakata and H. Itoh: Proc. 21st IEEE Photovol. Spec. Conf., Florida (1990) 1449.

5) T. Kobe, Y. Nakata, T. Machida, Y. Yamamoto and T. Tsuji: Proc. 18th IEEE Photovol. Spec. Conf., Las Vegas (1985) 1594.

6) A. Yokota, H. Sannomiya, S. Moriuchi, Y. Inoue, M. Itoh, Y. Nakata and T. Tsuji: Tech. Digest of 5th Int. Photovol. Sci. Engi. Conf., Kyoto (1990) 637.

7) Y. Nakata, A. Yokota, H. Sannomiya, S. Moriuchi, Y. Inoue, K. Nomoto, M. Itoh and T. Tsuji: Mat. Res. Soc. Symp. Proc., Vol. 219 (1991) 433.

8) Y. Nakata, A. Yokota, H. Sannomiya, S. Moriuchi, Y. Inoue, K. Nomoto, M. Itoh and T. Tsuji: Jpn. J. Appl. Phys., Vol. 31, Part 1, No. 2 (1992) (in press)

9) W. Y. Kim, H. Tasaki, M. Konagai and K. Takahashi: J. Appl. Phy. 61 (1987) 3071.

10) Y. Yamamoto, H. Sannomiya, A. Yokota, Y. Nakata and T. Inoguchi: Proc. 19th IEEE Photovol. Spec. Conf., New Orleans (1987) 302.

11) Y. Yamamoto, K. Nomoto, T. Okuno, S. Moriuchi, Y. Nakata and T. Inoguchi: Proc. 19th IEEE Photovol. Spec. Conf., New Orleans (1987) 901.

12) Y. Nakata, H. Sannomiya, S. Moriuchi, A. Yokota, Y. Inoue, M. Itoh and H. Itoh: Mat. Res. Soc. Symp. Proc., Vol. 192 (1990) 15.

13) H. Sannomiya, S. Moriuchi, Y. Inoue, K. Nomoto, A. Yokota, M. Itoh, Y. Nakata and T. Tsuji: Tech. Digest of 5th Int. Photovol. Sci. Engi. Conf., Kyoto (1990) 387.

14) Y. Nakata, H. Sannomiya, S. Moriuchi, Y. Inoue, K. Nomoto, A. Yokota, M. Itoh and T. Tsuji: OPTOELECTRONICS - Devices and Technologies, Vol. 5, No. 2, (1990) 209.

15) A. Matsuda and K. Tanaka: J. Non-Cryst. Solids 97&98 (1987) 1367.

16) A. Matsuda and K. Tanaka: Materials Science Reports Vol. 2, No. 4, August (1987) 139.

17) K. Nomoto, Y. Takeda, S. Moriuchi, H. Sannomiya, T. Okuno, A. Yokota, M. Kaneiwa, M. Itoh, Y. Yamamoto, Y. Nakata and T. Inoguchi: Tech. Digest of 4th Int. Photovol. Sci. Engi. Conf., Sydney (1989) 85.

III. CHARACTERIZATION OF COMPONENT CELLS IN a-Si ALLOY STACKED SOLAR CELL

3-1. Introduction

A multi-bandgap stacked solar cell using a-Si alloy materials [1] is one of the most promising cell structures to obtain both of high stability and high conversion efficiency. [2-5] For such stacked solar cells, it is essential to balance the output currents of component cells with each other because the output current of the stacked solar cells is limited by the lowest current among them of the component cells. To obtain a stacked solar cell with a high conversion efficiency, it is necessary to take account of the current balance in each component cell. After light exposure, however, since the changes in output current by light-induced degradation are different among the component cells, the currents are not balanced with each other even if the currents are balanced at initial stage. To obtain stacked solar cells with high stability, therefore, it is necessary to know individual current - voltage (I-V) characteristics of component cells after light exposure and to design the optimum i-layer thicknesses of component cells taking account of the current balance after light exposure. There was not a measuring method of individual I-V characteristics of component cells in stacked cells and it was required.

In this chapter, methods for measuring the spectral photo-response of a-Si alloy single-junction solar cells [6] and each component cell in a-Si alloy stacked solar cells [7,8] are first investigated. On the bases of these methods, a new method for measuring individual I-V characteristics of component cells in stacked solar cells is proposed. [2] Using this new method, the light-induced degradation characteristics of component cells in stacked solar cells are demonstrated. [2]

3-2 Measurement of Spectral Photo-response in a-Si Alloy Single-junction Solar Cells

At first, measuring method of the spectral response for a-Si single-junction solar cells was investigated to establish a measuring method of individual I-V characteristics of component cells in a-Si alloy stacked solar cells. [6] The spectral response for a-Si solar cells is significantly influenced by bias light and bias voltage. [9,10] Moreover, the spectral response changes with long exposure to light, this phenomenon is well-known as a Staebler-Wronski (S-W) effect. [11-15]

3-2-1. Experimental

An experimental apparatus for measuring the spectral response of a-Si single-junction solar cells is shown in Fig. 3-2-1. The chopped probe light and D.C. bias light simultaneously irradiated the samples. The probe light intensity was about $10 \sim 25\,\mu$ W/cm^2. AM1.5 standard light with various optical filters was used for the bias illumination. Figure 3-2-2 shows the transmission spectra of these optical filters. Red bias light was obtained by using 832* and IRA-05* filters, and blue bias light was obtained by using 829* and IRA-05 filters. AM1.5 standard light was used for white bias light, and the intensity was changed by using neutral density (ND) filters. A.C. photo-current generated by chopped probe light was measured by using a lock-in amplifier. Samples were prepared by RF glow discharge decomposition of SiH_4 and GeH_4. Stainless steel (S.S.)/ pi(a-Si)n/Transparent Conductive Oxide (TCO) cells and S.S./ni(a-Si)p/TCO cell were used for the measurement of the spectral response dependence on the bias light wavelength. S.S./ni(a-Si)p/TCO cells and S.S./ni(a-SiGe)p/TCO cells were used for the measurement of the spectral response dependence on the bias light intensity. Dangling bond densities in the photovoltaic active layers were changed by exposure to AM 1.5, 10 suns of light from a solar simulator.

The experimental parameters which were investigated for the analysis of spectral response are summarized in Table 3-2-1.

*829 and 832 filters were made by Nihonshinkukogaku and IRA-05 filter was made by Toshiba Glass Corporation.

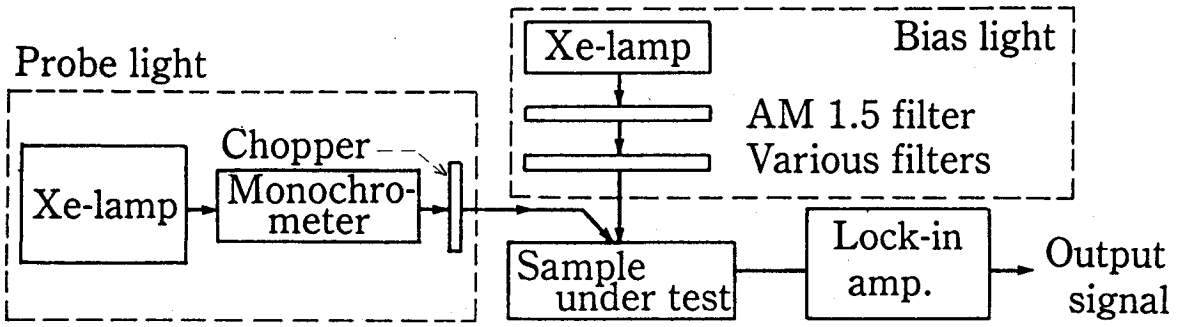

Fig. 3-2-1. Experimental apparatus for measuring spectral photo-response of a-Si alloy solar cells.

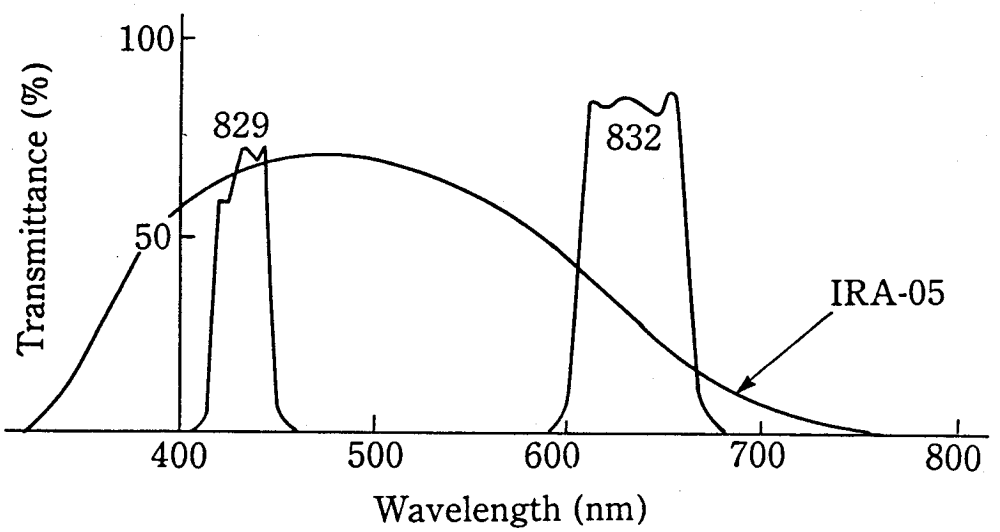

Fig. 3-2-2. Transmission spectra of various optical filters.

Table 3-2-1. Experimental parameters for study of spectral response in a-Si alloy single-junction solar cells.

Samples	Materials	(a-Si and a-SiGe)
	i-layer thickness	(a-Si: 320 nm, 760 nm, a-SiGe: 250 nm)
	Structure	(S.S./nip/TCO, S.S./pin/TCO)
	Dangling bond density	($3\times10^{16}\sim 3\times10^{17}cm^{-3}$)
Bias light	Wavelength	(blue, red, white)
	Intensity	(0～50 mW/cm^2)
Probe light	Chopping frequency	(6 Hz, 170 Hz)
Bias voltage	Voltage	(-2 V ～ +0.8 V)

3-2-2. Dependence of spectral photo-response on bias light wavelength

The spectral response dependence on the bias light wavelength in short circuit conditions was investigated. S.S./pi(a-Si)n/TCO solar cells were used, and their i-layer thicknesses were 320 nm and 760 nm. The spectral responses with the red or blue bias light and without bias light are shown in Fig. 3-2-3. The chopping frequencies of the probe light were 6 Hz and 170 Hz. As shown in this figure, in the case of the lower chopping frequency of the probe light and the solar cell with thicker i-layer, the spectral response at long wavelength is enhanced by the blue bias light.

To clarify the reason for this enhancement, the spectral response with the blue bias light was investigated. The bias voltage dependence of the spectral responses with and without the blue bias light was measured. The probe light wavelength was fixed at 630 nm, and the bias voltage was changed. The spectral response with the blue bias light depends on the bias voltage and shows a large enhancement. The bias voltage dependence is shown in Fig. 3-2-4 (a). Photo-current - bias voltage (I-V) characteristics (1) with only the blue bias light and those (2) with the blue bias light and the unchopped 630 nm probe light were measured, as shown in Fig. 3-2-4 (b). To explain the enhancement of the spectral response, Figs. 3-2-5 (a) and (b) are drawn as exaggerations of Figs. 3-2-4 (a) and (b). The difference in I-V characteristics ((2) - (1)) is measured as the spectral response with the 630 nm probe light. It is considered that there is a difference of fill factor (F.F.) between I - V characteristics (1) and (2), as shown in Fig. 3-2-5 (b), on the basis of the bias voltage dependence of spectral response which is shown in Fig. 3-2-4 (a). In other words, the F.F. under the blue bias light is modulated by the red probe light, and the spectral response, which is the difference between (1) and (2), is enhanced. In a-Si solar cells, the

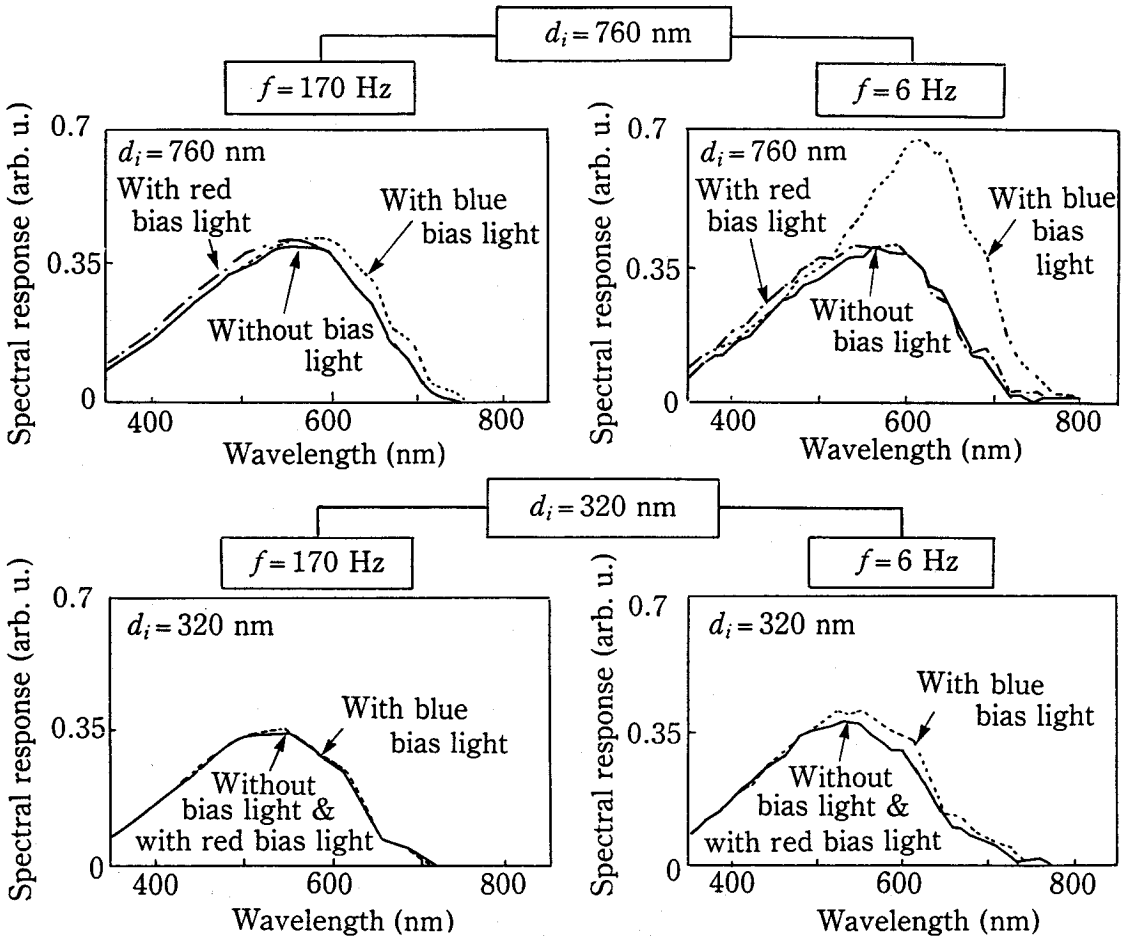

Fig. 3-2-3. Spectral response dependence on bias light wavelength in short circuit condition for a-Si solar cell with i-layer thicknesses of 320 nm and 760 nm under probe light of 6 Hz and 170 Hz chopping frequency.

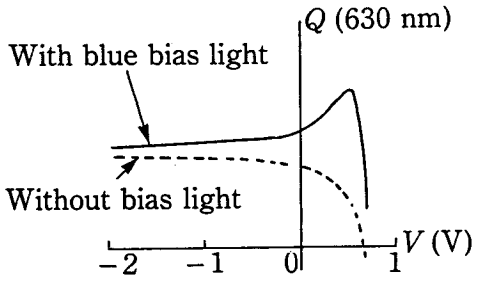

(a) Spectral response

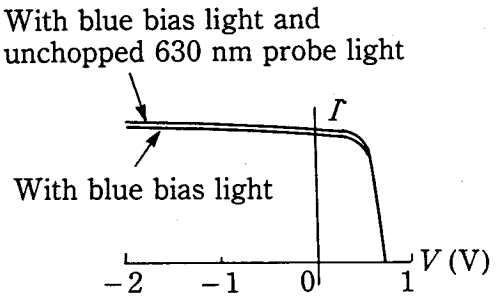

(b) *I-V* characteristics

Fig. 3-2-4. Dependence of spectral response on bias voltage (a) and photo-current - bias voltage characteristics (b). The wavelength of probe light is fixed at 630 nm.

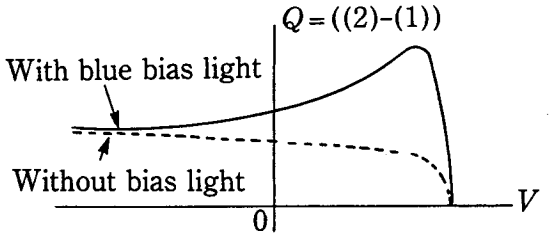

(a) Spectral response

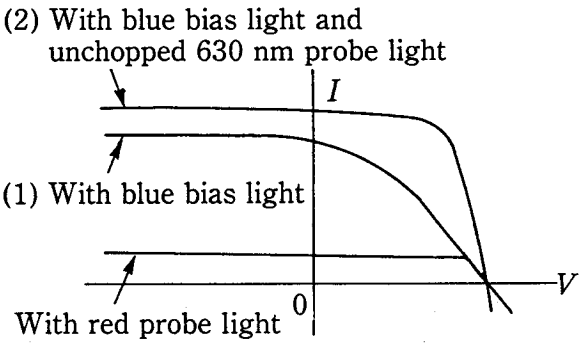

(b) *I-V* characteristics

Fig. 3-2-5. Schematic explanation of the observed effect shown in Fig. 3-2-4

electric fields in the photovoltaic active layers are utilized to increase the efficiency and the F.F. depends mainly on the electric field. In S.S./ni(a-Si)p/TCO cells, the spectral response at long wavelength was not enhanced by the blue bias light. However, the enhancement was observed after 1 hour's exposure of the cell to 10 suns of light. These results suggest that the region in the i-layer whose characteristics are modulated by the red probe light is located near the n-layer and the electrical properties of the region are changed by the light exposure.

As a result, the electric fields in the photovoltaic active layers are modulated under the blue bias light by the red probe light, and the spectral response at long wavelength is enhanced. Therefore, it is necessary to use the bias light which contains at least red light in order to prevent the modulation of the electric fields by the red probe light and to measure the spectral responses accurately.

3-2-3. Dependence of spectral photo-response on bias light intensity

The spectral response dependence on the bias light intensity in short circuit conditions was investigated. S.S./ni(a-Si)p/TCO cells with the i-layer thickness of 400 nm and S.S./ni(a-SiGe)p/TCO cells with thickness of 250 nm were used. The spectral response dependence is influenced by the dangling bond densities in the photovoltaic active layer. Therefore, the cells were exposed to AM 1.5, 10 suns of light in the open circuit condition to change the dangling bond densities. The 1 and 5.5 hours' exposure to 10 suns of light corresponds to 303 and 1545 hours' exposure to 1 sun of light in a-Si solar cells, and 46 and 184 hours' exposure to 1 sun of light in a-SiGe solar cells respectively, using the prediction method. [14,15] The dangling bond densities in the photovoltaic active layer of a-Si solar cell were estimated to be $\sim 3 \times 10^{16}$, $\sim 2 \times 10^{17}$, and $\sim 3 \times 10^{17}$ cm^{-3} after 0, 1 and 5.5 hours' exposure to 10 suns of light respectively, from the electron spin resonance (ESR) measurements on similar a-Si films. This implies that the dangling bond densities were varied over a wide range. Figures 3-2-6 (a) and (b) show the light-induced degradation characteristics of a-Si and a-SiGe solar cells under 10 suns of light which is normalized by the initial value.

The spectral responses of a-Si and a-SiGe solar cells before and after 1 and 5.5 hours' exposure to 10 suns of light were measured under AM 1.5 bias light, as shown in Figs. 3-2-7 (a) and (b). The intensity of AM 1.5 bias light was adjusted to 0, 0.05, 0.5, 5, and 50 mW/cm^2 by using ND filters. The spectral response of a-Si and a-SiGe solar cells before the light exposure did not change with the AM 1.5 bias light. But the spectral response of a-Si and a-SiGe solar cells after the light exposure was increased in the entire wavelength range by the AM 1.5 bias light. The higher the dangling bond densities were, the larger was the increase of the spectral responses caused by the AM 1.5 bias light was.

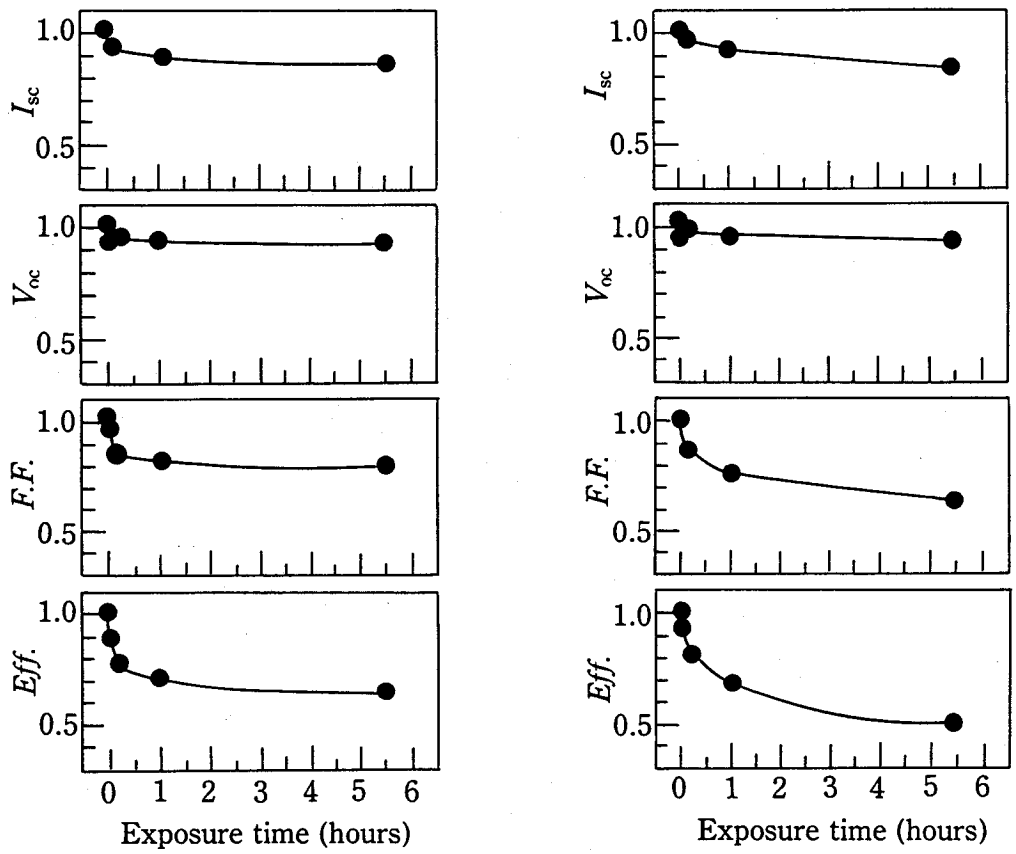

Fig. 3-2-6. Light-induced degradation characteristics of a-Si solar cell (a) and a-SiGe solar cell (b) under 10 suns of light which were normalized by the initial values.

[I_{sc} : Short circuit current V_{oc}: Open circuit voltage
F.F.: Fill factor Eff.: Conversion efficiency]

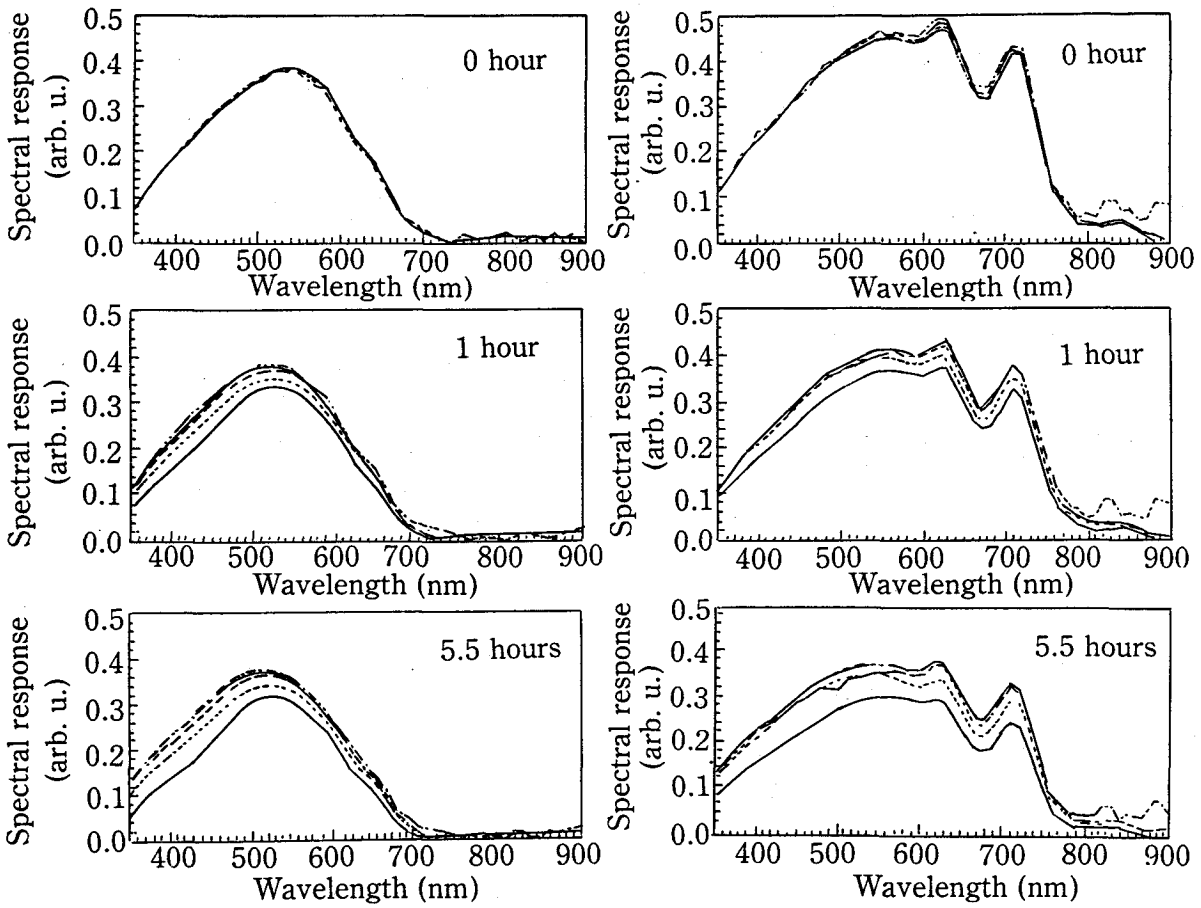

Fig. 3-2-7. Dependence of spectral responses on bias light intensity in short circuit condition for a-Si solar cell (a) and a-SiGe solar cell (b) before and after 1 and 5.5 hours' exposure to 10 suns of light.

[——— 0 mW/cm^2, ·····0.05 mW/cm^2, ----- 0.5 mW/cm^2
—·— 5 mW/cm^2, — — — 50 mW/cm^2]

In order to evaluate quantitatively, the increase of the spectral responses in the entire wavelength range, short circuit currents were calculated from the spectral responses and spectrum of AM 1.5 standard sunlight. The calculated short circuit currents of a-Si and a-SiGe cells, and those normalized by the values under the bias light of 50 mW/cm^2 are shown in Figs. 3-2-8 (a) and (b) and Figs. 3-2-9 (a) and (b). Even in a-Si and a-SiGe solar cells with high dangling bond densities, the calculated short circuit currents rapidly increased and almost saturated when the bias light intensity changed from 0 to 5 mW/cm^2. The difference between them under the bias light intensity of 5 and 50 mW/cm^2 is less than 3 %. The electric field in the photovoltaic active layer is determined by the charges which are trapped in the localized states. The localized states are originated from the dangling bonds and others. The many localized states which were induced by the light exposure are not occupied by carriers when the bias light does not irradiate. But, when the intensity of the bias light increase, those many localized states are rapidly occupied by carriers, and the electric field in the photovoltaic active layer comes not to change. So the short circuit currents rapidly increased and saturated with an increase in the intensity of the bias light. Therefore, if the spectral response does not change with the decrease in the intensity of the white bias light from low initial value to 50 % of it, the spectral response can be measured accurately under this low intensity bias light. It takes about 5 minutes to measure one spectral response. The 5 minutes' exposure to 5 mW/cm^2 bias light corresponds to less than 1 second's exposure to 100 mW/cm^2 light. [12] Therefore, the light-induced degradation of spectral response during the measurement is negligible if the bias light intensity of 5 $\sim$10 mW/cm^2 is used.

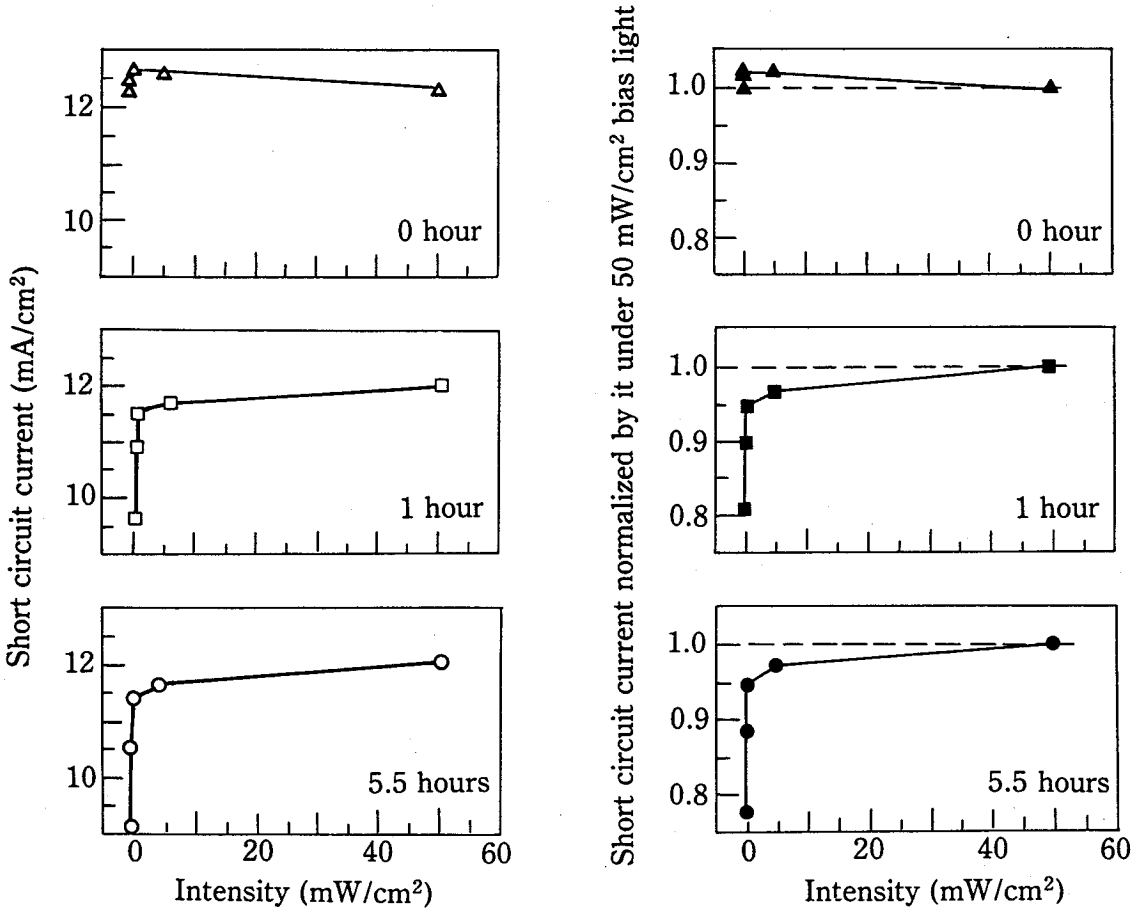

(a) Absolute short circuit current (b) Normalized short circuit current

Fig. 3-2-8. Dependence of short circuit currents on bias light intensity for a-Si solar cell before and after 1 and 5.5 hours' exposure to 10 suns of light. Short circuit currents are calculated from spectral responses and spectrum of AM 1.5 standard sunlight.

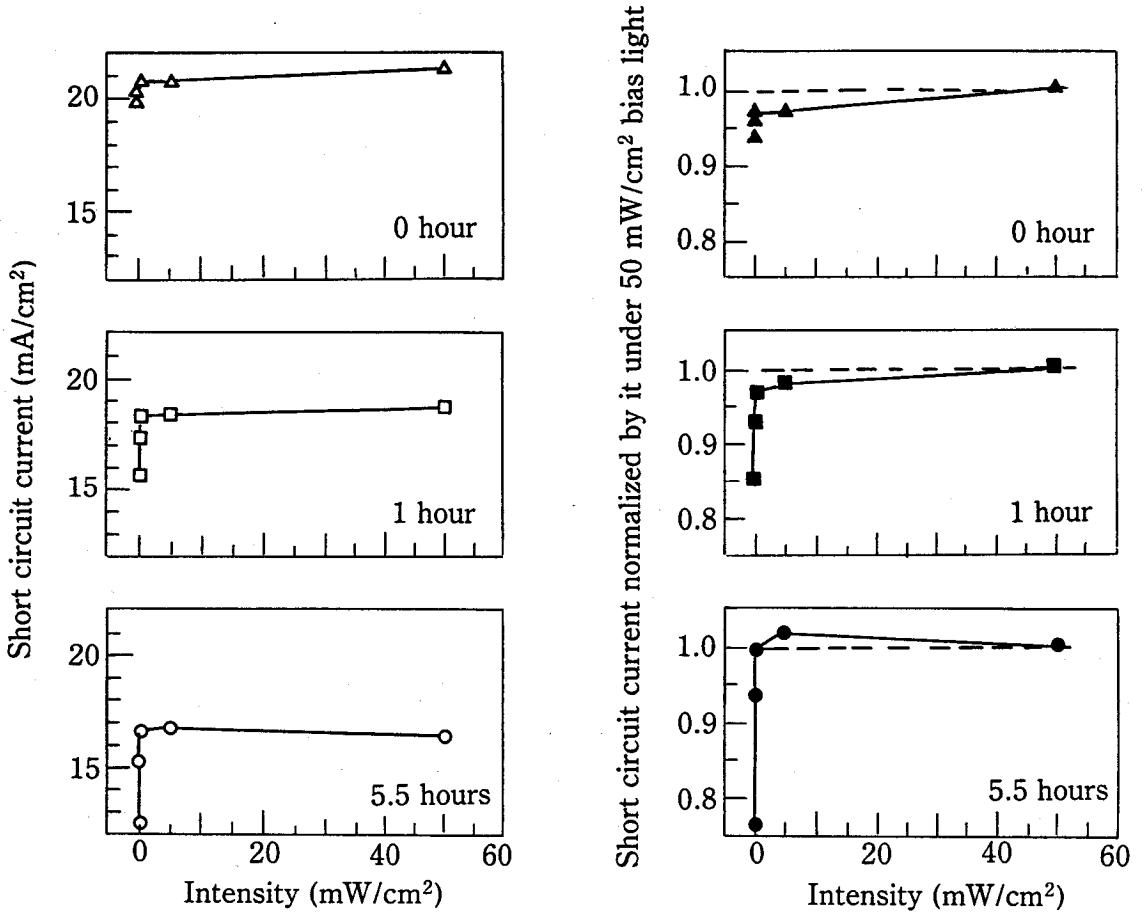

(a) Absolute short circuit current

(b) Normalized short circuit current

Fig. 3-2-9. Dependence of short circuit currents on bias light intensity for a-SiGe solar cell before and after 1 and 5.5 hours' exposure to 10 suns of light. Short circuit currents are calculated from spectral responses and spectrum of AM 1.5 standard sunlight.

3-2-4. Summary

The spectral response dependence on the bias light wavelength and the bias light intensity in a-Si and a-SiGe single-junction solar cells with the various i-layer thicknesses and with the various dangling bond densities were investigated. The results from this investigation are as follows.

(1) The spectral responses are enhanced in some cases by the blue bias light because the electric fields in the photovoltaic active layers are modulated by the red probe light under the blue bias light. Therefore, it is necessary to use the bias light which at least contains red light in order to prevent the modulation of the electric fields by the red probe light and to measure the spectral responses accurately.

(2) The spectral response rapidly increased and almost saturated when the white bias light intensity changed from 0 to 5 mW/cm^2, even in a-Si and a-SiGe solar cells with high dangling bond densities. Therefore, if the spectral response does not change with the decrease in the bias light intensity from low initial value to 50 % of it, the spectral response can be measured accurately under this low intensity bias light.

(3) The light-induced degradation of spectral response during the measurement is negligible if the bias light intensity of $5 \sim 10$ mW/cm^2 is used.

3-3. Measurement of Spectral Photo-response for Each Component Cell in a-Si Stacked Solar Cells

Next, measuring method of the spectral response for each component cell in a-Si stacked solar cells was investigated to establish a measuring method of individual I-V characteristics of component cells in a-Si stacked solar cells. [7,8] A method of measuring spectral response for each component cell in a stacked cell with blue and red bias light has been proposed. [16] However, spectral response for a-Si stacked cell under various measuring conditions has not been well-established.

3-3-1. Experimental

Stainless steel (S.S.)/pi(a-Si)npi(a-Si)n/TCO and S.S./ni(a-SiGe)pni(a-Si)p/TCO tandem cells (two-stacked cells) were used for measurements. The experimental apparatus is same as mentioned in section 3-2, which is shown in Fig. 3-2-1.

Bias light was irradiated through various optical filters, whose transmission spectra are shown in Fig. 3-3-1. Red bias light was obtained by using 833 and IRA-05 filters and blue bias light was obtained by using 829 and IRA-5 filters. The photo-current with chopped probe light was measured by using a lock-in amplifier. The probe light chopping frequency was changed from 6 to 170 Hz.

The detailed experimental conditions for measuring the spectral response are summarized in Table 3-3-1.

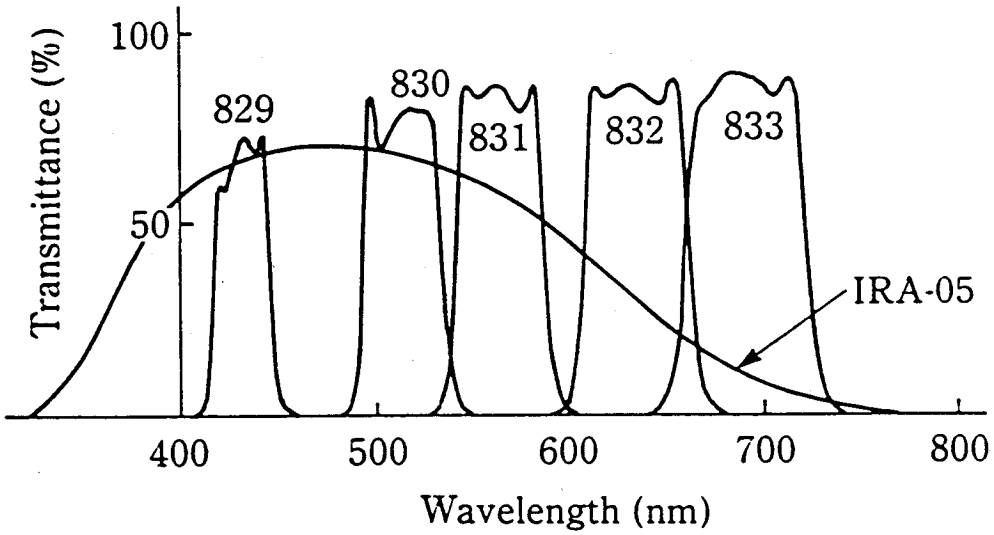

Fig. 3-3-1. Transmission spectra of various optical filters.

Table 3-3-1. Experimental conditions for measuring spectral response for each component cell in a stacked cell

Bias light	Chopping frequency of probe light	Bias voltage
Variable wavelength	8 6 Hz 6 Hz	0 V
Red and blue	8 6 Hz 6 Hz	0 V
None	8 6 Hz 6 Hz	0 V
Variable intensity red and blue	8 6 Hz 6 Hz	0 V
Red and blue	8 6 Hz	Variable

3-3-2. Measuring principle of spectral photo-response for each component cell in a stacked cell.

Figure 3-3-2 shows the measuring principle of the spectral response for each component cell of a tandem cell. Since a tandem cell is composed of two single cells connected in series, the photo-current of the tandem solar cell is basically limited by a component cell with a lower current level. As shown in Fig. 3-3-2 (a), under long wavelength bias light, the bottom cell has a higher photo-current than the top cell and the photo-current of the tandem cell is limited by the top cell. Therefore, in this case, the top cell spectral response can be measured. The bottom cell spectral response can be obtained under short wavelength bias light as shown in Fig. 3-3-2 (b).

Without bias light, as shown in Fig. 3-3-2 (d), under a short wavelength probe light the top cell has a higher photo-current than the bottom cell and the bottom cell spectral response can be measured, while the top cell spectral response can be measured under a long wavelength probe light without bias light.

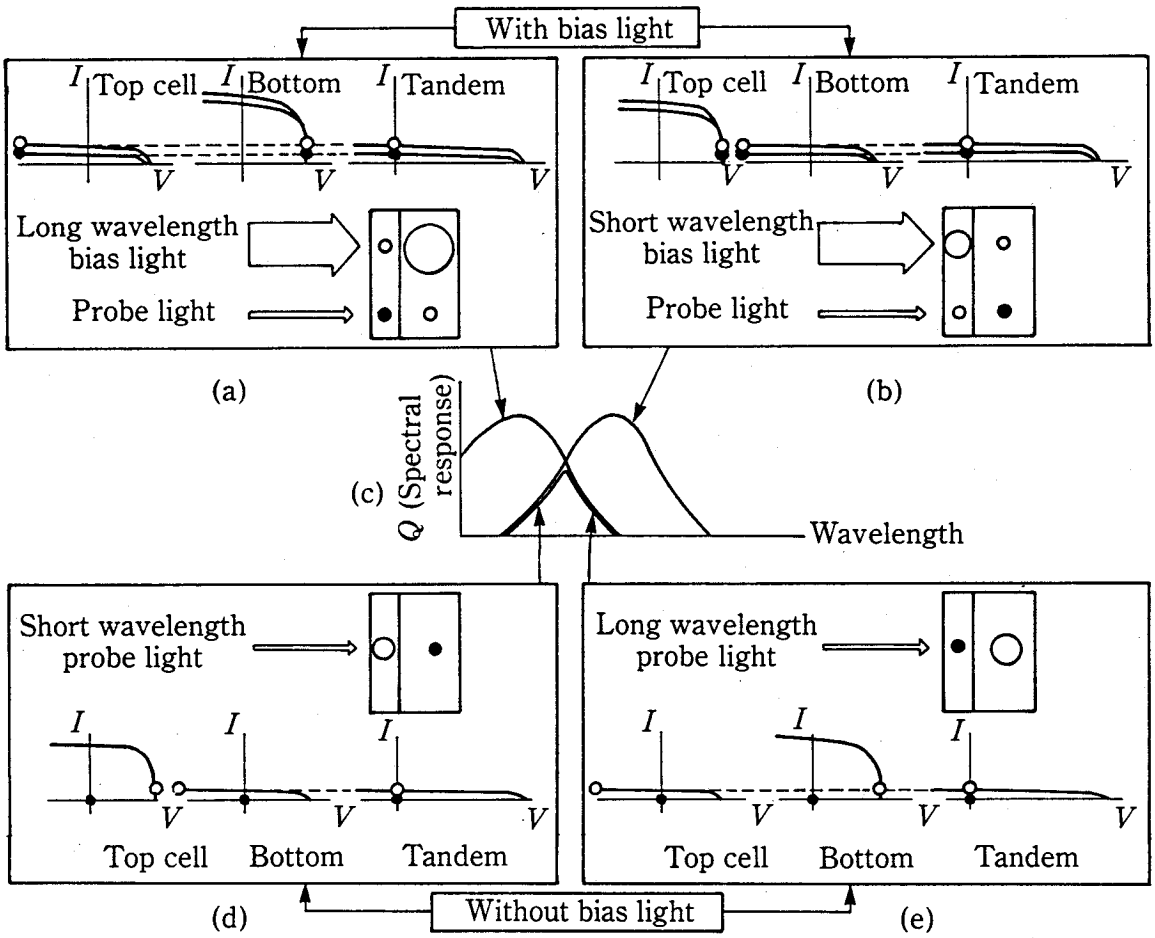

Fig. 3-3-2. Measuring principle of spectral response for each component cell in a stacked cell.

3-3-3. Dependence of spectral photo-response on probe light and bias light

In the external short circuit condition, spectral response dependence for each component cell in a stacked cell under probe light and bias light was investigated, in order to make clear the conditions of measuring exact spectral response. S.S./pi(a-Si)npi(a-Si)n/TCO tandem cells were used for measurements.

The measuring of exact spectral response depends on the probe light intensity and the fill factor of the component cell with higher photo-current level. However, the probe light intensity is about 10 ~ 25 μ W/cm^2, which is an ordinary value. Another experiment confirmed that each component cell in this stacked cell has an ordinary value of fill factor.

The spectral response dependence on bias light wavelength was studied. The same spectral responses for top cells were observed under various red bias lights, which were obtained with IRA-05 filter and with 830, 831, 832, or 833 filter. It was confirmed that spectral responses do not depend on the bias light wavelength when bias light induces a large difference between the photo-currents of the two component cells.

Next, the spectral response dependence on the probe light chopping frequency with and without bias light was investigated, as shown in Fig. 3-3-3. If the bias light intensity is high enough, the spectral response does not depend on the probe light chopping frequency, whether it is 86 Hz or 6 Hz. However, without bias light, the spectral response does depend on the probe light chopping frequency. Under high frequency chopped probe light, enhanced spectral response at long wavelength is observed. It is suggested that this enhancement is caused by the transient photo-current characteristics of deep traps. However, under low frequency chopped probe light, exact spectral response is observed according to the measuring principle.

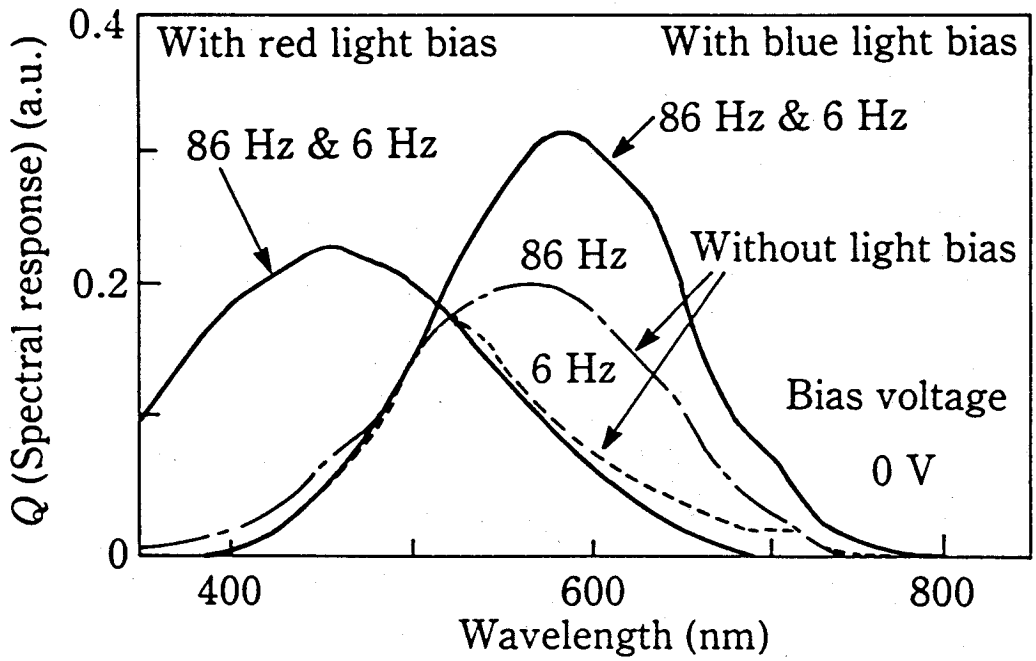

Fig. 3-3-3. Spectral response dependence for each component cell in a stacked cell on probe light chopping frequency with and without bias light.

Spectral response dependence on the bias light intensity was measured and is shown in Fig. 3-3-4 with 6 Hz and 86 Hz chopped probe light. In the case of 6 Hz, spectral response at short wavelength begins to decrease when red bias intensity reaches 2 % of its initial value ($\sim$5 mW/cm^2) and is consistent with that of the bottom cell without bias light. Similarly, spectral response at long wavelength begins to decrease when blue bias intensity reaches 2 % of its initial value ($\sim$3 mW/cm^2). In the case of 86 Hz, spectral response at short wavelength begins to decrease and that at long wavelength begins to increase when red bias light intensity reaches 10 % of initial value ($\sim$ 5 mW/cm^2). In other words, in the case of low-frequency chopped probe light, the minimum limit of the bias light intensity at which spectral response is exact can be expanded.

The above experiments showed that if the bias light intensity is high enough (higher than about 0.5 mW/cm^2 in these experiments), spectral response for each component cell in stacked cells at the external short circuit condition can be measured exactly in a wide range of bias light wavelengths and a probe light chopping frequency.

3-3-4. Dependence of spectral photo-response on bias voltage

The spectral responses of single and stacked a-Si solar cells depend on the bias voltage, and those behaviors are different from those of crystal solar cells. The spectral response dependence on bias voltage is useful to characterize a-Si solar cells. Therefore, the spectral response dependence for each component cell in a stacked a-Si cell on external bias voltage was investigated, using an S.S./ni(a-SiGe)pni(a-Si)p/TCO tandem cell.

When the stacked cell is in an external short circuit condition, the component cell which has a higher photo-current is almost in an open-circuit condition, and this voltage is applied to the other component cell, as shown in

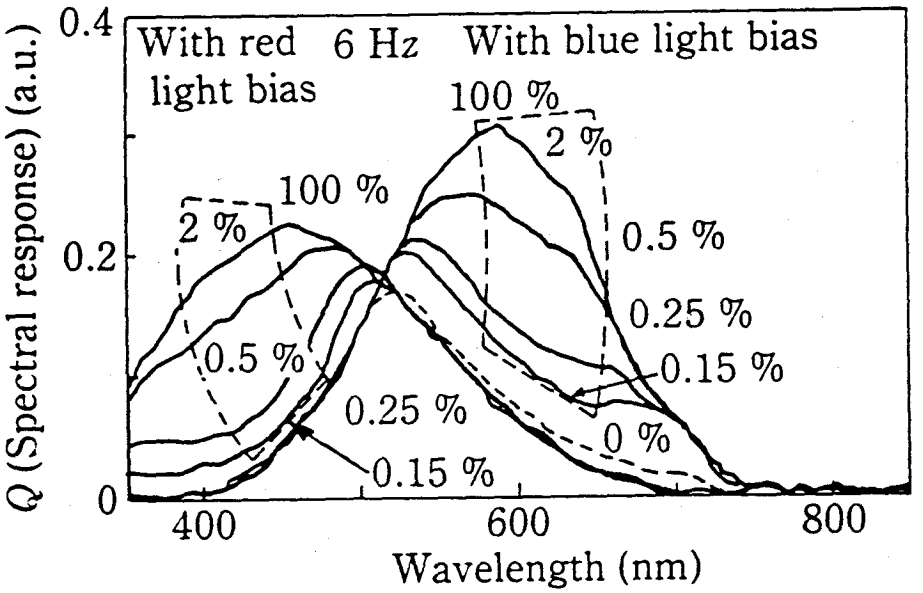

(a) 6 Hz chopped probe light

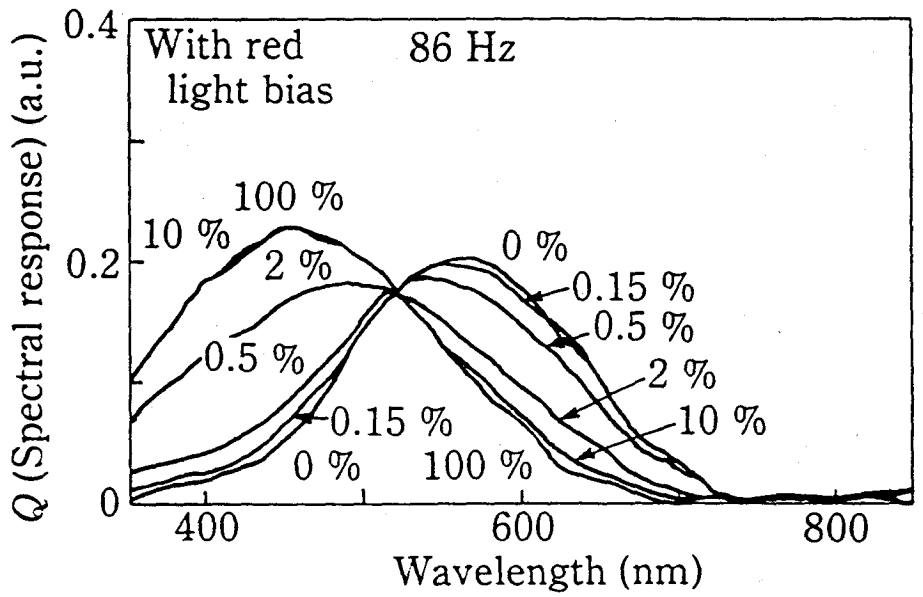

(b) 86 Hz chopped probe light

Fig. 3-3-4. Spectral response dependence for each component cell in a stacked cell on bias light intensity with 6 Hz (a) and 86 Hz (b) chopped probe light.

Figs. 3-3-2 (a) and (b). When external bias voltage is applied to the stacked cell, both the external bias voltage and the reversed open-circuit voltage are applied to the component cell with the lower photo-current level. To determine the internal bias voltage of each component cell, the open-circuit voltages of a stacked cell and another single cell which has the same structure as the front cell were measured under the same blue bias light. The reversed open-circuit voltages were estimated from these measured data. It was confirmed that these open-circuit voltages do not change in spite of the probe light wavelength, because the bias light intensity is high enough.

Spectral response dependence on external bias voltage (0 ~ 1.16 V) is shown in Fig. 3-3-5. The biased voltages of each component cell are - 0.56 ~ 0.60 V for top cells and - 0.76 ~ 0.40 V for bottom cells. In the case of nearly maximum output voltage (1.16 V), enhanced spectral response at long wavelength for the top cell and enhanced spectral response at short wavelength for the bottom cell are observed. As examples, schematic I - V curves under red bias light and red probe light are shown in Fig. 3-3-6, in order to discuss the cause of this enhanced spectral response. When the near-maximum output voltage is applied, the measured value at long wavelength for the top cell becomes larger than the exact value, because the internal bias voltage of each component cell is changed by the probe light. For this reason, spectral response at short wavelength for the top cell becomes smaller. The limit of external bias voltage in which spectral response is exact can be slightly expanded using higher intensity bias light and lower intensity probe light. However, this effect cannot be avoided by choosing a suitable measuring condition for the spectral response.

As a result, spectral response for each component cell in a stacked cell with external bias voltage can be measured exactly below the external bias voltage at which the enhanced spectral response is first observed.

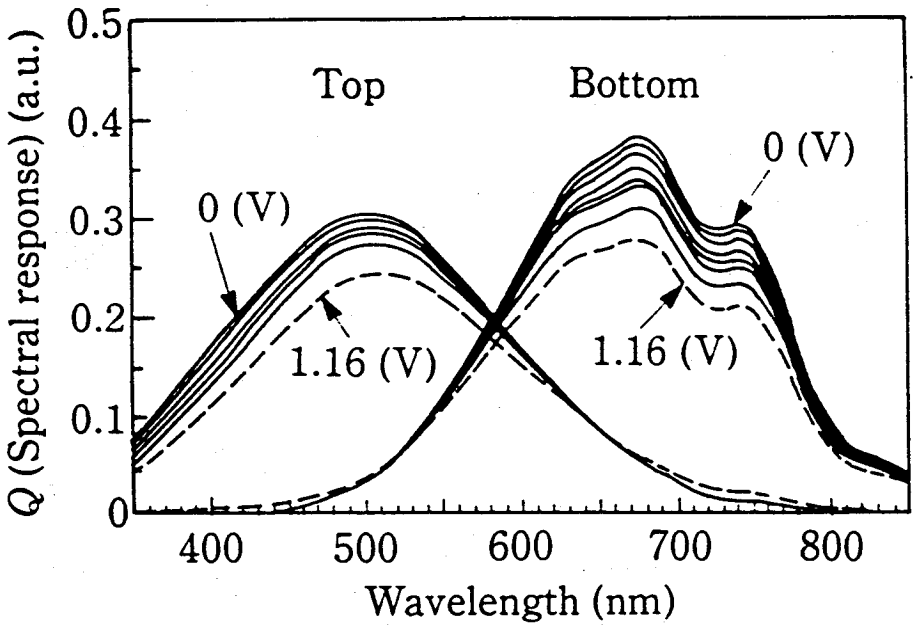

Fig. 3-3-5. Spectral response dependence for each component cell in a stacked cell on external bias voltage.

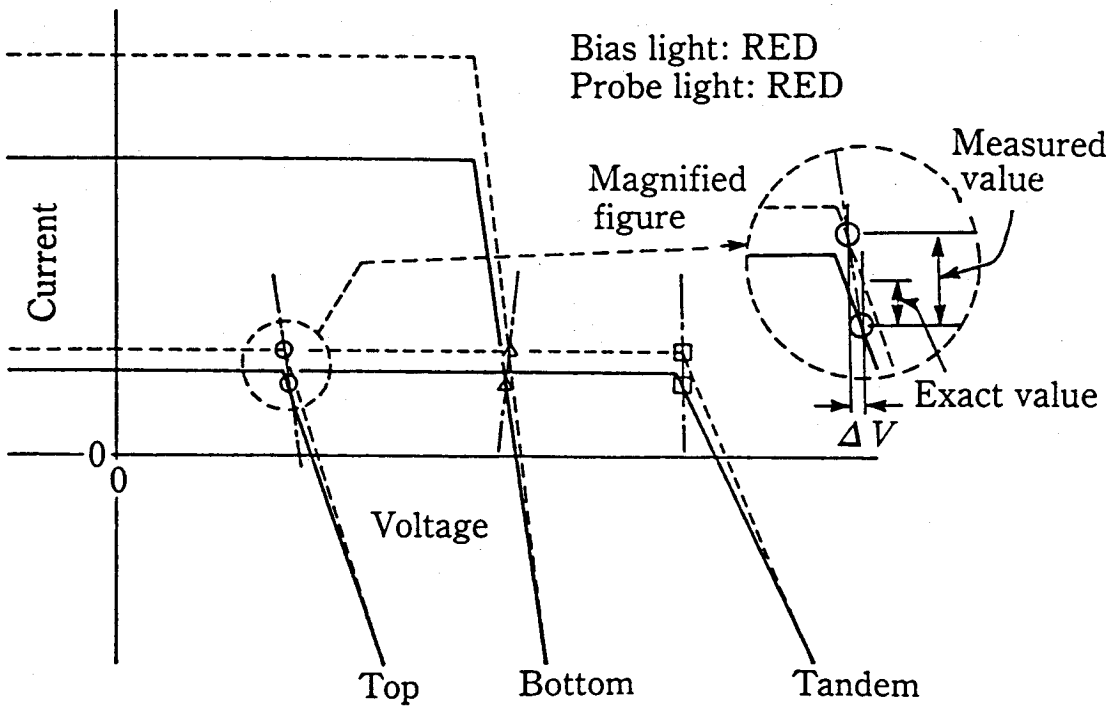

Fig. 3-3-6. Explanatory diagram of enhanced spectral response by external bias voltage for top cell in a stacked cell.

3-3-5. Summary

The spectral photo-response dependence for each component cell in a stacked a-Si alloy solar cell on various measuring conditions was investigated. The results from this investigation are the following:

(1) Under very low intensity or no bias light and high frequency chopped probe light, enhanced spectral response at long wavelength is observed, and it is suggested that this enhancement is caused by transient photo-current characteristics due to deep traps.

(2) If the intensity of bias light is high enough (higher than about 0.5 mW/cm^2 in this series of experiments), spectral response for component cells in stacked cells under external short circuit conditions can be measured exactly in a wide range of bias light wavelengths and probe light chopping frequencies.

(3) Under bias voltage, which is around the maximum output voltage of a stacked cell, enhanced spectral response at long wavelength for the top cell and enhanced spectral response at short wavelength for the bottom cell are observed, because the internal bias voltage of each component cell is changed by probe light. This effect cannot be avoided by choosing a suitable measuring condition. Therefore, spectral responses for component cells in a stacked cell with external bias voltage can be measured exactly below the external bias voltage at which enhanced spectral response is first observed.

3-4. Characterization of Component Cells in a-Si Alloy Stacked Solar Cell

3-4-1. Measuring method of individual current - voltage characteristics of component cells

To obtain stacked solar cells with high stability, it is necessary to know individual I-V characteristics of component cells after light exposure and to design the optimum i-layer thicknesses of component cells taking account of the current balance after light exposure. On the bases of the methods for measuring the spectral response as mentioned above, a new method for measuring individual full I-V characteristics of component cells in the stacked cells was investigated. [2)]

The spectral response for each component cell in a-Si stacked solar cell was measured by the method that is mentioned in section 3-3. By integration of the spectral responses multiplied by solar spectrum, output currents were calculated. The applied voltage for each component cell was evaluated by subtracting the open circuit voltages of two other component cells from applied voltage to the stacked cell. The open circuit voltages of two other component cells were estimated from the open circuit voltages of single cells and tandem cells measured under the similar bias light which was used for measuring the spectral response. These output currents against the applied voltages for each component cell are plotted in Fig. 3-4-1 (a) using marks. However, full I-V curve of each component cell can not be obtained only from such spectral response measurement, because the spectral response for each component cell can be measured exactly below around the maximum output voltage, as mentioned at section 3-3. Therefore, the full I-V curve of each component cell was extrapolated from the experimental data by fitting theoretical I-V characteristics to the experimental data of output currents, as shown in Fig. 3-4-1 (a). The theoretical I-V characteristics were obtained by using Crandall's model. [17)] The I-V curve in the stacked cell obtained by

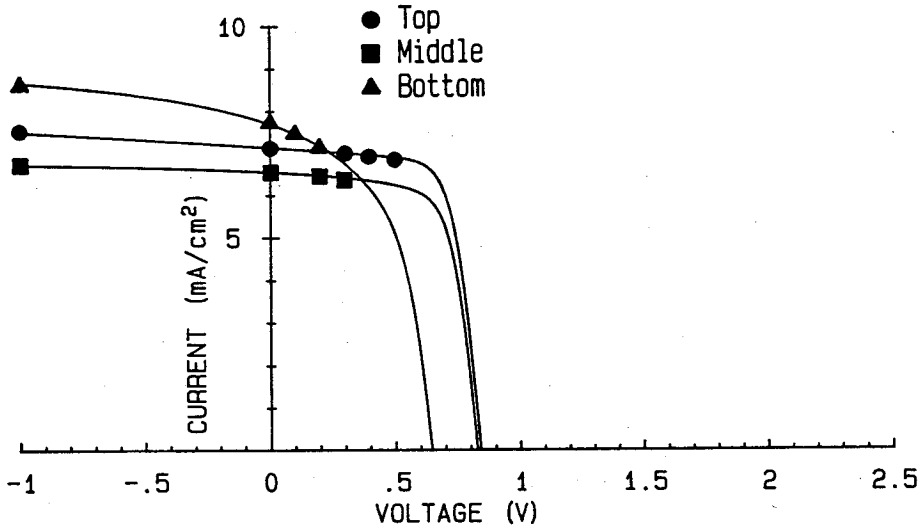

(a) Individual I-V curves of each component cell

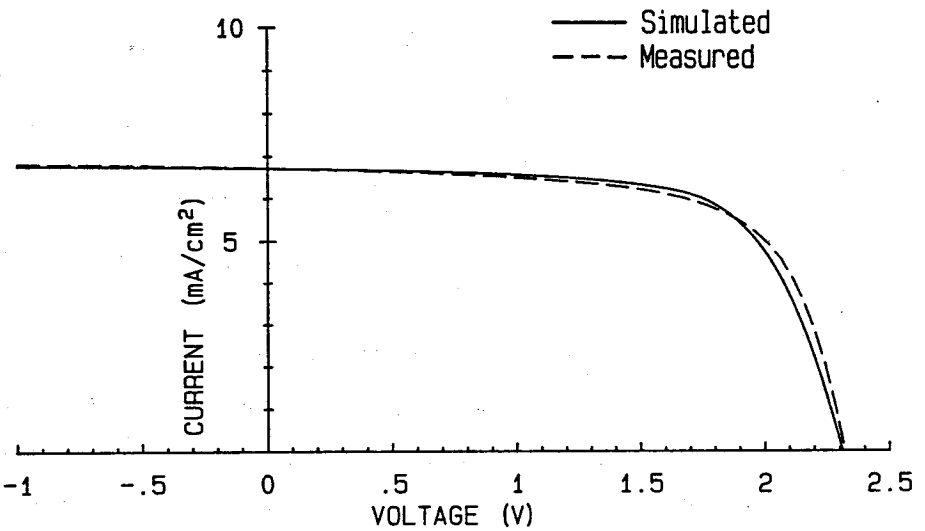

(b) I-V curves of a stacked cell

Fig. 3-4-1. Individual I-V curves of each component cell obtained from spectral responses (a) (experimental output current ●: top cell, ■: middle cell, ▲: bottom cell, solid lines: fitted curves) and I-V curves of a stacked cell (b). (solid line: synthesized, broken line: measured)

synthesizing these curves is in good agreement to the I-V curve measured under simulated AM 1 solar light even at a higher bias voltage range over the maximum output point, as shown in Fig. 3-4-1 (b). It shows that the I-V characteristic in each component cell can be precisely estimated in a wide range of voltage by using this new method.

3-4-2. Light-induced degradation of component cells in a-Si alloy stacked solar cell

By using the new method that is mentioned above, the light-induced degradation of component cells in stacked cells was analyzed. Figure 3-4-2 (a) shows I-V curves of the component cells in a a-Si/a-Si/a-SiGe stacked cell with an initial conversion efficiency of 10.3%. This cell was exposed to the 1 sun light during 550 hours. This exposure condition is equivalent to 1 year field test. [13-15] The I-V characteristics of the stacked cell after light exposure are shown in Fig. 3-4-2 (b). The output currents at the maximum output power point (Imax) of component cells are considered as the index of current balance among component cells. The Imax and their ratio to the initial values of this cell are shown in Table 3-4-1. Each component cell has almost the same Imax values in the initial state, whereas the bottom a-SiGe cell has the smallest Imax value after light exposure and has the largest degradation among the three component cells in this stacked cell. Thus the component cell limiting the output current of the stacked cell and the component cell having the largest degradation can be analyzed using the individual I-V characteristics of each component cell.

These results show that the new method for measuring the I-V characteristic of each component cell is very useful to analyze the light-induced degradation in stacked cells and to design the stacked cells with high stability.

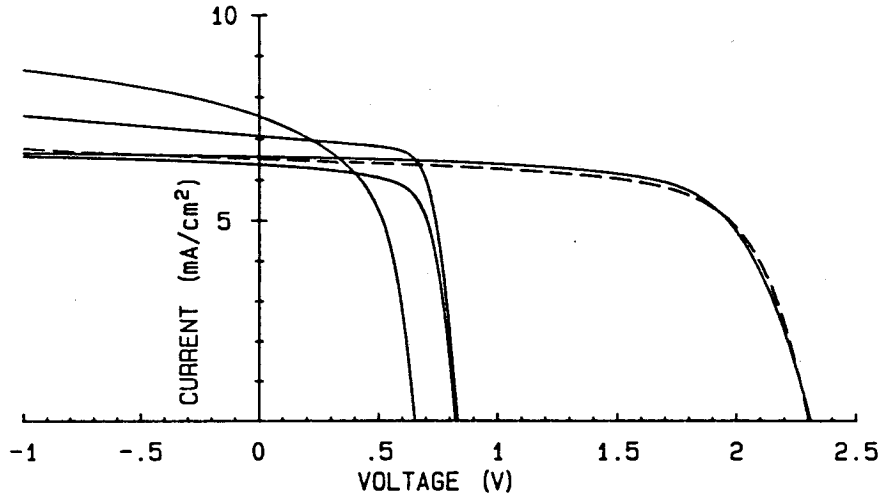

(a) Initial I-V curves

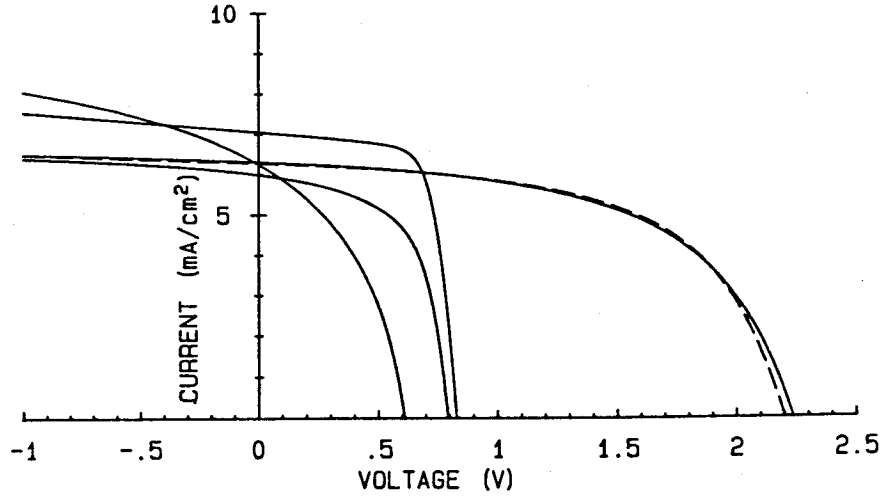

(b) I-V curves after 550 hours' exposure to 1 sun light

Fig. 3-4-2. Light-induced change in I-V curves of component cells and a stacked cell. (solid line: obtained from spectral responses, broken line: measured)

Table 3-4-1. Light-induced change in output currents at maximum output power point (Imax) of the same cell as shown in Fig. 3-4-2.

	Top cell	Middle cell	Bottom cell
(a) Initial Imax (mA/cm^2)	6．4	5．5	5．5
(b) After exposure (mA/cm^2)	6．3	4．6	3．9
Ratio (b／a)	0．98	0．84	0．71

3-5 Summary

The method for measuring individual I-V characteristics of component cells in a-Si alloy stacked solar cells was investigated to obtain stacked solar cells with high stability. The results from these investigations are the following:

(1) At first, the methods for measuring the spectral photo-response of a-Si single-junction solar cells and each component cell in a-Si alloy stacked solar cell have been well-established, since the cause of the enhanced spectral response and the measuring condition to obtain the accurate spectral response have been clarified.

(2) On the bases of the methods as mentioned above, a new method for measuring individual full I-V characteristics of component cells in stacked cell has been proposed, by fitting theoretical I-V characteristic to experimental data of output currents that are calculated from spectral response.

(3) Using this new method, the light-induced degradation of each component cell in a-Si alloy stacked solar cells has been demonstrated, and it was shown that the new method is very useful to analyze the light-induced degradation in stacked cells and to design the stacked cells with high stability.

REFERENCES

1) K. Nomoto, Y. Takeda, S. Moriuchi, H. Sannomiya, T. Okuno, A. Yokota, M. Kaneiwa, M. Itoh, Y. Yamamoto, Y. Nakata and T. Inoguchi: Tech. Digest of 4th Int. Photovol. Sci. Engi. Conf., Sydney (1989) 85.

2) S. Moriuchi, Y. Inoue, H. Sannomiya, A. Yokota, M. Itoh, Y. Nakata and H. Itoh: Proc. 21st IEEE Photovol. Spec. Conf., Florida (1990) 1449.

3) Y. Nakata, H. Sannomiya, S. Moriuchi, A. Yokota, Y. Inoue, M. Itoh and H. Itoh: Mat. Res. Soc. Symp. Proc., Vol. 192 (1990) 15.

4) H. Sannomiya, S. Moriuchi, Y. Inoue, K. Nomoto, A. Yokota, M. Itoh, Y. Nakata and T. Tsuji: Tech. Digest of 5th Int. Photovol. Sci. Engi. Conf., Kyoto (1990) 387.

5) Y. Nakata, H. Sannomiya, S. Moriuchi, Y. Inoue, K. Nomoto, A. Yokota, M. Itoh and T. Tsuji: OPTOELECTRONICS - Devices and Technologies, Vol. 5, No. 2, (1990) 209.

6) Y. Nakata, Y. Inoue, H. Sannomiya, K. Nomoto, A. Yokota, M. Itoh and T. Tsuji: OPTOELECTRONICS - Devices and Technologies, Vol. 6, No. 1, (1991) 141.

7) Y. Nakata and T. Inoguchi: OPTOELECTRONICS - Devices and Technologies, Vol. 4, No. 1, (1989) 75.

8) M. Kaneiwa, K. Nomoto, M. Itoh, Y. Yamamoto, Y. Nakata and T. Inoguchi: Tech. Digest of 4th Int. Photovol. Sci. Engi. Conf., Sydney (1989) 673.

9) R. Shimokawa, M. Nishiura, M. Horiguchi, and Y. Hamakawa: Solar Cells, 19 (1987) 149.

10) C.R. Wronski, B. Abeles G. D. Cody, D. L. Morel, and T. Tiedje: Proc. 14th IEEE Photovol. Spec. Conf., San Diego (1980) 1057.

11) D. Staebler and C. Wronski: Appl. Phys. Lett., 31 (1977) 292; J. Appl. Phys., 51 (1980) 3262.

12) T. Kobe, Y. Nakata, T. Machida, Y. Yamamoto and T. Tsuji: Proc. 18th IEEE Photovol. Spec. Conf., Las Vegas (1985) 1594.

13) A. Yokota, H. Sannomiya, S. Moriuchi, Y. Inoue, M. Itoh, Y. Nakata and T. Tsuji: Tech. Digest of 5th Int. Photovol. Sci. Engi. Conf., Kyoto (1990) 637.

14) Y. Nakata, A. Yokota, H. Sannomiya, S. Moriuchi, Y. Inoue, K. Nomoto, M. Itoh and T. Tsuji: Mat. Res. Soc. Symp. Proc., Vol. 219 (1991) 433.

15) Y. Nakata, A. Yokota, H. Sannomiya, S. Moriuchi, Y. Inoue, K. Nomoto, M. Itoh and T. Tsuji: Jpn. J. Appl. Phys., Vol. 31, No. 2A, Part 1(1992) (to be published)

16) J. Burdick and T. Glatfelter: Solar Cells, 18 (1986) 301.

17) R. S. Crandall: RCA Rev., Vol. 42, (1981) 441.

IV. ANALYSIS OF LIGHT-INDUCED DEGRADATION IN a-Si ALLOY SOLAR CELLS

4-1. Introduction

To increase practical power uses of amorphous silicon (a-Si) solar cells, an important key issue is the improvement of the stability as well as of the initial conversion efficiency. To improve the stability of a-Si solar cells, a stacked cell structure is one of the most useful candidates.[1-7] Moreover, if solar cells with different optical bandgap materials, for example, amorphous silicon carbon (a-SiC), amorphous silicon (a-Si) and amorphous silicon germanium (a-SiGe), are stacked in the order of decreasing optical bandgap from the light incident side, the cell structure is expected to obtain high efficiency. [5] To improve the stability of the stacked solar cell, it is necessary to understand the light-induced degradation characteristics of the a-SiC,[1] a-Si, and a-SiGe component cells, because the degradation of the stacked solar cells is determined entirely in terms of the degradation of the component cells. [8,9]

The light-induced degradation in a-Si solar cells is caused by the Staebler-Wronski (S-W) effect [10] in the photovoltaic active layer of the cells. Since its discovery in 1977, the light-induced changes in a-Si:H films have been studied extensively to clarify the mechanism. It is confirmed that the S-W effect is attributed to the increase in defect density. Namely, the increase in the defect density causes a reduction in the carrier lifetimes and leads to the degradation in the cell characteristics. There are a number of defect creation models, in which models it is generally accepted that defects are created by the recombination of photo-generated carriers. [11-13] In a-Si:H films, the rate of the recombination that

creates the defects is determined only by the light intensity. In a-Si solar cells, however, the recombination rate is determined by the bias voltage in addition to the light intensity. [14-16] Namely, both the light intensity and the bias voltage determine the increase in the defect density and the degradation characteristics of the solar cells. Therefore, to understand the degradation characteristics quantitatively, it is necessary to clarify the dependence of the light-induced degradation characteristics of the solar cells on the light intensity and the bias voltage.

On the other hand, it is a time-consuming process to investigate the degradation of a-Si alloy solar cells under lengthy outdoor exposure. An accelerated test method by which indoor measurement corresponds to outdoor testing is required. If the relationship between the light-induced degradation characteristics and the exposure conditions is clarified quantitatively, it becomes possible that the degradation under lengthy outdoor exposure can be estimated within a short time from the experimental data under simulated light.

This chapter describes the dependence of the light-induced degradation in single-junction solar cells made of a-Si alloys, namely a-SiC, a-Si, and a-SiGe, on the light intensity and the bias voltage.[15,17-19] In section 4-3, the quantitative relationship between the light-induced degradation characteristics and the exposure condition is experimentally clarified. It is attempted to describe the light-induced degradation characteristics of photovoltaic parameters under various light exposure conditions through a single function of certain normalized parameters of exposure condition. In section 4-4, the experimental results of the light-induced degradation in a-Si alloy solar cells are discussed by applying a defect creation model. In section 4-5, using the analytical formula, a new accelerated test method is proposed. By using the method, the light-induced

change of lengthy outdoor exposure can be predicted within a short time from the experimental data under the simulated light. The validity of this accelerated test method is confirmed experimentally.

4-2. Experimental

The single-junction solar cells were prepared by a conventional radio frequency (RF) glow discharge technique. The cell structure was stainless steel substrate / n i p / transparent conductive oxide (TCO) and cell area was 1.0 cm^2. The i-layer thickness, the bandgap of the i-layer, and the solar cell characteristics before light exposure are shown in Table 4-2-1. The solar cell characteristics were measured under 100 mW/cm^2 light with the spectrum of air mass (AM) 1. Changes in current-voltage characteristics during light exposure were investigated for various recombination rates. The recombination rate was controlled by the light intensity and the bias voltage, independently. The exposure light source is a high-intensity solar simulator having the AM 1.5 spectrum and the light intensity is controlled by changing the distance between the light source and the cell. The bias voltage was controlled to keep the recombination rate in the cell constant irrespective of the change in the cell characteristics during the light exposure. The cell temperature was kept at 48 degrees centigrade.

Table 4-2-1. Thickness (d_i) and optical bandgap (E_{gopt}) of i-layer and cell characteristics before light exposure for a-SiC, a-Si, and a-SiGe solar cells. [I_{sc}: Short circuit current V_{oc}: Open circuit voltage; F.F.: Fill factor η : Conversion efficiency]

	di (nm)	E_{gopt} (eV)	I_{sc} (mA/cm^2)	V_{oc} (V)	F.F.	η (%)
a-SiC	100	1.89	8.2	0.88	0.63	4.5
a-Si	300	1.75	16.8	0.84	0.60	8.4
a-SiGe	300	1.56	19.8	0.67	0.52	6.9

4-3. Dependence of Light-induced Degradation in a-Si Alloy Solar Cells on Exposure Condition

4-3-1. Light intensity dependence

First, the dependence of the light-induced degradation characteristics in a-SiC, a-Si, and a-SiGe single-junction solar cells on the light intensity was investigated. The cells were exposed to light of 0.3-, 1-, 3-, and 6-suns intensities under the open circuit condition. The changes in the conversion efficiencies (η) that are normalized by initial ones (η_0) are shown in Fig. 4-3-1 (a) for a-SiC, a-Si, and a-SiGe cells as a function of the exposure time. As is well known, the degradation is accelerated according to the light intensity. But when all the experimental data points are plotted as a function of $N_c^{\gamma} t$, where N_c is the ratio of the exposure light intensity to 1 sun and γ is the characteristic constant, they are approximately on a single curve, as shown in Fig. 4-3-1 (b). In this experiment, γ = 2.0 for the a-Si and a-SiC cells and γ = 1.2 for the a-SiGe cell. This result indicates that the light-induced degradation characteristics of the conversion efficiency of a-Si alloy single-junction solar cells under light of various intensities and the open circuit condition can be expressed by a single function as follows:

$$\eta(t) / \eta_0 = f_1(N_c^{\gamma} t) , \qquad (4\text{-}3\text{-}1)$$

where function f_1 differs according to the a-Si alloy materials of the i-layer.

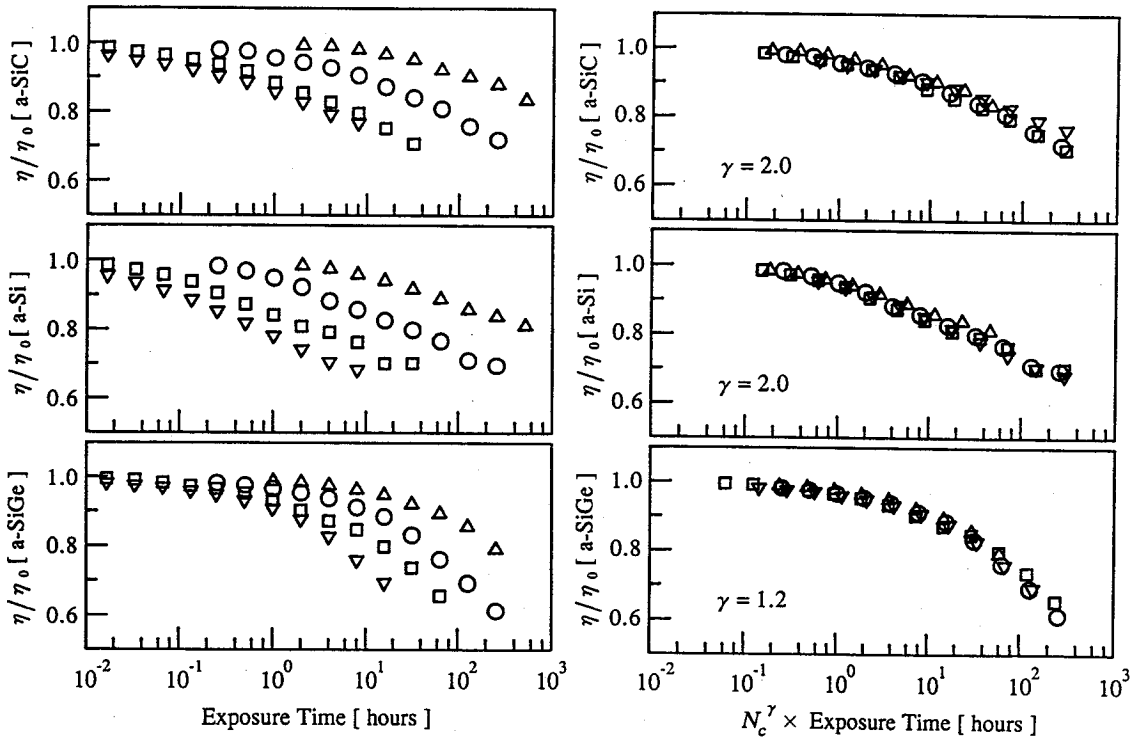

(a) Exposure time (b) $N_c^{\gamma} t$

Fig. 4-3-1. Light-induced degradation characteristics of normalized conversion efficiencies (η / η_0) for a-SiC, a-Si, and a-SiGe solar cells as a function of exposure time t (a), and $N_c^{\gamma} t$ (b) for various light intensities (△: 0.3 suns, ○: 1 sun, □: 3 suns, ▽: 6 suns). N_c is defined as the ratio of the exposure light intensity to 1 sun.

4-3-2. Bias voltage dependence

Next, the dependence of the light-induced degradation characteristics in a-SiC, a-Si, and a-SiGe single-junction solar cells on the bias voltage was investigated. The cells were exposed to light of 1-sun and 6-suns intensities under the open circuit and load condition. Under the open circuit condition, all the photo-generated carriers were recombined in the cells. Under the load condition, the bias voltage is controlled so that one-third of the photo-generated carriers are recombined in the cell. Namely, the bias voltage controls the recombination ratio R_r that is defined as the ratio of the recombined carriers to the photo-generated carriers in the cell. The changes in conversion efficiencies (η) that are normalized by initial ones (η_0) are shown in Fig. 4-3-2 (a) as a function of exposure time. As is well known, the degradation is accelerated according to the forward bias voltage, [20,21] but when all the experimental data points are plotted as a function of $R_r^{\beta} t$, where β is a characteristic constant, the data under the light of the same intensity are approximately each on a single curve, as shown in Fig. 4-3-2 (b). The β value is independent of the light intensity, and β = 1.0 for a-Si and a-SiC cells, and β = 0.6 for a-SiGe cell. This result indicates that the light-induced degradation characteristics of the conversion efficiency in the a-Si alloy single-junction solar cell under the various bias voltages and the same intensity light can be expressed by a single function expressed as follows:

$$\eta(t) / \eta_0 = f_2(R_r^{\beta} t) , \qquad (4\text{-}3\text{-}2)$$

where function f_2 differs according to the a-Si alloy materials of the i-layer.

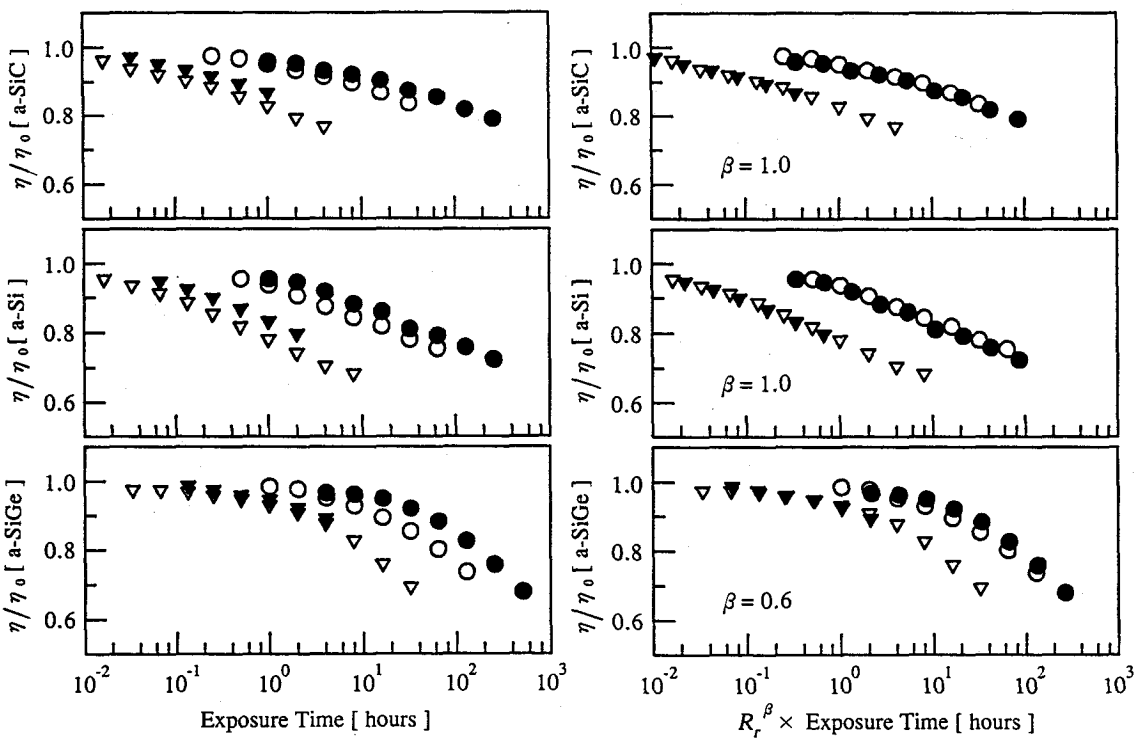

(a) Exposure time (b) $R_r^{\beta} t$

Fig. 4-3-2. Light-induced degradation characteristics of normalized conversion efficiencies (η / η_0) for a-SiC, a-Si, and a-SiGe solar cells as a function of exposure time t (a), and $R_r^{\beta} t$ (b) for various bias voltages. R_r is defined as the ratio of recombined carriers to photo-generated carriers.

● : 1 sun, load condition where one third of the photo-generated carriers are recombined.

▼ : 6 suns, load condition where one third of the photo-generated carriers are recombined,

○ : 1 sun, open circuit condition.

▽ : 6 suns, open circuit condition

4-3-3. Exposure condition dependence

The dependence of the light-induced degradation characteristics of the normalized conversion efficiencies (η / η_0) of a-SiC, a-Si, and a-SiGe cells on the light intensity and the bias voltage has been clarified, respectively. From eqs. (4-3-1) and (4-3-2) and the conclusion that the β value is independent of the light intensity, it is derived that all the experimental data points for various light intensities and various bias voltages are approximately on a single curve, as shown in Fig. 4-3-3, when they are plotted as a function of $N_c^{\gamma} R_r^{\beta} t$ instead of t. This indicates that all the light-induced degradation characteristics under the condition of various light intensities and various bias voltages can be described by the following single function:

$$\eta(t) / \eta_0 = f_m (N_c^{\gamma} R_r^{\beta} t) , \qquad (4\text{-}3\text{-}3)$$

where function f_m differs according to the a-Si alloy materials of the i-layer. This result also means that the light-induced degradation characteristics of the conversion efficiencies of a-Si alloy single-junction solar cells under arbitrary exposure condition can be predicted from a series of light-induced degradation data under certain exposure conditions with transformation by $N_c^{\gamma} R_r^{\beta} t$.

The only light-induced degradation characteristics of the conversion efficiency have been shown, as mentioned above. The other light-induced degradation characteristics of the a-Si solar cell, namely, short circuit current (I_{sc}), open circuit voltage (V_{oc}) and fill factor (F.F.), are shown with conversion efficiency (η) in Fig. 4-3-4 (a) as a function of t, and in Fig. 4-3-4 (b) as a function of $N_c^{\gamma} R_r^{\beta} t$. When all the experimental data points of each cell parameter are plotted as a function of $N_c^{\gamma} R_r^{\beta} t$ instead of t, all the data points

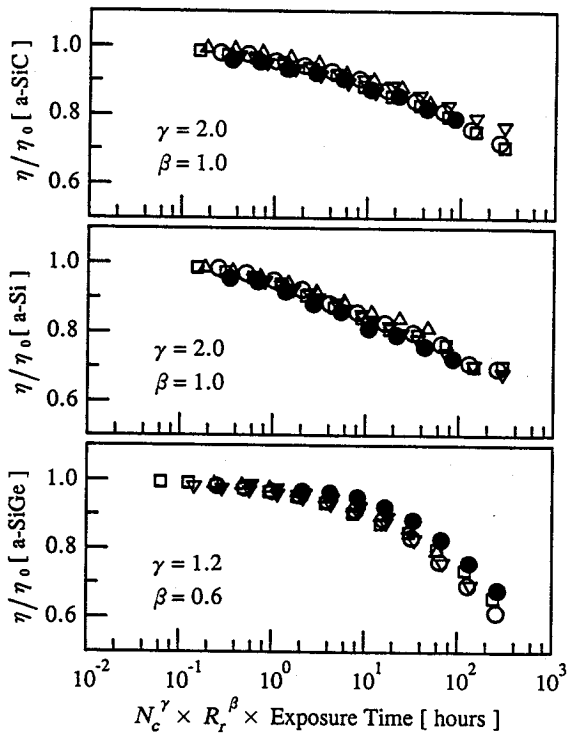

Fig. 4-3-3. Light-induced degradation characteristics of normalized conversion efficiencies (η / η_0) for a-SiC, a-Si, and a-SiGe solar cells as a function of $N_c^{\gamma} R_r^{\beta} t$ for various light intensities and various bias voltages. Symbols are the same as those in Figs. 4-3-1 and 4-3-2.

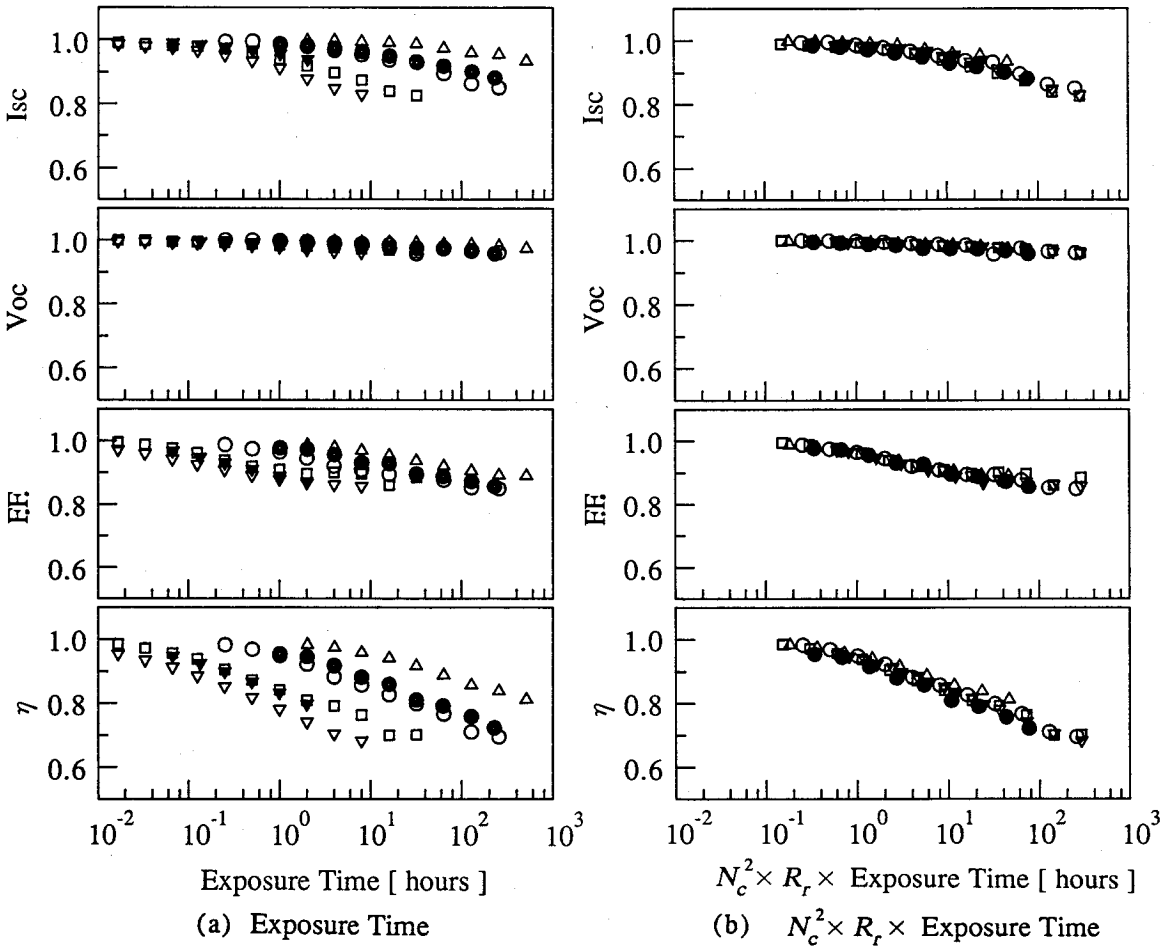

Fig. 4-3-4 Light-induced degradation characteristics of normalized I_{sc}, V_{oc}, FF, and η for a-Si solar cell as a function of exposure time t (a), and $N_c^2 R_r t$ (b) for various light intensities and bias voltages. Symbols are the same as those in Figs. 4-3-1 and 4-3-2.

$\left\{ \begin{array}{ll} I_{sc}: \text{Short circuit current} & V_{oc}: \text{Open circuit voltage} \\ \text{F.F.: Fill factor} & \eta : \text{Conversion efficiency} \end{array} \right\}$

are approximately on a single curve. Namely, the dependence of the light-induced degradation characteristics of I_{sc}, V_{oc}, and F.F. on the light intensity and the bias voltage can be expressed by the single function, in the same manner as that of conversion efficiencies.

Moreover, the light-induced degradation characteristics of mobility · lifetime ($\mu\tau$) products of the i-layers in a-SiC, a-Si and a-SiGe single-junction solar cells under much exposure condition were investigated. The cells were exposed to light of 0.3-, 1-, 3- and 6-suns intensities. The $\mu\tau$ products of the i-layers in the cells were estimated from current-voltage characteristics under uniformly absorbed light using Crandall's model. [16] The initial $\mu\tau$ products of the i-layers in the a-SiC, a-Si and a-SiGe solar cells are 3.2×10^{-10}, 1.6×10^{-8}, and 1.5×10^{-9} cm^2/V, respectively. The light-induced degradation characteristics of the normalized $\mu\tau$ products are shown in Fig. 4-3-5 (a) as a function of t and in Fig. 4-3-5 (b) as a function of $N_c^{\gamma} R_r^{\beta} t$. As shown in Fig. 4-3-5, the light-induced degradation characteristics of $\mu\tau$ products can be expressed by the equation in the same manner as well.

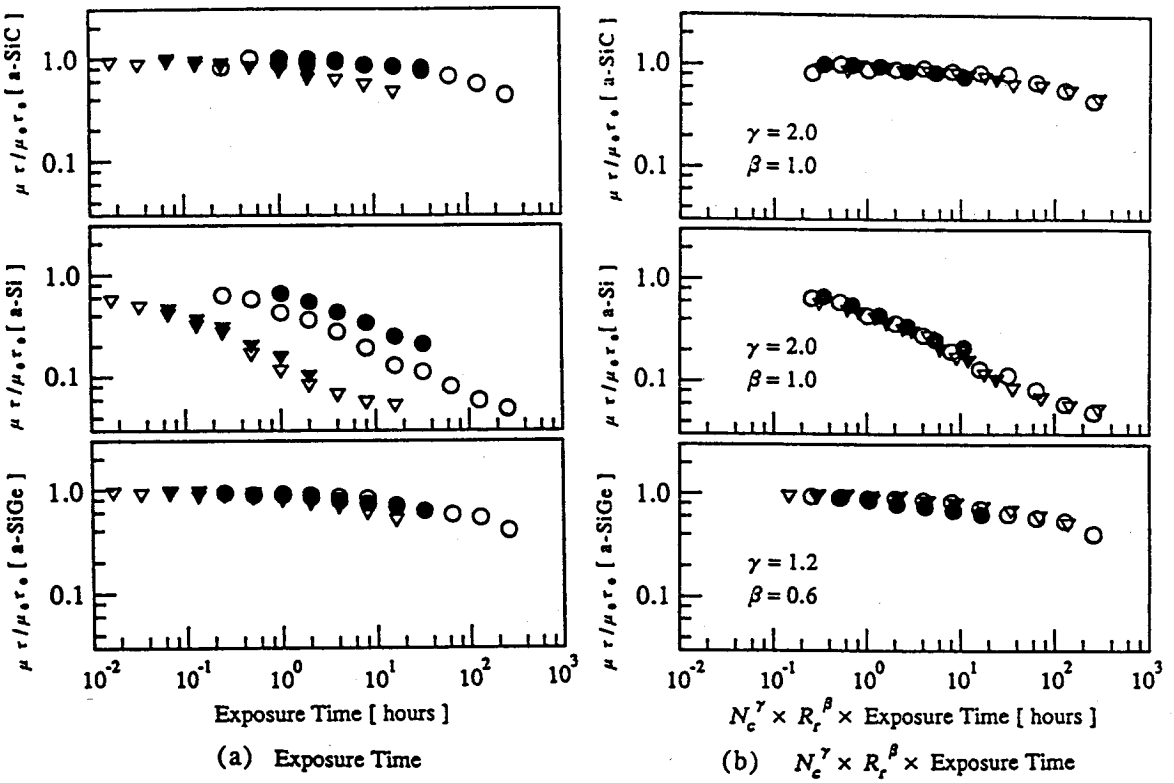

Fig. 4-3-5 Light-induced degradation characteristics of normalized $\mu\tau$ products ($\mu\tau/\mu_0\tau_0$) in a-SiC, a-Si and a-SiGe single-junction solar cells as a function of exposure time t (a), and $N_c^{\gamma} R_r^{\beta} t$ (b) for various light intensities and bias voltages. Symbols are the same as those in Figs. 4-3-1 and 4-3-2.

4-4. Discussions of Light-induced Degradation in a-Si Alloy Solar Cells

In this section, the relation expressed by eq. (4-3-3) is discussed. It is considered that characteristics of the a-Si alloy solar cells are determined by total defect density (Ns) in the i-layer and the light-induced degradation is caused by the increase in the N_s. [14-16] Therefore, it is expected that the light-induced degradation characteristics of the cells can be expressed by a function that does not depend on the exposure condition when it is expressed as a function of $N_s(t)$ instead of t. Namely,

$\eta(t)$: function that depends on the exposure condition,

$\eta(N_s(t))$: function that does not depend on the exposure condition.

Therefore, our experimental results suggest that there is one-to-one correspondence between $N_c^{\gamma} R_r^{\beta} t$ and $N_s(t)$.

There are a number of defect creation models to explain the S-W effect. Stutzmann et al. investigated the changes in dangling bond density under light of various intensities and proposed a defect creation model where nonradiative tail-to-tail recombination of photo-generated carriers creates the defect. [11] According to their model, the increase in N_s is described as follows:

$$dN_s/dt = C_{SW} A_t n p \qquad (4\text{-}4\text{-}1)$$

where A_t is the rate constant for the nonradiative tail-to-tail recombination, C_{SW} the fraction that leads to the defects, n and p the free electrons and holes. In this model, it is assumed that the number of captured electrons and holes by the tail states are proportional to the number of free electrons and holes.

The number of free electrons and holes can be obtained by solving the rate equation in which bi- and monomolecular recombination processes are included. Therefore, the dependence of n and p on light intensity changes according to the dominant recombination process in the i-layer. To determine the dominant recombination process in a-SiC:H, a-Si:H, and a-SiGe:H films, the light intensity dependence of the photo-conductivities (σ_p) was investigated. The results are shown in Fig. 4-4-1. The light intensity dependence of photo-conductivity can be expressed by $\sigma_p \propto N_c^{\alpha}$. It was obtained that α = 0.9 for a-SiC:H and a-Si:H, and α = 0.6 for a-SiGe:H were obtained. This result indicates that a monomolecular recombination process is dominant in a-SiC:H and a-Si:H films, and a bimolecular recombination process is dominant in a-SiGe:H film.

In the solar cells, the recombination rate can be controlled by the bias voltage in addition to the light intensity. Namely, some of the photo-generated carriers are taken out of the cell. In this case, the generation rate of N_s is expressed by

$$dN_s / dt = C_{SW} A_t (n\,p)_{open} R_{1/op} \qquad (4\text{-}4\text{-}2)$$

where $A_t(n\,p)_{open}$ is the nonradiative tail-to-tail recombination rate at open circuit condition and $R_{1/op}$ is defined as the ratio of the np product under the load condition to it under the open circuit condition, $[(np)_{load} / (np)_{open}]$. This $R_{1/op}$ can be obtained only by solving the continuity equations and the Poisson equation numerically. [22-27)]

Under the open circuit condition, however, most of the photo-generated carriers scarcely drift, because the electric fields in almost the entire photovoltaic

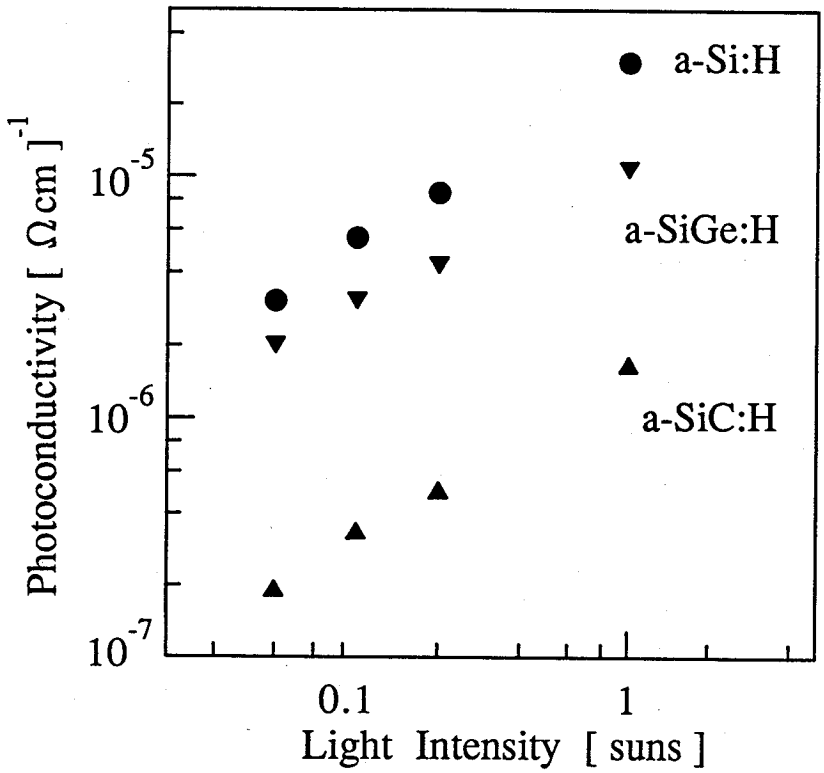

Fig. 4-4-1. Light intensity dependence of photo-conductivities in a-SiC:H, a-Si:H, and a-SiGe:H films.

active layer are weak, except the narrow p/i and i/n interface regions. [24] In this case, therefore, the number of np product in the cell is very close to those in film, and eq. (4-4-2) is approximated by eq. (4-4-1). In the case where the monomolecular recombination process is dominant, N_s can be expressed as

$$N_s(t) = (N_s^3(0)+CN_c^2t)^{1/3}$$
$$= g_1(N_c^2t) , \qquad (4\text{-}4\text{-}3)$$

where C is a suitable constant. Therefore, there is one-to-one correspondence between $N_s(t)$ and N_c^2t, and η $(N_s(t))$ can be expressed by a function of N_c^2t. This corresponds to the experimental results of a-Si and a-SiC cells expressed by eq. (4-3-1). On the other hand, in the case where a bimolecular recombination process is dominant, the N_s can be expressed as

$$N_s(t) = N_s(0) + C' N_c t$$
$$= g_2(N_c t) , \qquad (4\text{-}4\text{-}4)$$

where C' is a suitable constant. In this case, there is one-to-one correspondence between $N_s(t)$ and $N_c t$, and η $(N_s(t))$ can be expressed by a function of $N_c t$. This corresponds approximately to the experimental results of a-SiGe cells.

At load condition, it is suggested from our experimental results that there is one-to-one correspondence between $N_c^{\gamma} R_r^{\beta} t$ and $N_s(t)$ under various light intensities and various bias voltages.

Thus far, the functional shapes of f_m $(N_c^{\gamma} R_r^{\beta} t)$ in Fig. 4-3-3 have not referred. The functional shape depends on the i-layer material, as mentioned sub-section 4-3-3. In addition, it depends on other such factors as i-layer

thickness and cell structure. For example, in the case where the i-layer thickness is different from that in this experiment, the function f_m changes to another function, h_m. But the dependence on light intensity and bias voltage does not change because γ and β values are determined only by the i-layer material, not by other cell parameters. Namely, in the case where cell structural parameters are different from those in this experiment, function $f_m\,(N_c^{\gamma} R_r^{\beta} t)$ only becomes another function, $h_m\,(N_c^{\gamma} R_r^{\beta} t)$.

4-5. Accelerated Test Method of Light-induced Degradation

4-5-1 Proposal of new accelerated test method

To predict the light-induced changes under lengthy outdoor exposure within a short time, the above analytical function obtained under solar simulator light is expanded into the function under natural outdoor sunlight. According to the above discussion, $N_c^{\gamma} R_r^{\beta} t$ corresponds to the total defect density, and the above result can be applied even in a case where exposure condition changes with time. Under the outdoor exposure, the N_c and the R_r change with time. Thus to describe the light-induced degradation in a-Si alloy cells, the photo-degradation time scale is defined as follows:

$$S_d(t) = \int_0^t N_c^{\gamma}(t) R_r^{\beta}(t) \mathrm{dt}\,, \qquad (4\text{-}5\text{-}1)$$

where $N_c\,(t)$ is the ratio of light intensity to 1 sun at time t and $R_r\,(t)$ is the recombination ratio at time t. In the case where $N_c(t)$ and $R_r(t)$ are independent of exposure time, such as under simulated light, the $S_d\,(t)$ becomes $N_c^{\gamma} R_r^{\beta} t$ as shown in eq. (4-3-3).

The exposure time T_a for which the light-induced degradation ratio of the conversion efficiency under simulated light is equivalent to that under the outdoor exposure for one year is given by

$$T_a = \frac{1}{N_c'^{\gamma} R_r'^{\beta}} \int_0^{t_1} N_c^{\gamma}(t) R_r^{\beta}(t) \mathrm{dt}, \tag{4-5-2}$$

where N_c' is the ratio of the simulated light intensity to 1 sun, R_r' the recombination ratio under the simulated light, $N_c(t)$ the ratio of outdoor exposure light intensity to 1 sun at time t, $R_r(t)$ the recombination ratio under outdoor exposure at time t, and $t_1 = 1$ year.

The absolute value of the recombination rate of photo-generated carriers changes drastically according to the light intensity. But the R_r does not change greatly according to the light intensity in the case of an ordinary constant bias voltage condition. Therefore, at the first-order approximation, the R_r can be considered as the constant during the outdoor exposure, and eq. (4-5-2) can be reduced to

$$T_a = \left(\frac{R_r}{R_r'}\right)^{\beta} \frac{1}{N_c'^{\gamma}} \int_0^{t_1} N_c^{\gamma}(t) \mathrm{dt}$$

$$= K_b T_{ac}, \tag{4-5-3}$$

where t_1 = 1 year, K_b is the correction factor by bias voltage defined by $(R_r / R_r')^{\beta}$ and T_{ac} is defined by

$$T_{ac} = \frac{1}{N_c'^{\gamma}} \int_0^{t_1} N_c^{\gamma}(t) \mathrm{dt}. \tag{4-5-4}$$

When the bias voltage under outdoor exposure and that under simulated light are the same, namely K_b = 1, then T_a= T_{ac}. The T_{ac} can be calculated by using insolation data for 1 year. HASP (Heating, Air-Conditioning and Sanitary Engineers Program in JAPAN) data are hourly outdoor standard insolation data and they are widely used in simulations of photovoltaic systems and solar thermal systems in Japan. Figure 4-5-1 shows the T_{ac} calculated from the HASP data in Tokyo as a function of light intensity and γ . From Fig. 4-5-1, the exposure time under the simulated light to evaluate the light-induced degradation ratio under the outdoor exposure for one year can be obtained. For example, the light-induced degradation ratio under outdoor exposure for one year can be predicted by that for only 22 hours under 5 suns simulated light in the case of γ = 2.0. When the bias voltages under outdoor exposure and that under simulated light are not the same, the K_b is calculated and the T_a can be obtained from eq. (4-5-3). When the higher-intensity simulated light is used, the exposure time becomes shorter but the accuracy of the converted data becomes lower.

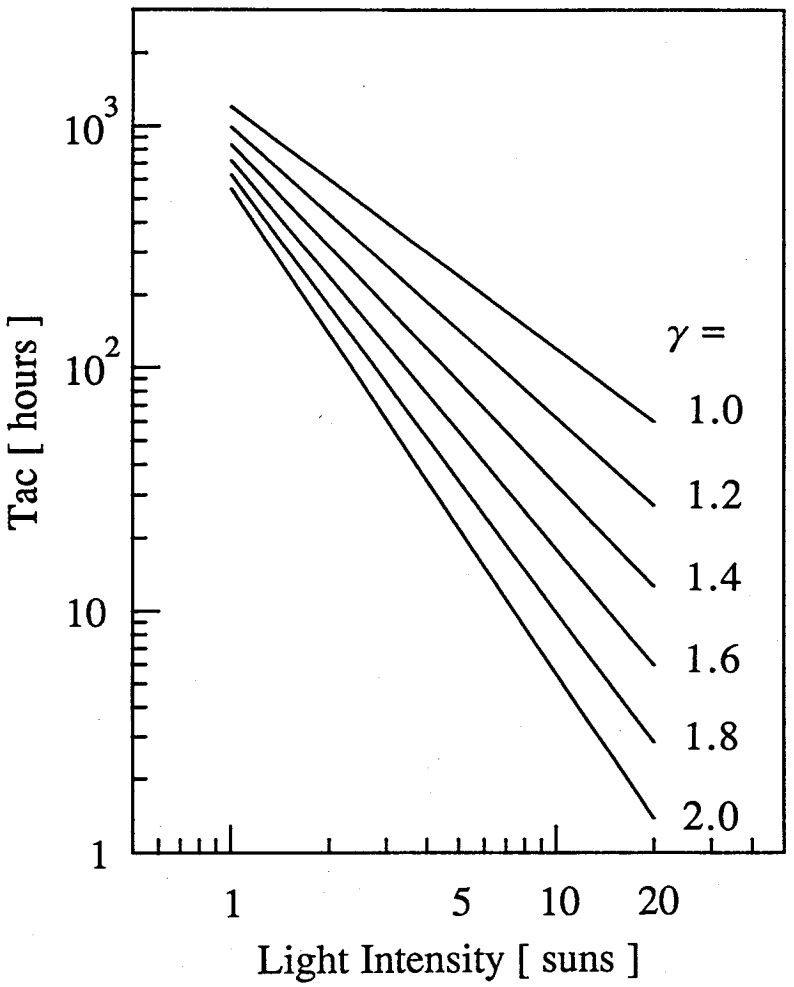

Fig. 4-5-1. Exposure time (T_{ac}) equivalent to one year outdoor test as a function of light intensity and γ.

4-5-2 Experimental confirmation of accelerated test method

To confirm the validity of the new accelerated test method, the light-induced degradation characteristics of normalized conversion efficiency in a-Si solar cells under simulated light and outdoor exposure were compared, and are shown in Fig. 4-5-2. The intensity of the simulated light was 1 sun. The bias voltages were open circuit condition in both cases. The T_{ac} is 550 hours from Fig. 4-5-1 because $\gamma = 2.0$ in the a-Si solar cells. Therefore, the two horizontal axes were taken as 550 hours for the data under the simulated light, corresponding to 365 days for the data under outdoor exposure. As shown in this figure, the light-induced degradation characteristics under the simulated light correspond quite well to those seen under outdoor exposure. Therefore, the validity of the new accelerated test method has been confirmed experimentally.

This accelerated test method is useful for evaluating and designing a-Si alloy solar cells, including stacked cells, with high stability.

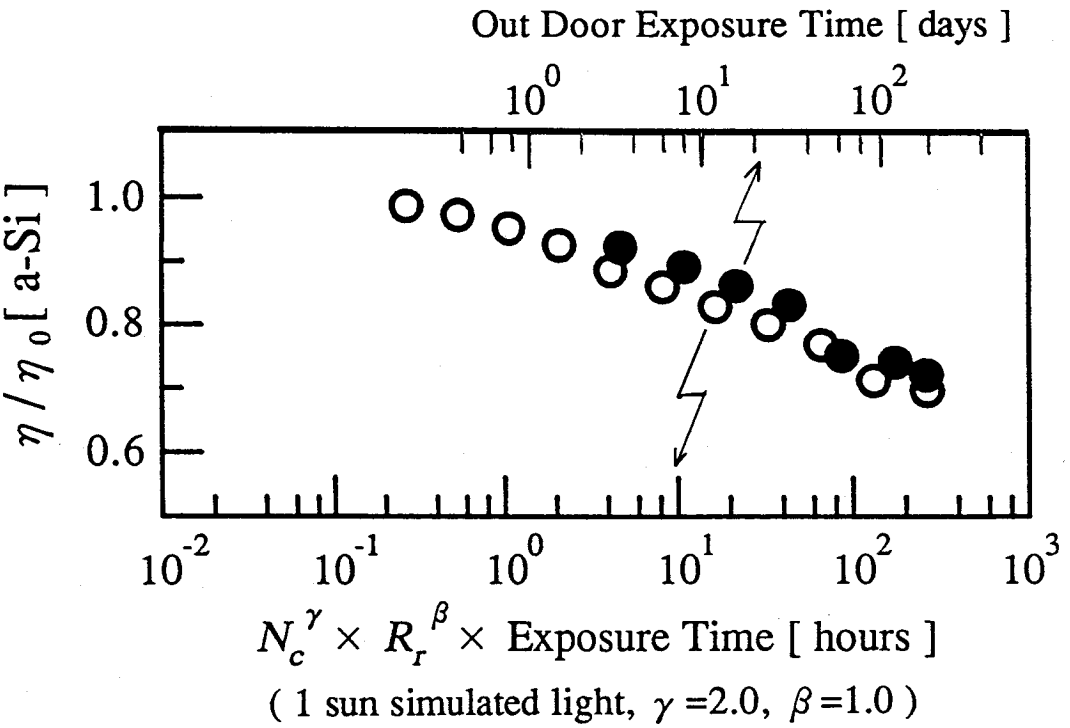

Fig. 4-5-2. Comparison of light-induced degradation characteristics of normalized conversion efficiency (η / η_0) in a-Si solar cells under 1 sun simulated light (○) and under outdoor exposure (●). Bias voltage is maximum output voltages in both cases.

4-6. Summary

The light-induced degradation in current-voltage characteristics of amorphous single-junction solar cells made of silicon alloys, namely a-SiC, a-Si, and a-SiGe, has been studied systematically. The dependence of the light-induced degradation characteristics of the photovoltaic parameters on the light intensity and the bias voltage has been investigated quantitatively. The results of this study can be summarized as follows:

(1) The light-induced degradation characteristics of the conversion efficiency and the other photovoltaic parameters under the condition of the various light intensities and bias voltages can be described by the following function:

$$\eta(t) / \eta_0 = f(N_c^{\gamma} R_r^{\beta} t),$$

where N_c is the ratio of the exposure light intensity to 1 sun, R_r is the ratio of recombined carriers in the cell to photo-generated carriers, and γ and β are characteristic constants. In this experiment, it is determined that γ = 2.0, β = 1.0 for a-SiC and a-Si cells, and γ =1.2, β = 0.6 for a-SiGe cell. The result also indicates that the light-induced degradation characteristics of a-Si alloy solar cells, which contain a-Si alloy component cells in stacked cells, under the condition of arbitrary light intensities and bias voltages can be predicted from a series of light-induced degradation data under certain light intensities and bias voltages.

(2) It was suggested that $N_c^{\gamma} R_r^{\beta} t$ corresponds to the total defect density by applying a defect creation model modified to an active layer of the a-Si alloy solar cells.

(3) Using this analytical formula, a new accelerated test method by solar simulator indoor measurement instead of natural sunlight outdoor testing has been proposed. The validity of the new accelerated test method has been confirmed experimentally.

REFERENCES

1) K. Nomoto, Y. Takeda, S. Moriuchi, H. Sannomiya, T. Okuno, A. Yokota, M. Kaneiwa, M. Itoh, Y. Yamamoto, Y. Nakata and T. Inoguchi: Tech. Digest of 4th Int. Photovol. Sci. Engi. Conf., Sydney (1989) 85.

2) S. Moriuchi, Y. Inoue, H. Sannomiya, A. Yokota, M. Itoh, Y. Nakata and H. Itoh: Proc. 21st IEEE Photovol. Spec. Conf., Florida (1990) 1449.

3) Y. Nakata, H. Sannomiya, S. Moriuchi, A. Yokota, Y. Inoue, M. Itoh and H. Itoh: Mat. Res. Soc. Symp. Proc., Vol. 192 (1990) 15.

4) H. Sannomiya, S. Moriuchi, Y. Inoue, K. Nomoto, A. Yokota, M. Itoh, Y. Nakata and T. Tsuji: Tech. Digest of 5th Int. Photovol. Sci. Engi. Conf., Kyoto (1990) 387.

5) Y. Nakata, H. Sannomiya, S. Moriuchi, Y. Inoue, K. Nomoto, A. Yokota, M. Itoh and T. Tsuji: OPTOELECTRONICS - Devices and Technologies, Vol. 5, No. 2, (1990) 209.

6) J. Yang, R. Ross, T. Glatfelter, R. Mohr, G. Hammond, C. Bernotaitis, E. Chen, J. Burdick, M. Hopson and S. Guha: Proc. 20th Photovol. Spec. Conf. Las Vegas (1988) 241.

7) M. S. Bennett and K. Rajan: J. Appl. Phys. 67 (1990) 4161.

8) Y. Nakata and T. Inoguchi: OPTOELECTRONICS - Devices and Technologies, Vol. 4, No. 1, (1989) 75.

9) M. Kaneiwa, K. Nomoto, M. Itoh, Y. Yamamoto, Y. Nakata and T. Inoguchi: Tech. Digest of 4th Int. Photovol. Sci. Engi. Conf., Sydney (1989) 673.

10) D. L. Staebler and C. R. Wronski: Appl. Phys. Lett. 31 (1977) 292; J. Appl. Phys. 51 (1980) 3262.

11) M. Stutzmann, W. B. Jackson, and C. C. Tsai: Phys. Rev. B 23 (1985) 23.

12) M. Hack, S. Guha, and W. den Boer: Phys. Rev. B 33 (1986) 2512.

13) D. Redfield and R. H. Bube: Appl. Phys. Lett. 54 (1989) 1037.

14) D. L. Staebler, R. S. Crandall, and R. Williams: Appl. Phys. Lett. 54 (1981) 733.

15) T. Kobe, Y. Nakata, T. Machida, Y. Yamamoto and T. Tsuji: Proc. 18th IEEE Photovol. Spec. Conf., Las Vegas (1985) 1594.

16) Z. E. Smith and S. Wagner: Appl. Phys. Lett. 46 (1985) 1078.

17) A. Yokota, H. Sannomiya, S. Moriuchi, Y. Inoue, M. Itoh, Y. Nakata and T. Tsuji: Tech. Digest of 5th Int. Photovol. Sci. Engi. Conf., Kyoto (1990) 637.

18) Y. Nakata, A. Yokota, H. Sannomiya, S. Moriuchi, Y. Inoue, K. Nomoto, M. Itoh and T. Tsuji: Mat. Res. Soc. Symp. Proc., Vol. 219 (1991) 433.

19) Y. Nakata, A. Yokota, H. Sannomiya, S. Moriuchi, Y. Inoue, K. Nomoto, M. Itoh and T. Tsuji: Jpn. J. Appl. Phys.,Vol. 31, Part 1, No. 2 (1992) (in press)

20) Y. Uchida, M. Nishiura, H. Sakai, and H. Haruki: Solar Cells 9 (1983) 3.

21) S. Tsuda, N. Nakamura, K. Watanabe, T. Takahama, H. Nishiwaki, M. Ohnishi, and Y. Kuwano: Solar Cells 9 (1983) 25.

22) R. S. Crandall: RCA Rev. 42 (1981) 441.

23) R. S. Crandall: J. Appl. Phys. 53 (1982) 3350.

24) G. A. Swartz: J. Appl. Phys. 53 (1982) 712.

25) H. Okamoto, H. Kida, S. Nonomura, and Y. Hamakawa: Solar Cells 8 (1983) 317.

26) I. Sakata and Y. Hayashi: Appl. Phys. A 37 (1985)153.

27) M. Hack and M. Shur: J. Appl. Phys. 58 (1985) 997.

V. BANDGAP PROFILING IN a-Si ALLOY SOLAR CELLS

5-1. Introduction

It was already explained that an important key issue to use a-Si solar cells as one of future new energy sources is improvement of the stability for the light-induced degradation as well as the conversion efficiency. This key issue has to be approached from three directions of material,[1] analytical, [2-8] and device technologies. A multi-bandgap stacked solar cell using a-Si alloy materials [1] is one of the most promising cell structures to obtain both of high stability and high conversion efficiency. [1,9]

It has been reported that characteristics of an a-SiGe cell applied as the bottom cell in a stacked cell can be improved by bandgap profiling in a photovoltaic active layer.[10-12] Many other experiments of bandgap profiling have been done as a-Si alloy films [13-15] and solar cells. [16] Based on the results of a computer simulation, it is claimed that the improvement of the solar cell characteristics is caused by the increase in the electric field for holes inside the cell. [10] But the physical mechanism has not yet been clarified. It is important to clarify the physical mechanism in order to design the bandgap profiles. Therefore, a series of systematic experiments on the bandgap profiling using a-SiGe:H and a-SiC:H cells was made. [17-20]

In this chapter, effect of the bandgap profiling on solar cell characteristics and design of the bandgap profiles are described.

5-2. Experimental

a-SiGe:H, a-Si:H and a-SiC:H were used to control the bandgap. These materials were deposited under high hydrogen dilution conditions to obtain the high quality by a chemical vapor deposition, as mentioned in chapter II. [1,21] The bandgap profiles were prepared by changing GeH_4 or CH_4 gas ratio to SiH_4 gas during the depositions of the i-layers.

Indium Tin Oxide (ITO)/pi(a-SiGe or a-SiC)n/stainless steel (S.S.) cells having i-layers with saddle shaped graded bandgap profiles were prepared for measurements of I-V characteristics and light-induced degradation characteristics. And cells with transparent electrodes at both sides, namely ITO/pi(a-SiGe)n/ITO and ITO/pi(a-SiC)n/ITO cells, were prepared for analysis.

Composition profiles were measured by Auger electron spectroscopy (AES). Carrier transports were evaluated by time-of-flight technique using a dye laser with 470 nm light.

5-3. Composition Profile

The bandgap profile was formed by changing the source gas ratio of GeH_4 or CH_4 to SiH_4 and the Si and Ge composition profiles in the i-layer were measured to confirm by Auger electron spectroscopy (AES). The experimental data are shown in Fig. 5-3-1. [17] The film thickness was 250 nm and the optical bandgap was changed from 1.45 eV to 1.75 eV. The Si and Ge composition can be controlled continuously by only changing the source gas ratio.

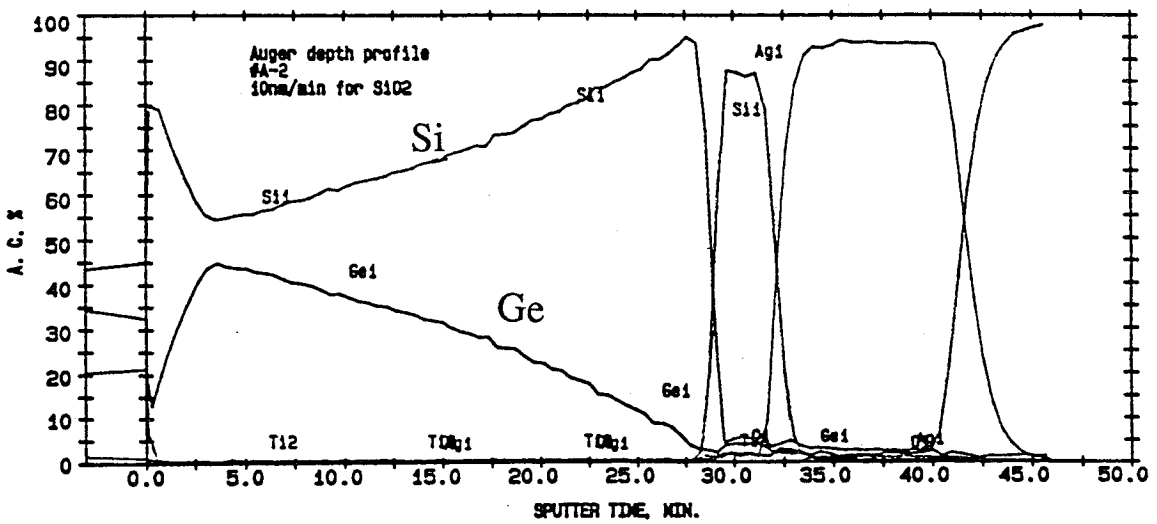

Fig. 5-3-1. Si and Ge composition profiles by Auger electron spectroscopy

5-4. Improvement of a-SiGe Cell Characteristics by Bandgap Profiling

5-4-1. Initial characteristics

To clarify the dependence of minimum bandgap position on a-SiGe solar cell characteristics, a-SiGe cells with different minimum bandgap position were prepared. Their minimum bandgap distances from the p-layer were 40 nm (Type P), 125 nm (Type M) and 210 nm (Type N) respectively, as shown in Fig. 5-4-1.[17] The total i-layer thicknesses were 250 nm. The characteristics of the a-SiGe cells with bandgap profiles were measured under red light [AM 1, 100 mW/cm^2 light through a red (>660 nm) cut-on filter]. The characteristics are shown in Fig. 5-4-2 including characteristics of a-SiGe cell with constant bandgap of 1.52 eV. The short circuit current (I_{sc}), fill factor (F.F.) and output power (P_{max}) increase as the position of the minimum bandgap changes from the n-layer side to the p-layer side. These characteristics of Type P cell are improved compared with those of the constant bandgap cell.

To analyze the characteristics, spectral responses were measured. The ordinary spectral responses and the spectral responses under bias voltage of 0.3 V normalized by the spectral responses under bias voltage of 0 V are shown in Figs. 5-4-3 (a) and (b).[17] The spectral response and the bias voltage dependence of Type P cell are improved at longer wavelengths comparing with the other cells. It is understood from the spectral response that the increases of I_{sc} and F.F. are caused by the improvement in characteristics at longer wavelengths where bottom cells have sensitivity.

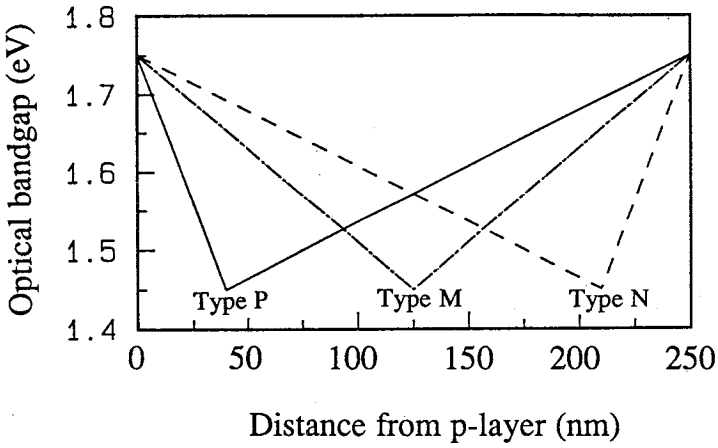

Fig. 5-4-1. Bandgap profiles of a-SiGe cells (Type P, M, N).

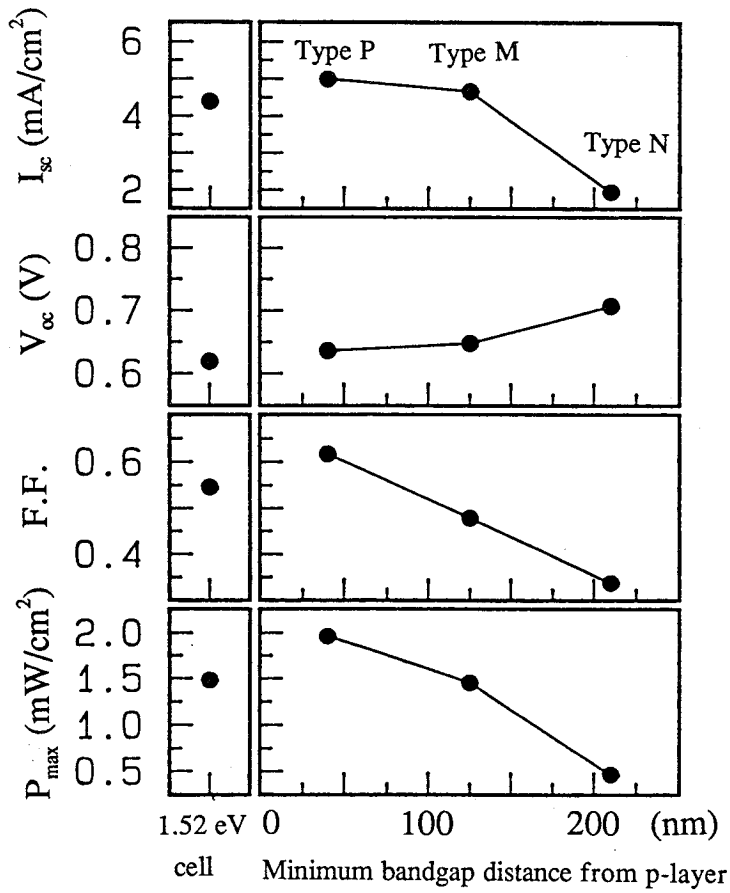

Fig. 5-4-2. Solar cell characteristics of a-SiGe cells (Type P, M, N and 1.52 eV constant bandgap cell) under red light.

(I_{sc}: Short circuit current V_{oc}: Open circuit voltage
F.F.: Fill factor P_{max}: Maximum output power)

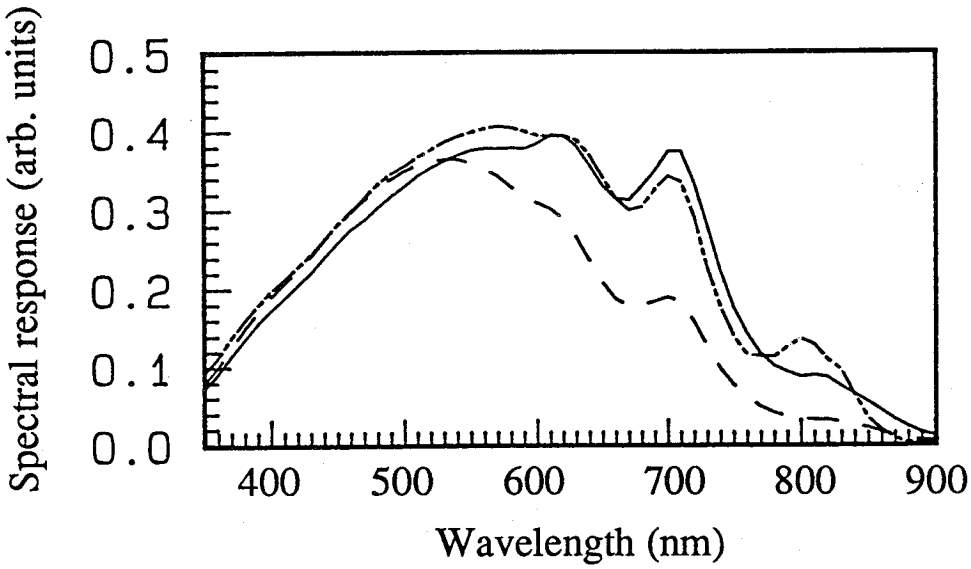

(a) Spectral responses

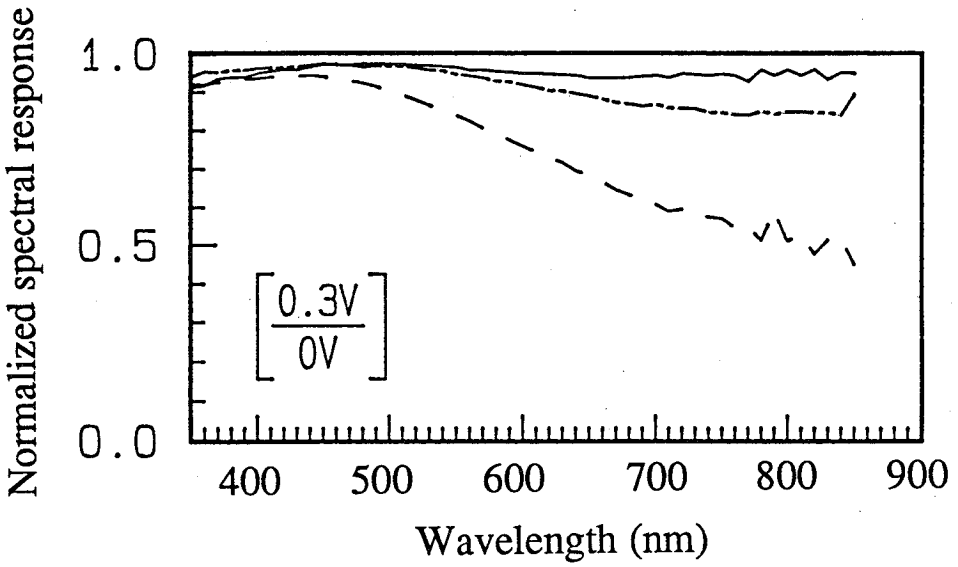

(b) Normalized spectral responses

Fig. 5-4-3. Spectral responses (a) and normalized spectral responses (b) of a-SiGe Type P (———), Type N (— — —) and 1.52 eV constant bandgap cell (—·—·—).

5-4-2. Light-induced degradation

The light-induced degradation of the a-SiGe cells with bandgap profiles (Type P, N and 1.52 eV constant bandgap cell) was investigated. They were exposed to AM 1.5, 10 suns of light, and their characteristics were measured under the red light [AM 1, 100 mW/cm^2 light through a red (>660 nm) cut-on filter]. The cells kept on open circuit condition during the exposure. The original characteristics and the normalized characteristics by the initial values are shown in Figs. 5-4-4 (a) and (b).[17] The initial output power of the Type P cell is larger than that of the other cells. And the degradation ratio of the Type P cell is smaller than that of the other cells.

It is indicated that the bandgap profiling is useful to obtain more efficient and more stable solar cells than conventional solar cells.

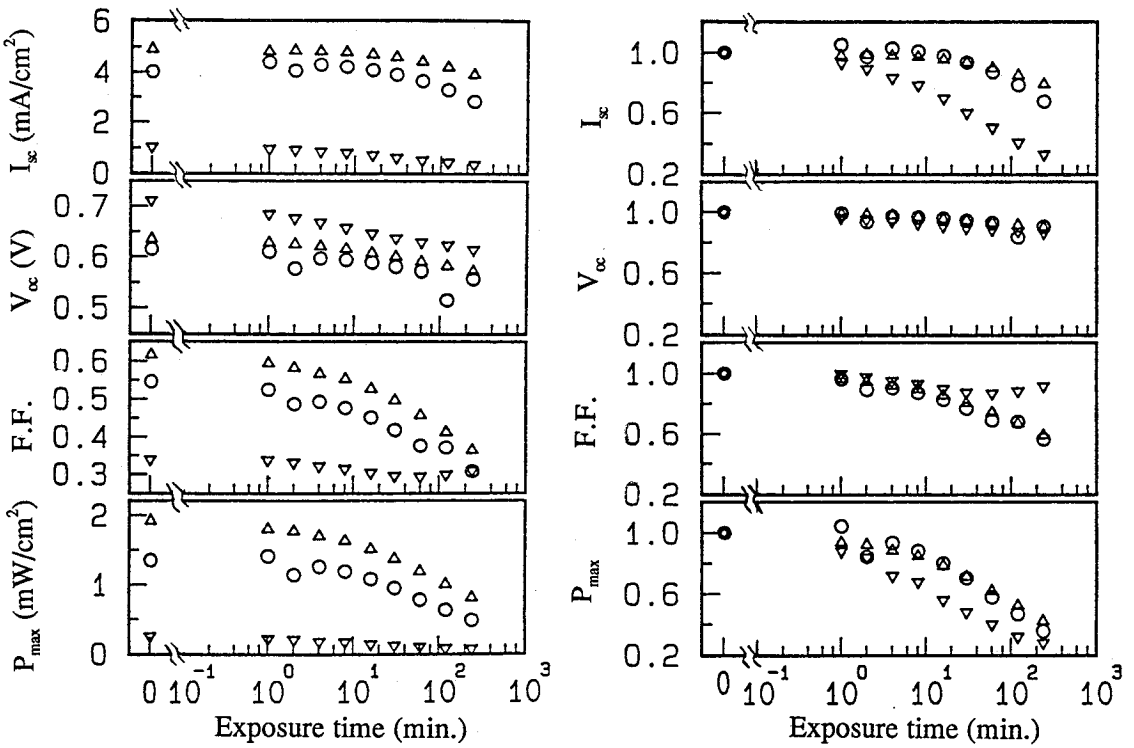

(a) Light-induced degradation (b) Normalized light-induced degradation

Fig. 5-4-4. Light-induced degradation characteristics under red light of a-SiGe Type P (△), Type N (▽) and 1.52 eV constant bandgap cell (○) which is exposed to AM 1.5, 10 suns light [Original (a) and normalized (b) data] .

[I_{sc}: Short circuit current V_{oc}: Open circuit voltage
F.F.: Fill factor P_{max}: Maximum output power]

5-5. Physical Mechanism of Bandgap Profiling on Solar Cell Characteristics

5-5-1. Carrier transport

The characteristics of a-SiGe cells can be improved by the bandgap profiling as mentioned above. It is claimed that the improvement of the solar cell characteristics is caused by the increase in the electric field for holes inside the cell.[10] But the physical mechanism has not yet been clarified. It is important to clarify the physical mechanism in order to design the bandgap profiles. Therefore, a series of systematic experiments on bandgap profiling using a-SiGe and a-SiC cells was made.[17]

To evaluate the effect of the bandgap profiling on the carrier transport, four type cells were prepared. The cells have the transparent electrodes at the both sides, as shown in Fig. 5-5-1. The i-layers were made of a-SiGe:H or a-SiC:H. The bandgap profiles of these cells are shown in Fig. 5-5-2 (a-SiGe Type P, N and a-SiC Type P, N).

By time-of-flight technique using a dye laser with 470 nm light, the charge collections of the a-SiGe Type P and N cells were measured as a function of externally applied voltage. The light was entered from the p-layer side to measure the electron collection and it was entered from the n-layer side to measure the hole collection. The experimental data are shown in Figs. 5-5-3 (a) and (b). At the same applied voltage, the electron collection of the Type P cell is smaller than that of the Type N cell, but the hole collection of the Type P cell is larger. These experimental data suggest that the electron transport is reduced but the hole transport is improved in the Type P cell by the bandgap profiling.

Moreover, the hole and electron transports were evaluated under a steady light like an operating condition. The blue light [AM 1, 100 mW/cm^2 light through a blue (<420 nm) cut-on filter] was irradiated to the a-SiGe Type P, N and a-SiC

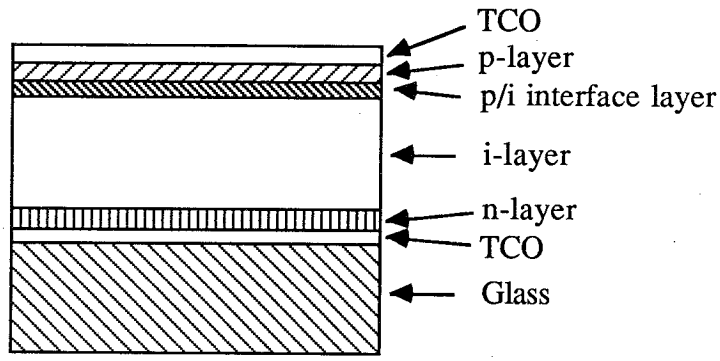

Fig. 5-5-1. a-SiGe and a-SiC cell structure for analysis

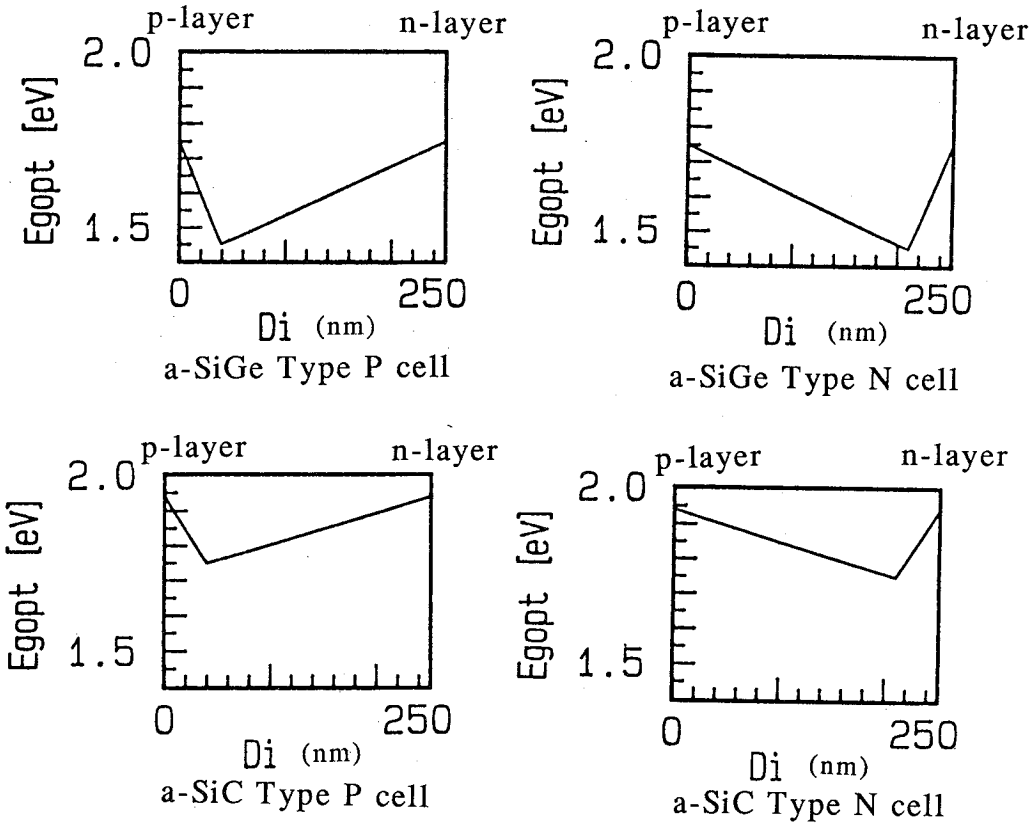

Fig. 5-5-2. Bandgap profiles of a-SiGe cells (Type P, N) and a-SiC cells (Type P, N). (Egopt: Optical bandgap)

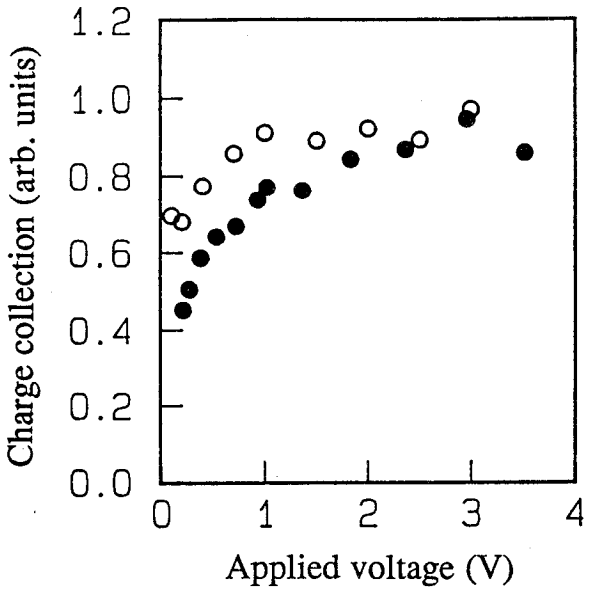

(a) Electron collection

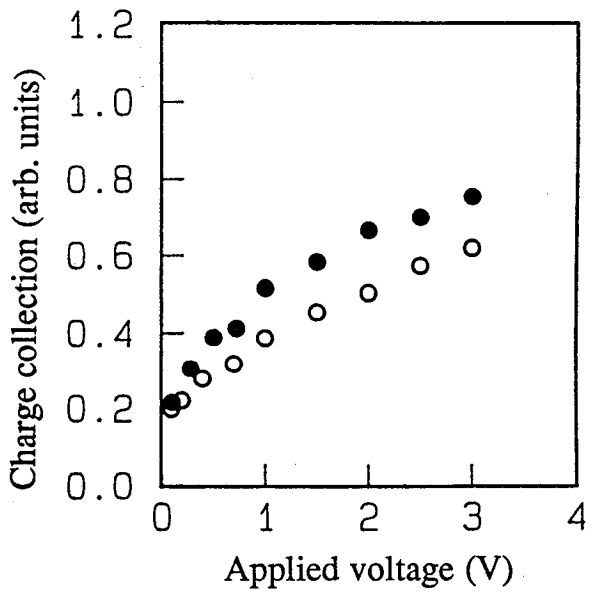

(b) Hole collection

Fig. 5-5-3. Electron collection (a) and hole collection (b) of a-SiGe Type P (●) cell and a-SiGe Type N (○) cell.

Type P, N cells from the n-layer side. Under this condition, carriers were generated near the n-layer side and electrons were collected to the n-layer immediately, but holes were transported to the p-layer through the i-layer. The hole transport can be evaluated by the bias voltage dependence of an output current under this condition. In other words, the hole transport can be evaluated by the F.F. of the solar cell characteristics under the blue light from the n-layer side. In the same manner as these experiments, the electron transport can be evaluated by the F.F. under the blue light from the p-layer side. The solar cell characteristics under the blue light from the n-layer side and the p-layer side are shown in Table 5-5-1 and Table 5-5-2. In the a-SiGe cells, the F.F. of the Type P cell is larger than that of the Type N cell under the blue light from the n-layer, but the F.F. is almost same under the blue light from the p-layer. These results suggest that the hole transport is improved but the electron transport is not improved in the Type P cell by the bandgap profiling and these results agree with the results of the time-of-flight measurement. But, in the a-SiC cells, the F.F. of the Type P cell is smaller than that of the Type N cell under the blue light from the n-layer side contrary to the experimental result of the a-SiGe cell. This result suggests that hole transport gets worse in the a-SiC Type P cell.

The effect of the bandgap profiling on the hole transport was considered. It can be considered that the electric field for holes within the cell is increased in the a-SiGe cell. But, in the a-SiC cell, if the increase of the electric field within the cell was a more effective cause to improve the cell characteristics, the F.F. of the Type P cell would be larger than that of the Type N cell. But, the experimental results are contrary and can not be explained only by the increase of the electric field within the cell. In comparing the a-SiGe Type P cell with the a-SiC Type P cell, it can be considered that the bandgap profiling produces an almost equivalent

increase in the electric field within the cell. But, the mobility · lifetime ($\mu\ \tau$) products of holes and electrons near the n-layer of a-SiGe Type P cell are larger than that of the a-SiC Type P cell, because the region near the n-layer of a-SiGe cell contains a few germanium like a-Si:H and the region near the n-layer of a-SiC cell contains much carbon. Therefore, in the a-SiGe Type P cell which has a larger $\mu\ \tau$ product of holes near the n-layer, the transport of holes which is generated near the n-layer is improved, even if the electric field near the n-layer is small. But, the $\mu\ \tau$ product of holes near the n-layer of a-SiC Type P cell is small, and the hole transport is worse. With these ideas about the increase of the electric field for holes within the cell and the spatial distribution of $\mu\ \tau$ product for holes, the characteristics of these four cells can be explained.

As a result, the hole transport is improved in the a-SiGe cell and reduced in the a-SiC cell by the bandgap profiling. It can be considered that these characteristics are caused by the spatial distribution of $\mu\ \tau$ product for holes and the increase of the electric field for holes within the cell.

The AM 1, 100 mW/cm^2 light was irradiated to the a-SiGe Type P, N and a-SiC Type P, N cells from the p-layer sides. These cell characteristics correspond to usual solar cell characteristics and they are shown in Table 5-5-3. In the a-SiGe cells, the output power of Type P cell is larger than that of type N cell and this result agree with the characteristic which is shown in Fig. 5-4-2. In the a-SiC cells, the output power of the Type P cell is larger than that of the Type N cell in spite of the poor hole transport. This experimental result can not be explained by the only hole transport.

In both a-SiGe cells and a-SiC cells, since the output powers of the Type P cells are larger than those of the Type N cells, the profile of photo-generated carriers was investigated.

Table 5-5-1. Cell characteristics of a-SiGe Type P, N and a-SiC Type P, N cells under blue light from the n-layer side.

Cell type			Isc mA/cm^2	Voc V	F.F.	Pmax mW/cm^2
a-SiGe	TYPE P	p ⋈ n ⇦	1.34	0.517	0.522	0.36
	TYPE N	p ⋈ n ⇦	0.82	0.681	0.477	0.27
a-SiC	TYPE P	p ⋈ n ⇦	0.65	0.804	0.420	0.22
	TYPE N	p ⋈ n ⇦	0.76	0.828	0.550	0.35

Table 5-5-2. Cell characteristics of a-SiGe Type P, N and a-SiC Type P, N cells under blue light from the p-layer side.

Cell type			Isc mA/cm^2	Voc V	F.F.	Pmax mW/cm^2
a-SiGe	TYPE P	⇨ p ⋈ n	2.37	0.584	0.546	0.76
	TYPE N	⇨ p ⋈ n	2.17	0.767	0.545	0.91
a-SiC	TYPE P	⇨ p ⋈ n	1.97	0.882	0.670	1.16
	TYPE N	⇨ p ⋈ n	1.79	0.856	0.627	0.96

Table 5-5-3. Cell characteristics of a-SiGe Type P, N and a-SiC Type P, N cells under AM 1, 100 mW/cm^2 light from the p-layer side.

Cell type			Isc mA/cm^2	Voc V	F.F.	Pmax mW/cm^2
a-SiGe	Type P	⇨ p ⋈ n	19.5	0.669	0.489	6.37
	Type N	⇨ p ⋈ n	14.0	0.841	0.472	5.56
a-SiC	Type P	⇨ p ⋈ n	11.3	0.949	0.618	6.63
	Type N	⇨ p ⋈ n	11.2	0.933	0.597	6.26

I_{sc}: Short circuit current V_{oc}: Open circuit voltage

F.F.: Fill factor P_{max}: Maximum output power

5-5-2. Profile of photo-generated carriers

To evaluate the effect of bandgap profiling on the light absorption, the profiles of the light absorption amount were calculated.[17-20] The calculated data in the a-SiGe Type P, N and 1.52 eV constant bandgap cells under 690 nm light are shown in Fig. 5-5-4. These results show that the profile of the light absorption amount corresponds closely with the bandgap profile under the long wavelength light. In other words, the profile of photo-generated carriers can be designed by using the bandgap profiling, especially under the long wavelength light. As a result, the light is absorbed in the narrow bandgap region near the p-layer of the a-SiGe Type P cell and the carriers are photo-generated near the p-layer and the holes are collected to the p-layer efficiently.

To confirm the effect of the profile of photo-generated carriers, an a-SiGe solar cell with well type bandgap profile was made, as shown in Fig. 5-5-5 (a). It is considered that there is not the increase of the electric field within the cell at this cell structure. The long wavelength light is almost absorbed at narrow bandgap layer, as shown in Fig. 5-5-5 (b). The F.F. of the well type cell were improved compared with that of the constant bandgap cell, as shown in Fig. 5-5-5 (c). This result suggests that the effect of the profile of photo-generated carriers is larger than the effect of the electric field.

As a result in sub-sections 5-5-1 and 5-5-2, it is considered that the profile of photo-generated carriers is the most effective cause on the improvement of the solar cell characteristics.

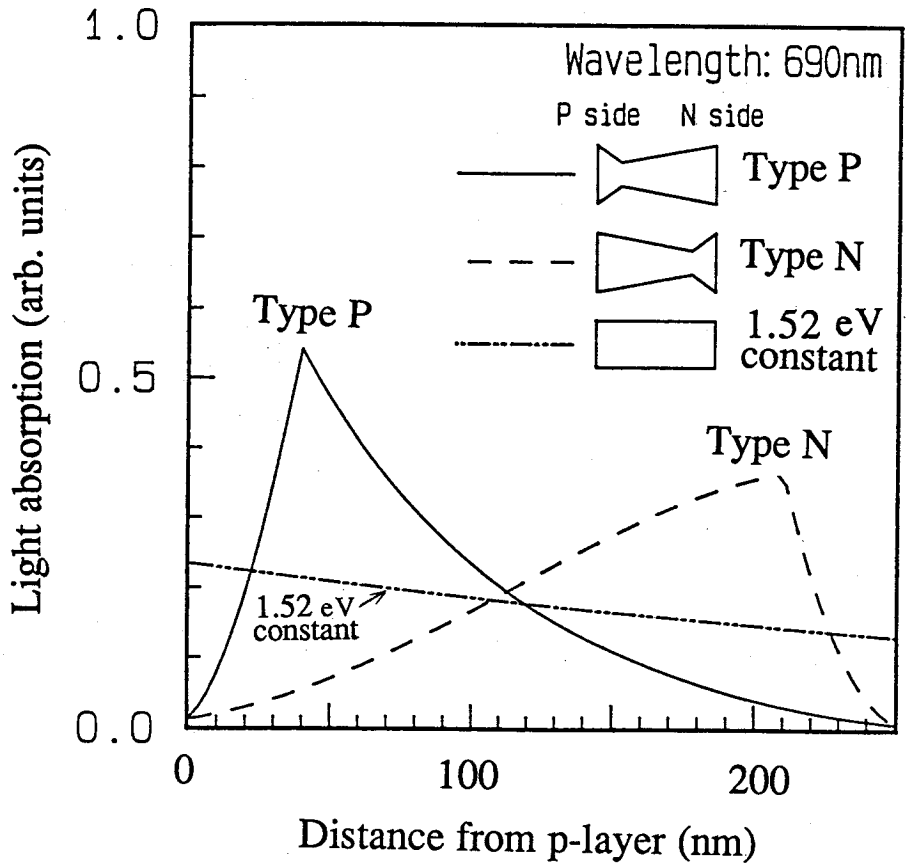

Fig. 5-5-4. Calculated profiles of light absorption in a-SiGe Type P, N and 1.52 eV constant bandgap cell under 690 nm light.

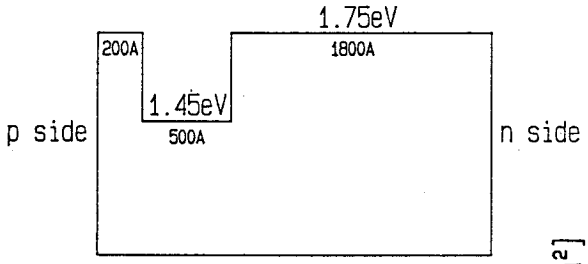

(a) Bandgap profile

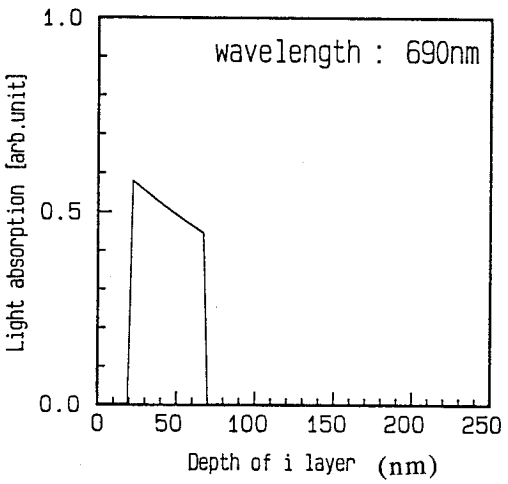

(b) Profile of light absorption

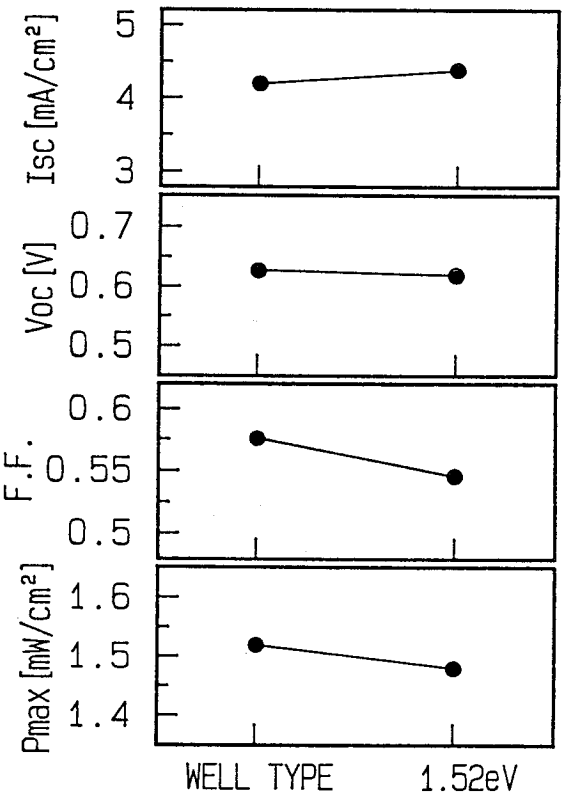

(c) Characteristics under red light

Fig. 5-5-5. Bandgap profile (a), profile of light absorption (b), and characteristics under red light (c) of a-SiGe well type cell

I_{sc}: Short circuit current V_{oc}: Open circuit voltage

F.F.: Fill factor P_{max}: Maximum output power

5-5-3. Effect of bandgap profiling on solar cell characteristics

Characteristics of a-Si solar cells are usually determined by the behavior of holes, which are called "limiting carriers", because the hole mobility is smaller than the electron mobility.[22] To improve the solar cell characteristics, it is necessary to increase the collection of photo-generated holes even if the collection of electrons is decreased slightly. In other words, it is important to optimize the collection of photo-generated holes and electrons.

On the basis of that idea and the experimental data as mentioned above, the qualitative effects of the bandgap profiles in the a-SiGe:H and a-SiC:H cells on the solar cell characteristics are summarized in Table 5-5-4. [17,19,20] An upward arrow means an increasing effect on the solar cell characteristics, and a downward arrow means a decreasing effect. The size of the arrow indicates the qualitative degree of the effect. It has been shown as mentioned above that the bandgap profiling affects the carrier transport and the profile of photo-generated carriers. It can be considered that the carrier transport is changed by an increase of the electric field for holes inside the cell and a spatial distribution of the $\mu\tau$ products of holes and electrons. And it is possible to consider that the most effective cause is the profile of the photo-generated carriers, which can be designed by using bandgap profiling. When a narrow bandgap region is positioned near the p-layer, the carriers are photo-generated near the p-layer. Although the collection of electrons photo-generated near the p-layer is decreased, that of holes is increased and the solar cell efficiency is improved. Therefore, bandgap profiling is useful to optimize the collection of photo-generated electrons and holes, and to increase the solar cell efficiency.

Table 5-5-4. Qualitative effect of bandgap profiles in a-SiGe and a-SiC cells on solar cell characteristics.

(⇧= increasing effect, ⇩= decreasing effect)

			a-SiGe cell	a-SiC cell
Carrier collection	Carrier transport	Electric field	⇧	⇧
		Distribution of mobility, lifetime	⇧	⇩
	Profile of photo-generated carriers	Distribution of light absorption	⇧	⇧
Total effect			⇧	⇧

5-6. Design of Bandgap Profiles

5-6-1. Design of bandgap profiles in a-SiC solar cells

On the basis of the effects of bandgap profiling on the cell characteristics, the bandgap profile of the a-SiC cell was designed to apply it to the top cell in the multi-bandgap cell.[17-20] To increase the carriers photo-generated near the p-layer, the minimum bandgap of the a-SiC cells at a distance of 35 nm from the p-layer was decreased from 1.98 eV to 1.80 eV, as shown in Fig. 5-6-1 (a). The maximum bandgap at both interfaces is 1.98 eV, and the total i-layer thickness is about 130 nm. A silver rear reflector was not deposited on the S.S. substrate in order to make the cell similar to the top cell in the stacked cell. The calculated absorption of 500 nm wavelength light is shown in Fig. 5-6-1 (b). The solar cell characteristics under the AM 1 light are shown in Fig. 5-6-2. As the minimum bandgap is decreased, the short circuit current (I_{sc}) and fill factor (F.F.) increase and the open circuit voltage (V_{oc}) decreases slightly. The increase of the F.F. is caused not only by the bandgap profiling but also by the improvement of the a-SiC quality because the carbon content is decreased. As a result, the a-SiC cell with the high F.F. and the high V_{oc} has been obtained.

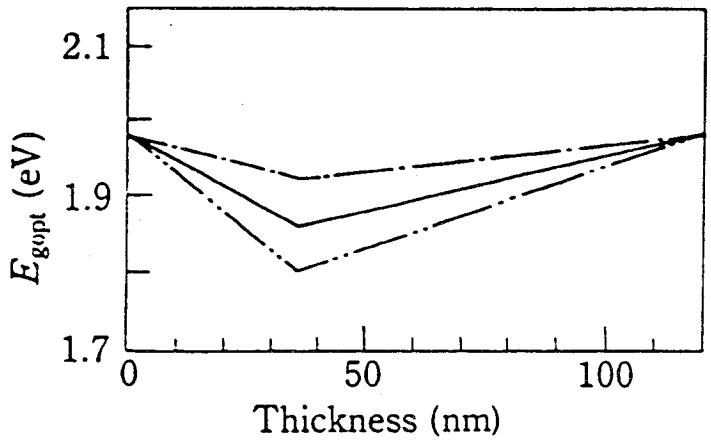

(a) Bandgap profiles

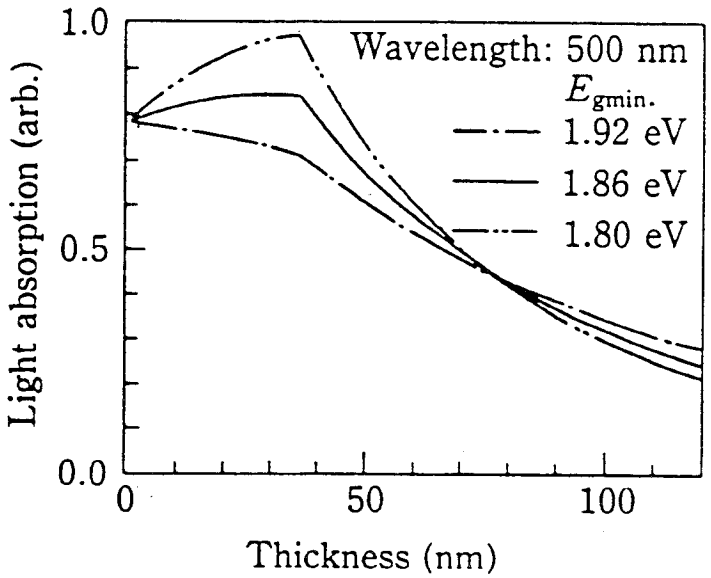

(b) Calculated absorption of 500 nm wavelength light

Fig. 5-6-1. Bandgap profiles (a) and calculated absorption of 500 nm wavelength light (b) in a-SiC cells.

(Egopt: Optical bandgap Egmin: Minimum bandgap)

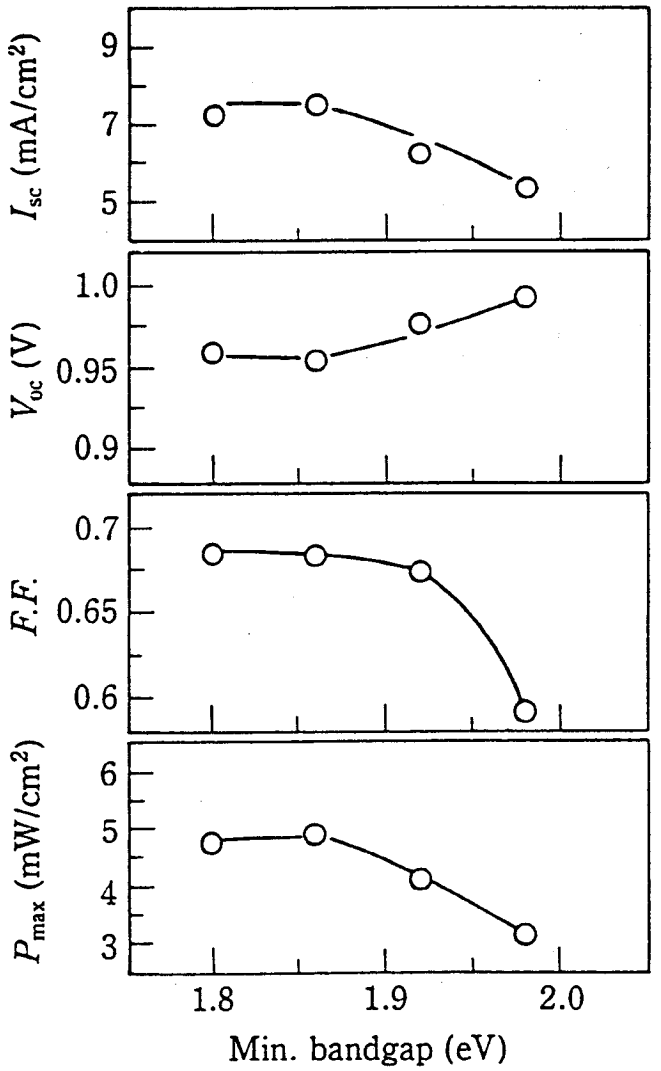

Fig. 5-6-2. Solar cell characteristics of a-SiC cells with bandgap profiles under AM 1 light versus the minimum bandgap

{ I_{sc}: Short circuit current V_{oc}: Open circuit voltage
F.F.: Fill factor P_{max}: Maximum output power }

5-6-2. Design of bandgap profiles in a-SiGe solar cells

On the basis of the effect of bandgap profiling on the solar cell characteristics, the bandgap profile of an a-SiGe cell was designed to obtain high efficiency also.[17-20] To increase the carriers photo-generated near the p-layer, the minimum bandgap at the distance of 40 nm from the p-layer was decreased from 1.50 eV to 1.39 eV, as shown in Fig. 5-6-3 (a). The maximum bandgap at both interfaces is 1.75 eV, and the total i-layer thickness is 250 nm. The calculated absorption of 690 nm wavelength light in the cells is shown in Fig. 5-6-3 (b). They correspond closely with the bandgap profiles. The photo-generated carriers near the p-layer increase as the minimum bandgap is decreased. The characteristics of the cells under red light [AM 1, 100 mW/cm^2 light through a red (wavelength >660 nm) cut-on filter] are shown in Fig. 5-6-4, including the characteristics of the cell with a constant bandgap of 1.52 eV. The rear reflector is a smooth silver film or a ZnO/textured silver multi-film. The characteristics of the bandgap profiling cells with the smooth reflector are improved compared with these of the cell with the constant bandgap and the smooth reflector. The short circuit current (I_{sc}) of the cell with the ZnO/textured silver reflector is higher than that of the cell with the smooth silver reflector. These effects of the reflectors will be discussed in chapter VI. As the minimum bandgap is decreased, the I_{sc} increases remarkably, and the fill factor (F.F.) and the open circuit voltage (V_{oc}) decrease slightly. The slight decrease of the F.F. is caused by the quality debasement of the a-SiGe as the germanium content is increased. The maximum output power (P_{max}) is almost constant. The current of the stacked cell is limited by the lowest current of the component cells. Therefore, the a-SiGe cells having the small minimum bandgap and the large I_{sc} are useful to adjust the current of each component cell at the stacked cell because the other component cells have large I_{sc}.

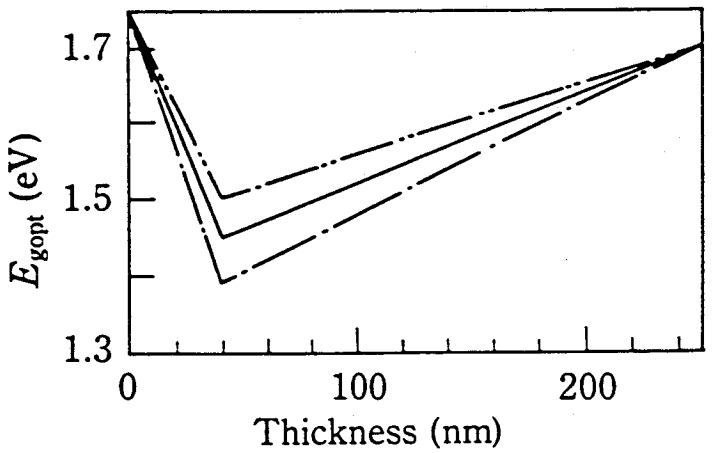

(a) Bandgap profiles

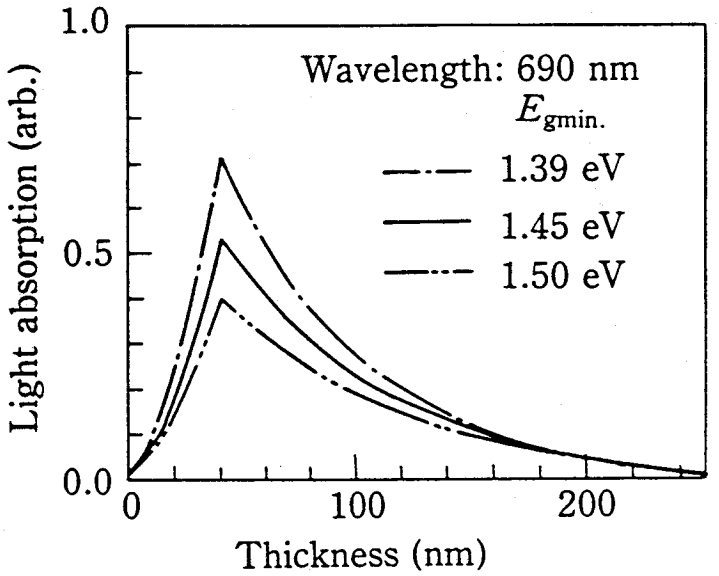

(b) Calculated absorption of 690 nm wavelength light

Fig. 5-6-3. Bandgap profiles (a) and calculated absorption of 690 nm wavelength light (b) in a-SiGe cells.

(Egopt: Optical bandgap Egmin: Minimum bandgap)

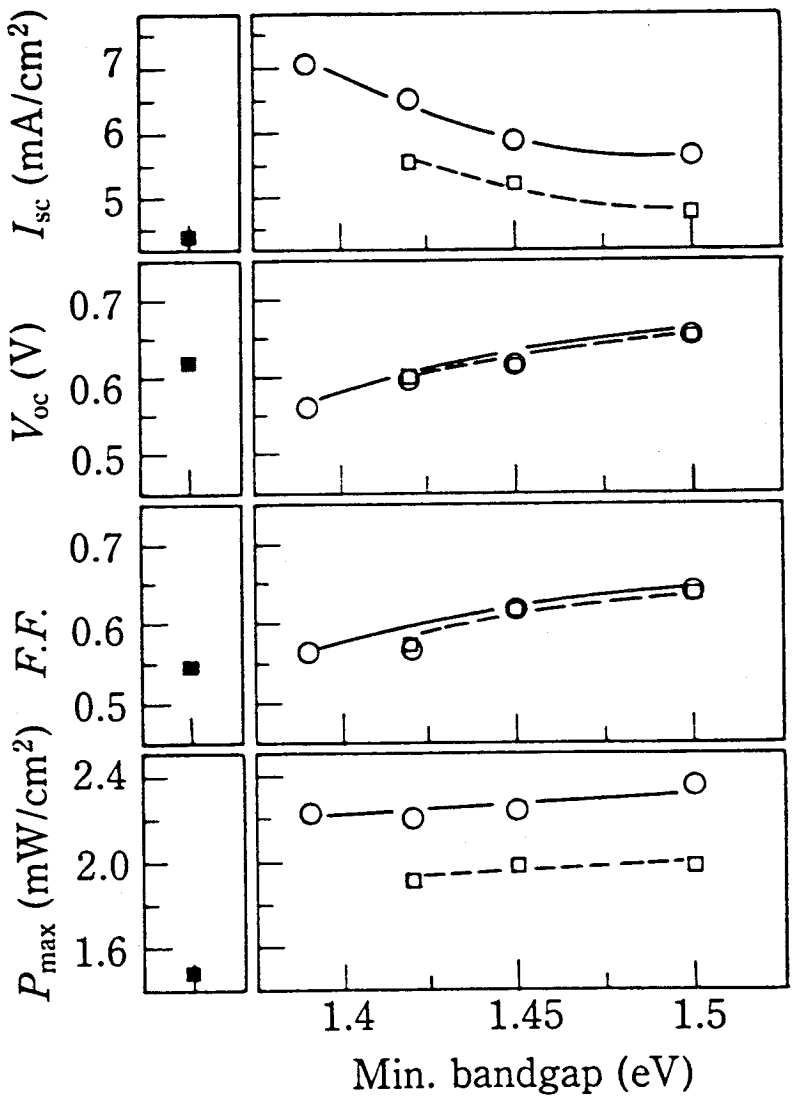

Fig. 5-6-4. Solar cell characteristics of a-SiGe cells with bandgap profiles under red light versus the minimum bandgap. (○: cell with ZnO/textured silver reflector, □: cell with smooth silver reflector, ■: cell with constant bandgap of 1.52 eV and smooth silver reflector)

[I_{sc}: Short circuit current V_{oc}: Open circuit voltage
F.F.: Fill factor P_{max}: Maximum output power]

Next, the bandgap profile of the a-SiGe cell was designed to obtain high stability,[20] because the light-induced degradation of multi-bandgap stacked solar cells was mainly determined by the light-induced degradation of a-SiGe bottom cells, as mentioned in sub-section 3-4-2. It is considered that the light-induced degradation of hole collection by light exposure becomes smaller when the minimum bandgap is positioned near the p-layer, because the holes photo-generated near the p-layer are collected efficiently to the p-layer even after light exposure. Therefore, the dependence of minimum bandgap position on the light-induced degradation of a-SiGe solar cell was investigated. For this purpose, a-SiGe cells with different minimum bandgap position were prepared. The characteristics of the a-SiGe cells before and after 4 hours' exposure to AM 1.5, 10 suns of light under open circuit condition were measured under red light [AM 1, 100 mW/cm^2 light through a red (>660 nm) cut-on filter], as shown in Fig. 5-6-5. The light-induced degradation ratio is decreased as the position of the minimum bandgap changes from the n-layer side to the p-layer, and the light-induced degradation ratio of the solar cell, whose minimum bandgap distance from the p-layer is 10 nm, is decreased by approximately one-half as compared with that of the solar cell with a constant bandgap of 1.52 eV.

As a result, by designing the bandgap profiles, a-SiGe component solar cells with high efficiency and high stability have been obtained.

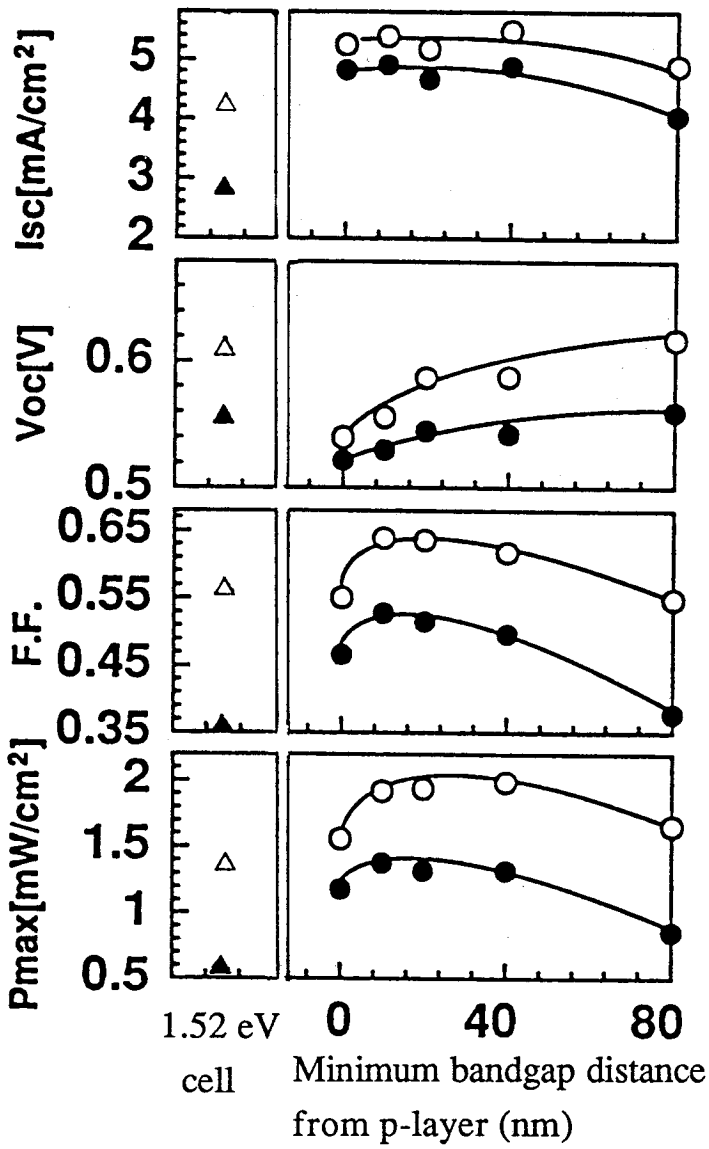

Fig. 5-6-5. Solar cell characteristics of a-SiGe cells with different minimum bandgap position under red light before (○) and after 4 hours' exposure to 10 suns light (●) including a-SiGe cell with 1.52 eV constant bandgap cell(△,▲) .

[I_{sc}: Short circuit current V_{oc}: Open circuit voltage
F.F.: Fill factor P_{max}: Maximum output power]

5-7. Summary

A series of systematic experiments on the bandgap profiling using a-SiGe:H and a-SiC:H cells was made. The results from these investigations are the following:

(1) Both initial characteristics and light-induced degradation of a-SiGe:H solar cells are improved by the bandgap profiling. The bandgap profiling is useful to obtain more efficient and more stable a-Si alloy multi-bandgap stacked solar cells.

(2) The physical mechanism of the bandgap profiling on the solar cell characteristics has been clarified. The largest effect is the profile of the photo-generated carriers. The bandgap profiling is effective to optimize the collection of photo-generated electrons and holes.

(3) On the basis of the physical mechanism of the bandgap profiling on the solar cell characteristics, the bandgap profiles of the a-SiC:H cells and the a-SiGe:H cells were designed to apply them to the multi-bandgap a-Si alloy staked solar cells. As a result, the component cells with the high efficiency and the high stability have been obtained.

REFERENCES

1) K. Nomoto, Y. Takeda, S. Moriuchi, H. Sannomiya, T. Okuno, A. Yokota, M. Kaneiwa, M. Itoh, Y. Yamamoto, Y. Nakata and T. Inoguchi: Tech. Digest of 4th Int. Photovol. Sci. Engi. Conf., Sydney (1989) 85.

2) Y. Nakata, Y. Inoue, H. Sannomiya, K. Nomoto, A. Yokota, M. Itoh and T. Tsuji: OPTOELECTRONICS - Devices and Technologies, Vol. 6, No. 1, (1991) 141.

3) M. Kaneiwa, K. Nomoto, M. Itoh, Y. Yamamoto, Y. Nakata and T. Inoguchi: Tech. Digest of 4th Int. Photovol. Sci. Engi. Conf., Sydney (1989) 673.

4) Y. Nakata and T. Inoguchi: OPTOELECTRONICS - Devices and Technologies, Vol. 4, No. 1, (1989) 75.

5) T. Kobe, Y. Nakata, T. Machida, Y. Yamamoto and T. Tsuji: Proc. 18th IEEE Photovol. Spec. Conf., Las Vegas (1985) 1594.

6) A. Yokota, H. Sannomiya, S. Moriuchi, Y. Inoue, M. Itoh, Y. Nakata and T. Tsuji: Tech. Digest of 5th Int. Photovol. Sci. Engi. Conf., Kyoto (1990) 637.

7) Y. Nakata, A. Yokota, H. Sannomiya, S. Moriuchi, Y. Inoue, K. Nomoto, M. Itoh and T. Tsuji: Mat. Res. Soc. Symp. Proc., Vol. 219 (1991) 433.

8) Y. Nakata, A. Yokota, H. Sannomiya, S. Moriuchi, Y. Inoue, K. Nomoto, M. Itoh and T. Tsuji: Jpn. J. Appl. Phys., Vol. 31, No. 2A, Part 1 (1992) (in press)

9) S. Moriuchi, Y. Inoue, H. Sannomiya, A. Yokota, M. Itoh, Y. Nakata and H. Itoh: Proc. 21st IEEE Photovol. Spec. Conf., Florida (1990) 1449.

10) S. Guha, J. Yang, A. Pawlikiewicz, T. Glatfelter, R. Ross, and S.R.Ovshinsky: Proc. 20th. IEEE Photovol. Spec. Conf., Las Vegas, 1988, pp. 79-84.

11) A. H. Pawlikiewicz and S. Guha, in: Proc. 20th. IEEE Photovol. Spec. Conf., Las Vegas, 1988, pp. 251-255.

12) J. Yang, R. Ross, T. Glatfelter, R. Mhr, S. Guha: Tech. Digest of 4th Int. Photovol. Sci. Engi. Conf., Sydney, 1989, pp. 409-414.

13) H. Shirai, S. Oda, T. Nakamura and I. Shimizu: Jpn J. Appl. Phys. 3 (1987) L169-L172.

14) J. P. Conde, D. S. Shen, V. Chu and S. Wagner: IEEE Trans. Electron Devices 12 (1989) 2834-2838.

15) J. P. Conde, D. S. Shen, V. Chu and S. Wagner: Proc. 4th Int. Photovol. Sci. Engi. Conf., Sydney, 1989, pp. 205-210.

16) C. M. Fortman: Mat. Res. Soc. Symp. Proc., Vol. 192 (1990) 27-38.

17) Y. Nakata, H. Sannomiya, S. Moriuchi, A. Yokota, Y. Inoue, M. Itoh and H.Itoh: Mat. Res. Soc. Symp. Proc., Vol. 192 (1990) 15-26.

18) H. Sannomiya, S. Moriuchi, Y. Inoue, K. Nomoto, A. Yokota, M. Itoh, Y.Nakata and T. Tsuji, in: Tech. Digest of 5th Int. Photovol. Sci. Engi. Conf., Kyoto (1990) 387-390.

19) Y. Nakata, H. Sannomiya, S. Moriuchi, Y. Inoue, K. Nomoto, A. Yokota, M. Itoh and T. Tsuji, OPTOELECTRONICS - Devices and Technologies, 2 (1990) 209-221.

20) Y. Nakata (Editors: Y. Sakurai, K. Suzuki, T. Masumoto, K. Shirae, Y. Hamakawa): PROGRESS IN AMORPHOUS MATERIALS - Science and Technology- (Elsevier Science Publishers B. V., Amsterdam, to be published in 1992) sub-section 4.5.4.

21) A. Matsuda and K. Tanaka, J. Non-Cryst. Solids 97&98 (1987) 1367.

22) M. Hack and M. Shur, J. Appl. Phys. 58(2) (1985) 997.

VI. OPTICAL CONFINEMENT IN a-Si ALLOY SOLAR CELLS

6-1. Introduction

To use a-Si solar cells as a future new energy source, an important key issue is improvement of the stability for the light-induced degradation and the conversion efficiency. This key issue has to be approached from three directions of material, analytical, [1-7] and device technologies. A multi-bandgap stacked solar cell using a-Si alloy materials is one of the most promising cell structures to obtain both of high stability and high conversion efficiency. [8-12]

To improve the conversion efficiency of the multi-bandgap stacked solar cells, the electric properties have been improved by using high quality materials [8] and bandgap profiling.[10-12] In addition, improvement of optical confinement is required. Therefore, texturing of rear reflector, inserting of oxide film and double anti-reflector coating are investigated to confine incident light to solar cells.

In this chapter, technologies of optical confinement at front and rear sides of solar cells are described. Texturing of rear silver reflector, inserting of ZnO film, glass / textured SnO_2 substrates and MgF_2 / Indium Tin Oxide (ITO) double anti-reflection coating are investigated. [11,12] Using these technologies of the optical confinement, the solar cells with high conversion efficiency are demonstrated.

6-2. Texturing of Rear Silver Reflector

Light reflected by a rear reflector is absorbed again in solar cells. Then, to increase short circuit current (I_{sc}), scattering of reflected light is required because the path of the light in the cell is extended. When an evaporated silver film is deposited on a stainless steel (S.S.) substrate as a rear reflector, the film is usually smooth and the reflected light is not scattered enough. To increase the light scattering, texturing of rear silver reflector has been investigated. Figure

6-2-1 shows the Scanning Electron Microscopy (SEM) images of the silver films which were deposited at a substrate temperature of 350℃. As the film thickness is increased, the island structure begins to connect and grow. To evaluate the light scattering of the films, the total and direct reflectance were measured. The diffuse reflectance was obtained by subtracting the direct reflectance from the total reflectance. The ratios of the diffuse reflectance to the total reflectance are shown in Fig. 6-2-2. The 50 nm thick silver reflector has the highest ratio of the diffuse reflectance, and it is considered that the reflector has the highest light scattering.

The a-SiGe cells with the bandgap profile [optical bandgap (Egopt): 1.42 eV ~ 1.75 eV] were prepared by using the S.S. substrates with various silver rear reflectors. The characteristics of the a-SiGe cells with the 100 nm and 50 nm thick silver rear reflectors under the red light [AM 1, 100 mW/cm^2 light through a red (wavelength> 660 nm) cut-on-filter] are shown in Table 6-2-1 (a) and (b). The cell with the 50 nm thick silver rear reflector has high light scattering, as mentioned before, but at the same time it has lower I_{sc}. From the SEM images and the low total reflectance, as shown in Fig. 6-2-3, it is considered that the film with the average thickness of 50 nm has a rough island structure and high light scattering. It has low reflectance because it cannot cover the whole substrate surface. Therefore, to obtain high light scattering and high reflectance, a double-layer reflector was employed. The 50 nm thick first layer was deposited at a substrate temperature of 350℃, and the 50 nm thick second layer was deposited at a substrate temperature of 150℃ to cover the whole substrate while keeping the roughness. The cell characteristics under the red light and the spectral response of the cell with the double-silver rear reflector are shown in Table 6-2-1 (c) and Fig. 6-2-4, respectively. The I_{sc} is increased by 9% as compared with that of the cell with single 100 nm thick silver rear reflector because the spectral response at long wavelengths of light is improved.

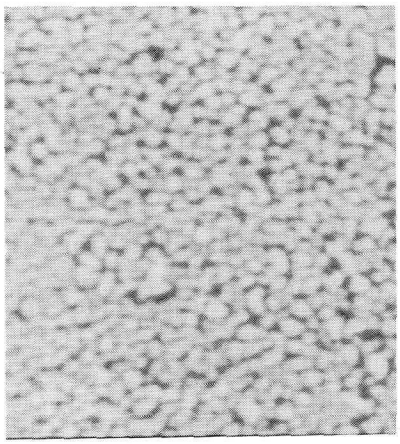

(a) 20 nm

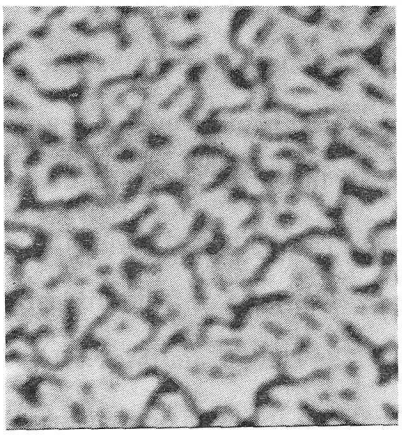

(b) 50 nm

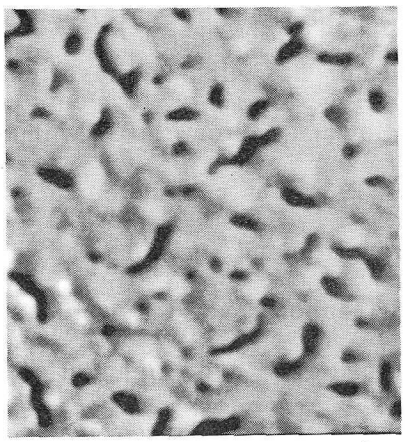

(c) 100 nm

Fig. 6-2-1. Scanning Electron Microscopy (SEM) images of silver films with various thicknesses.

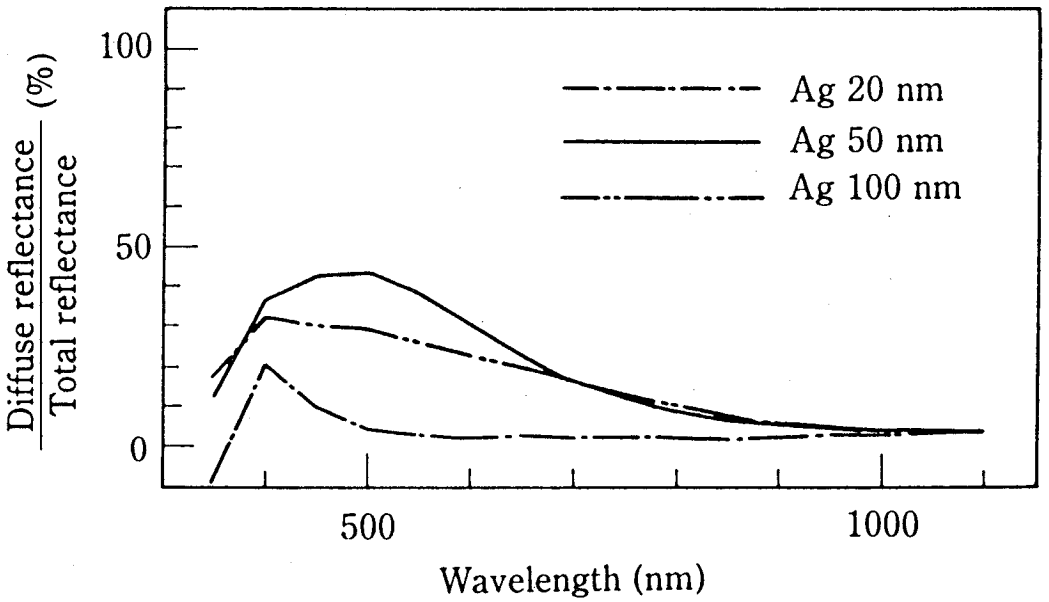

Fig. 6-2-2. Ratios of diffuse reflectance to total reflectance of silver rear reflectors.

Table 6-2-1. Characteristics of a-SiGe cells with bandgap profiles and various rear reflectors under red light.

[I_{sc}: Short circuit current V_{oc}: Open circuit voltage
F.F.: Fill factor P_{max}: Maximum output power]

	I_{sc} (mA/cm^2)	V_{oc} (V)	F.F.	P_{max} (mW/cm^2)
(a) Ag (100 nm)	5.28	0.62	0.61	1.99
(b) Ag (50 nm)	4.81	0.61	0.60	1.77
(c) Ag / Ag	5.74	0.62	0.61	2.15
(d) Ag / Ag / ZnO	7.02	0.63	0.59	2.63

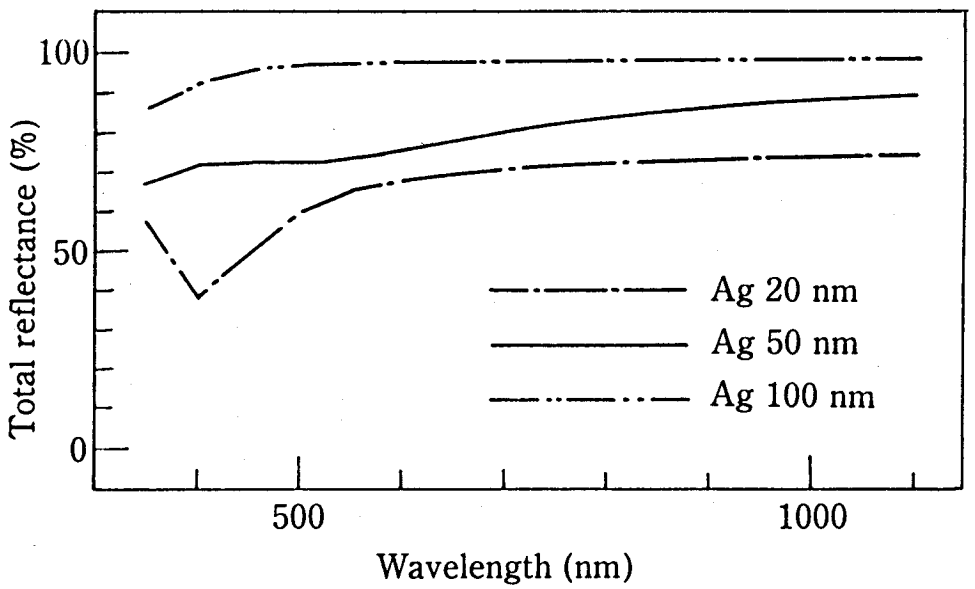

Fig. 6-2-3. Total reflectance of silver rear reflectors.

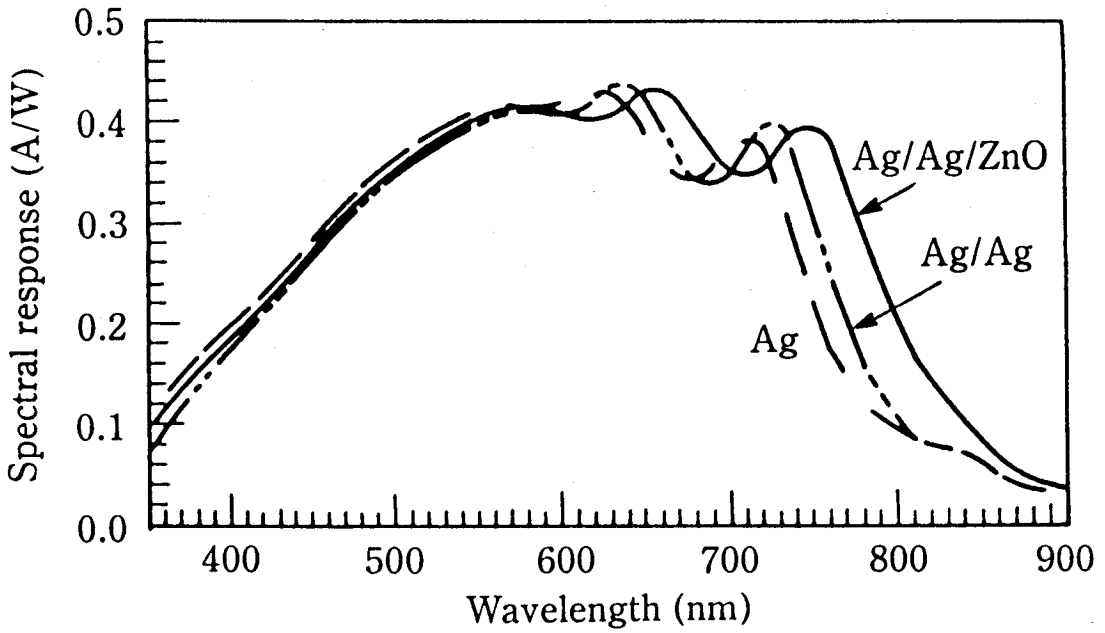

Fig. 6-2-4. Spectral responses of a-SiGe cells with various rear reflectors.

6-3. Inserting of ZnO film

To improve the optical confinement moreover, inserting of a ZnO film between the textured double-silver rear reflector and the a-Si alloy layer was investigated. The ZnO film was deposited by electron beam evaporation. The refractive index of ZnO film was about 2.0 at wavelengths of visible light, the resistivity was 1.7×10^{-2} $(S/cm)^{-1}$, and the absorption of visible light was very small. The a-SiGe cell with a bandgap profile and a ZnO / textured double-silver reflector was prepared. The thickness of the ZnO film was 100 nm. The characteristics under the red light and the spectral response of the a-SiGe cell are shown in Table 6-2-1 (d) and Fig. 6-2-4. The spectral response at long wavelengths of light is improved and the I_{sc} is increased by 22% over that of the cell with the textured double-silver reflector. The I_{sc} of the cell with a ZnO / smooth silver reflector is not increased. Therefore, it is considered that the I_{sc} is improved by optical confinement owing to the combination of the ZnO film and the textured silver film.

As a result, using the ZnO / textured double-silver reflector, the Isc of the bandgap profiling a-SiGe cell under the red light is increased by 33% as compared with that of the cell with single 100 nm thick silver rear reflector.

6-4. Glass / Textured SnO_2 Substrates

Texturing of rear silver reflector has been investigated to increase the light scattering, as mentioned above. Next, to increase the light scattering more over, use of glass / textured SnO_2 substrates was investigated. The SnO_2 films were deposited by Chemical Vapor Deposition (CVD) technique and their roughness could be made large. Silver films were evaporated at a substrate temperature of 150℃ to cover the whole substrates while keeping the roughness.

The total reflectance increases as the thickness of the evaporated silver film is increased, as shown in Fig. 6-4-1, and it shows a tendency of saturation when the silver film is evaporated more than 125 nm. Figure 6-4-2 (a) and (b) shows the Scanning Tunneling Microscopy (STM) images of the glass / textured SnO_2 and the glass / textured SnO_2 /Ag (125 nm).

From Fig. 6-4-1 and Fig. 6-4-2, glass / textured SnO_2 /Ag (125 nm) has high total reflectance keeping the roughness.

The a-SiGe cells with bandgap profile were prepared by using S.S. / Ag / Ag / ZnO, glass / textured SnO_2 / Ag(125 nm) and glass / textured SnO_2 / Ag(125 nm)/ ZnO(10 nm) substrates. The characteristics of a-SiGe cells with various substrates under the red light [AM 1, 100 mW/cm^2 light through a red (wavelength > 660 nm) cut-on-filter] are shown in Table 6-4-1. The Isc is increased by 4% furthermore as compared with that of the cell with the S.S./Ag/Ag/ZnO substrate.

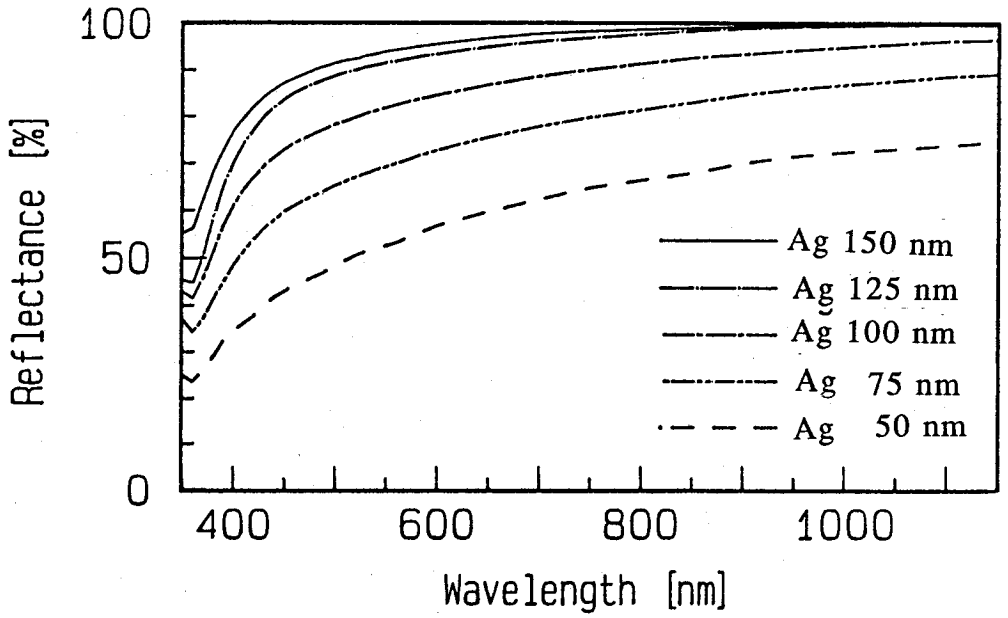

Fig. 6-4-1. Reflectance of a-SiGe cells with glass / textured SnO_2 /Ag substrates versus thicknesses of Ag.

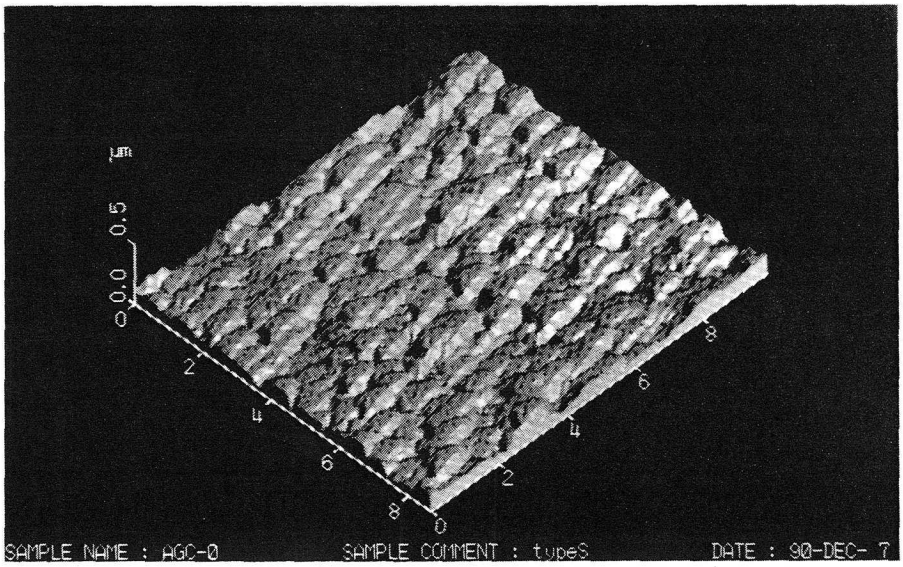

(a) Glass / textured SnO_2

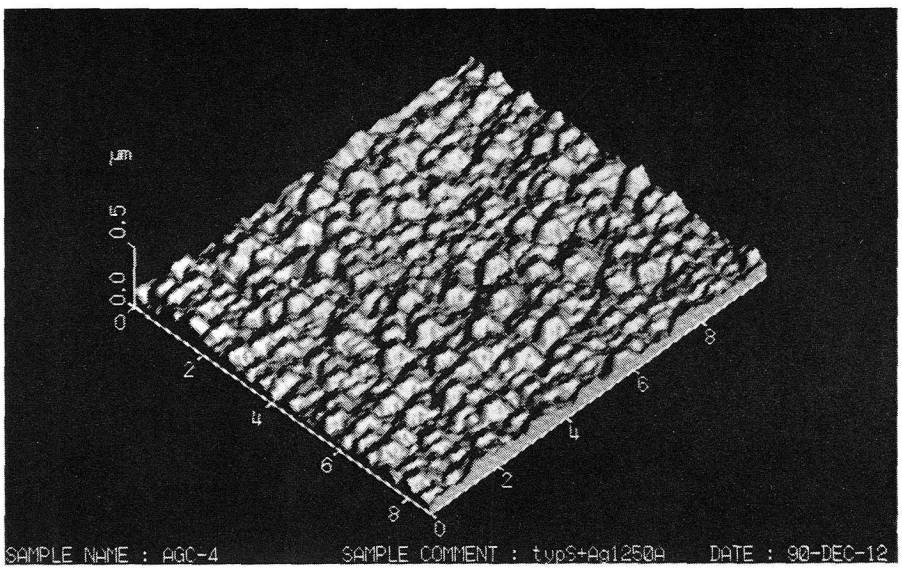

(b) Glass / textured SnO_2 /Ag (125 nm)

Fig. 6-4-2. Scanning Tunneling Microscopy (STM) images of glass / textured SnO_2 (a) and glass / textured SnO_2 /Ag(125 nm) (b).

Table 6-4-1. Characteristics of a-SiGe cells with bandgap profiles and various substrates under red light.

[I_{sc}: Short circuit current V_{oc}: Open circuit voltage
F.F.: Fill factor P_{max}: Maximum output power]

	I_{sc} (mA/cm^2)	V_{oc} (V)	F.F.	P_{max} (mW/cm^2)
(a) Ag / Ag / ZnO	7.73	0.62	0.58	2.75
(b) Glass / textured SnO_2 / Ag	6.03	0.54	0.62	2.01
(c) Glass / textured SnO_2 / Ag / ZnO	8.07	0.56	0.62	2.80

6-5. MgF_2 / ITO Double Anti-reflection Coating

Technologies of optical confinement at the rear side of the solar cells, namely texturing of rear reflector and inserting of oxide film, was investigated, as mentioned above. Next, technology of optical confinement at the frond side of the solar cells was investigated.

Indium Tin Oxide (ITO) films are usually deposited as both transparent conductive electrodes and anti-reflection coatings (ARC). But, the reflectance of single ARC can be made zero at one wavelength and the reflectance is larger at the other wavelengths. Therefore, MgF_2 / ITO double ARC was investigated to decrease the reflectance for a wide range of wavelengths. The refractive indexes of MgF_2 and ITO are 1.38 and 2.0 respectively.

The a-SiGe cell with the bandgap profile [optical bandgap (Egopt): 1.42 eV~ 1.75 eV] and MgF_2 / ITO double ARC was prepared. The glass / textured SnO_2 / Ag / ZnO substrate was used. The film thicknesses of MgF_2 and ITO were 79 nm and 63 nm respectively. The reflectance, spectral response and solar cell characteristics under the AM 1, 100 mW/cm^2 light of the a-SiGe cell are shown in Fig. 6-5-1 (a), (b) and Table 6-5-1. Figure 6-5-1 shows that the reflectance decreases and the spectral response increases for a wide range of wavelengths by using the MgF_2 / ITO double ARC.

As a result, the Isc of the cell with MgF_2 / ITO double ARC under the AM 1, 100 mW/cm^2 light is increased by 3 % as compared with that of the cell with ITO single ARC.

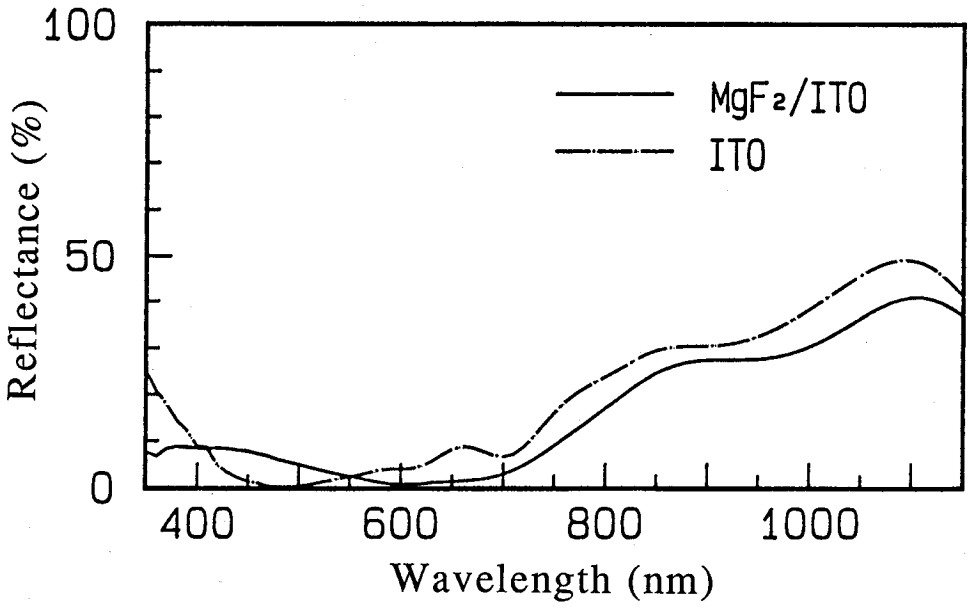

(a) Reflectance

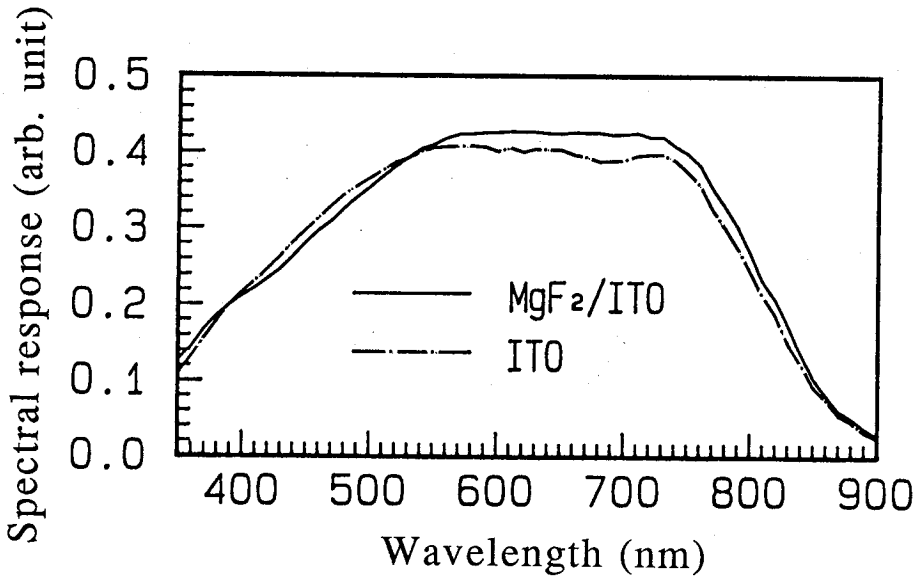

(b) Spectral response

Fig. 6-5-1. Reflectance (a) and spectral response (b) of the a-SiGe cell with MgF_2 / ITO double ARC.

Table 6-5-1. Characteristics of a-SiGe cells with MgF_2 / ITO double ARC under AM 1, 100 mW/cm^2 light.

[I_{sc}: Short circuit current V_{oc}: Open circuit voltage
F.F.: Fill factor P_{max}: Maximum output power]

	I_{sc} (mA/cm^2)	V_{oc} (V)	F.F.	P_{max} (mW/cm^2)
(a) ITO single ARC	23.3	0.64	0.56	8.45
(b) MgF_2 / ITO double ARC	24.0	0.64	0.56	8.61

6-6. Summary

The technologies of the optical confinement, namely rear reflector and anti-reflection coating, were investigated to improve the conversion efficiency. The results from these investigations are the following:

(1) Using the S.S. / Ag / Ag / ZnO reflector, the short circuit current of the a-SiGe cell with bandgap profile under the red light is increased by 33% as compared with that of the cell with single silver rear reflector.

(2) Using the glass / textured SnO_2 / Ag / ZnO substrate, the short circuit current of the a-SiGe cell with bandgap profile under the red light is increased by 4 % furthermore as compared with that of the cell with the S.S. / Ag / Ag / ZnO substrate.

(3) Using the MgF_2 / ITO double ARC, the short circuit current of the a-SiGe cell with bandgap profiling under the AM 1, 100 mW/cm^2 light is increased by 3 % as compared with that of the cell with ITO single ARC.

REFERENCES

1) Y. Nakata, Y. Inoue, H. Sannomiya, K. Nomoto, A. Yokota, M. Itoh and T. Tsuji: OPTOELECTRONICS - Devices and Technologies, Vol. 6, No.1, (1991) 141.

2) M. Kaneiwa, K. Nomoto, M. Itoh, Y. Yamamoto, Y. Nakata and T. Inoguchi: Tech. Digest of 4th Int. Photovol. Sci. Engi. Conf., Sydney (1989) 673.

3) Y. Nakata and T. Inoguchi: OPTOELECTRONICS - Devices and Technologies,Vol. 4, No. 1, (1989) 75.

4) T. Kobe, Y. Nakata, T. Machida, Y. Yamamoto and T. Tsuji: Proc. 18th IEEE Photovol. Spec. Conf., Las Vegas (1985) 1594.

5) A. Yokota, H. Sannomiya, S. Moriuchi, Y. Inoue, M. Itoh, Y. Nakata and T. Tsuji: Tech. Digest of 5th Int. Photovol. Sci. Engi. Conf., Kyoto (1990) 637.

6) Y. Nakata, A. Yokota, H. Sannomiya, S. Moriuchi, Y. Inoue, K. Nomoto, M. Itoh and T. Tsuji: Mat. Res. Soc. Symp. Proc., Vol. 219 (1991) 433.

7) Y. Nakata, A. Yokota, H. Sannomiya, S. Moriuchi, Y. Inoue, K. Nomoto, M. Itoh and T. Tsuji: Jpn. J. Appl. Phys., Vol. 31, No. 2A, Part 1 (1992) (in press)

8) K. Nomoto, Y. Takeda, S. Moriuchi, H. Sannomiya, T. Okuno, A. Yokota, M. Kaneiwa, M. Itoh, Y. Yamamoto, Y. Nakata and T. Inoguchi: Tech. Digest of 4th Int. Photovol. Sci. Engi. Conf., Sydney (1989) 85.

9) S. Moriuchi, Y. Inoue, H. Sannomiya, A. Yokota, M. Itoh, Y. Nakata and H. Itoh: Proc. 21st IEEE Photovol. Spec. Conf., Florida (1990) 1449.

10) Y. Nakata, H. Sannomiya, S. Moriuchi, A. Yokota, Y. Inoue, M. Itoh and H. Itoh: Mat. Res. Soc. Symp. Proc., Vol. 192 (1990) 15.

11) H. Sannomiya, S. Moriuchi, Y. Inoue, K. Nomoto, A. Yokota, M. Itoh, Y. Nakata and T. Tsuji: Tech. Digest of 5th Int. Photovol. Sci. Engi. Conf., Kyoto (1990) 387.

12) Y. Nakata, H. Sannomiya, S. Moriuchi, Y. Inoue, K. Nomoto, A. Yokota, M. Itoh and T. Tsuji: OPTOELECTRONICS - Devices and Technologies , Vol. 5, No. 2, (1990) 209.

VII. DEVELOPMENT OF HIGHLY STABLE MULTI-BANDGAP a-Si ALLOY STACKED SOLAR CELLS

7-1. Introduction

To use a-Si solar cells as a future new energy source, an important key issue is improvement of the stability as well as the conversion efficiency. A multi-bandgap stacked solar cell using a-Si alloy materials is one of the most promising cell structures to obtain both of high stability and high conversion efficiency. The material technologies, analytical technologies, and device technologies which include bandgap profiling [1-4] and optical confinement, [3] have been investigated in order to apply these technologies to this multi-bandgap a-Si alloy stacked solar cells, as mentioned in the previous chapters. By using these technologies totally, multi-bandgap a-Si alloy stacked solar cells were developed to obtain high stability and high conversion efficiency.

In this chapter, potential of multi-bandgap a-Si alloy stacked solar cells on stability and conversion efficiency is described. The characteristics of a-Si/a-Si/a-SiGe stacked solar cells [5] and a-SiC/a-Si/a-SiGe multi-bandgap stacked solar cells [1-4] with high stability and high conversion efficiency are presented.

7-2. Potential of Multi-bandgap Stacked Solar Cells

7-2-1. Light-induced degradation of stacked solar cells

Potential of multi-bandgap stacked cells on light-induced degradation was investigated. [3] To confirm the light-induced degradation of stacked solar cells, single, tandem, and triple cells were prepared. The p-, p/i- and n-layers were made from a-SiC:H, a-SiC:H where carbon composition was graded, and a-Si:H, respectively. The i-layer of each component cell was made from a-SiC:H, a-Si:H and a-SiGe:H. The substrate of the cells is stainless steel (S.S.) sheet. They were coated by evaporated 50 nm thick Ti films to increase the adhesion between the S.S. sheets and the silver rear reflectors.

Light-induced degradation in the characteristics of single, tandem, and triple cells were compared. The cells were exposed to AM 1, 100 mW/cm^2 light under the maximum output condition. The conversion efficiencies which are normalized by initial values are shown in Fig. 7-2-1. As the number of component cells is increased from one to three, the light-induced degradation of the cell is decreased. The thickness of each component cell in the stacked cell is thinner and the electric field inside the cell is higher than in the case of the single cell. Therefore, the light-induced defects are decreased because recombination of photo-generated carriers, which creates the defects, is decreased owing to the high electric field. Moreover, the light-induced defects in the i-layers cause small degradation in the conversion efficiency because photo-generated carriers are drifted efficiently by the high electric field. If the number of the component cells is increased to more than four, the initial efficiency is decreased, because the photo-generated carriers at the p- and n-layers cannot be collected and the loss of the collection at the layers is increased. Therefore, the three-stacked cell structure is useful in obtaining high stability.

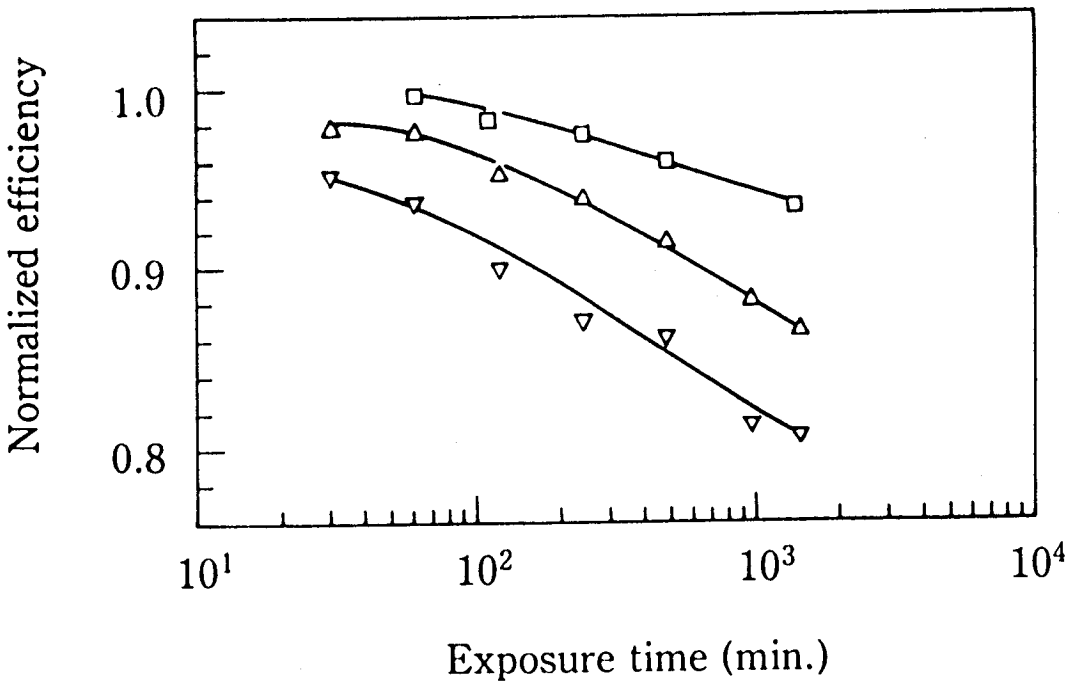

Fig. 7-2-1. Light-induced degradation in conversion efficiencies of single, tandem, and triple amorphous silicon solar cells under AM 1, 100 mW/cm^2 light which is normalized by initial values. (▽:a-Si single cell, △:a-Si/a-Si tandem cell, □: a-SiC/a-Si/a-SiGe triple cell).

7-2-2. Theoretical efficiency of multi-bandgap stacked solar cells

As shown above, the three-stacked cell structure is useful to obtain high stability. Moreover, if the solar cells with different optical bandgap materials are stacked in the order of decreasing optical bandgap from the light incident side, they would be expected to obtain high efficiency. As an ideal estimate, it was reported that a multi-bandgap three-stacked cell with an initial efficiency of 24% was possible.[6] The realistic initial efficiency of the multi-bandgap three-stacked cells have been estimated by applying Crandall's model.[7] Figure 7-2-2 shows the initial efficiency of the multi-bandgap three-stacked cells plotted for the two optical bandgaps of the top and bottom cells. The optical bandgap of the middle cell was fixed at 1.75 eV. It was assumed that the mobility · lifetime ($\mu\ \tau$) products of a-SiC:H, a-Si:H, and a-SiGe:H can be improved to 4, 16, and 7 $\times$ 10^{-9} cm^2/V, respectively, and they were twice as high as the present values. If a-Si alloy materials with optical bandgap of about 1.85 eV, 1.75 eV and 1.45 eV are applied to the i-layers of the multi-bandgap stacked cells, an initial efficiency of 15 % is achieved. As i-layer thickness of a-Si cell is decreased, efficiency is usually decreased but stability is improved. If the i-layer thickness of each component cell is decreased to obtain high stability for the stacked cell with the initial efficiency of 15%, an initial efficiency of 12% and a degradation ratio of 5% in the first year are estimated for the multi-bandgap three-stacked solar cell using the same model.

To summarize the potential of the stability and the efficiency of the cell, the multi-bandgap three-stacked solar cell is expected to be one of the most promising cell structures with high efficiency and high stability.

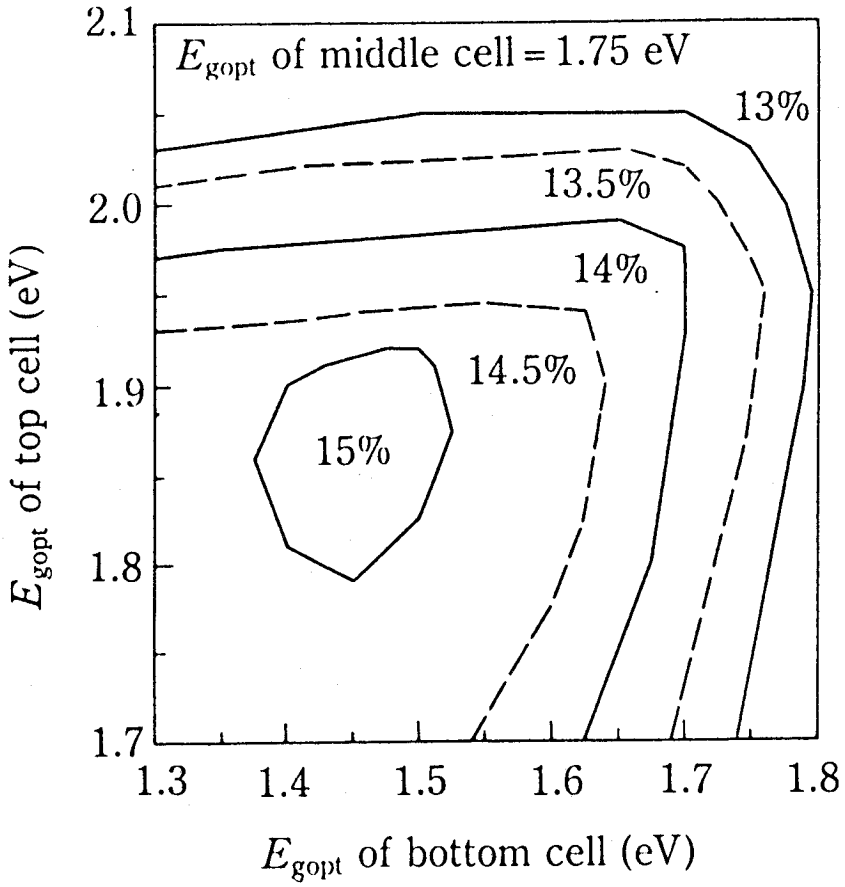

Fig. 7-2-2. Calculated initial efficiency of multi-bandgap three stacked solar cells for two optical bandgaps (E_{gopt}) of the top and bottom cells. (E_{gopt} of middle cell = 1. 7 5 eV).

7-3. Characteristics of a-Si/a-Si/a-SiGe Stacked Solar Cells

7-3-1. a-Si/a-Si/a-SiGe stacked solar cell with high initial efficiency

First, a-Si/a-Si/a-SiGe stacked solar cells were developed.[5] The cell structure and bandgap profile are shown in Figs. 7-3-1 (a) and (b). High quality a-SiGe:H, which is mentioned in section 2-3, was applied to the bottom cell and high quality a-SiC:H were applied to the three p/i interface layers, [8] as described in sub-section 2-2-3. In this case, single silver rear reflector was used and bandgap profiling has not applied yet. The cell size is 1 cm $\times$ 1 cm.

For the stacked solar cells, it is essential to balance the output currents of component cells with each other because the output current of the stacked solar cells is limited by the lowest current among them of the component cells. [9,10] To obtain a stacked solar cell with a high conversion efficiency, it is necessary to design the optimum i-layer thicknesses of the component cells taking account of the current balance in each component cell. Therefore, the i-layer thicknesses of the component cells were designed to obtain high short circuit current at the initial stage by using the new method for measuring full current-voltage (I-V) characteristic of each component cell, [5] which was stated in sub-section 3-4-1.

As a result, an initial efficiency of 10.7 % (I_{sc} = 6.77 mA/cm^2, V_{oc}= 2.36 V, and F.F. = 0.67) has been obtained, as shown in Fig. 7-3-2.[5]

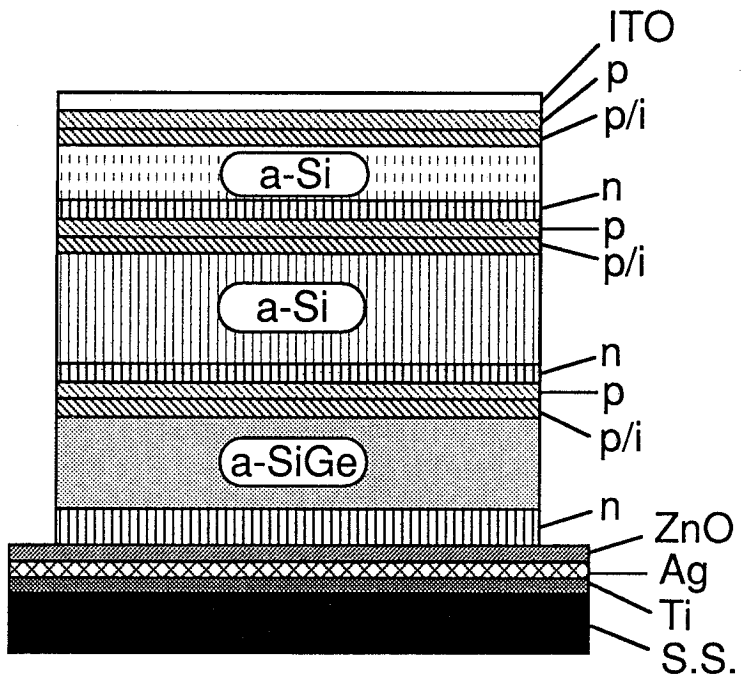

(a) Cell structure

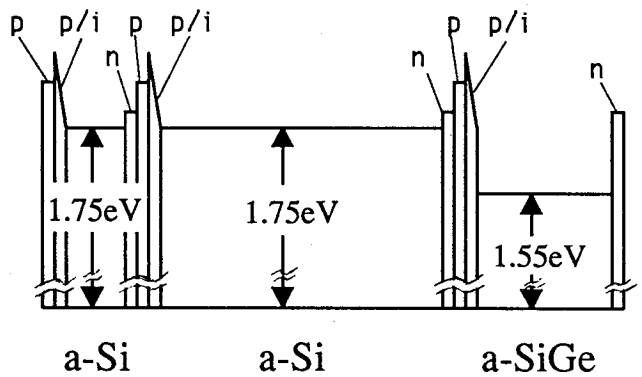

(b) Bandgap profile

Fig. 7-3-1. Cell structure (a) and bandgap profile (b) of a-Si/a-Si/a-SiGe stacked solar cell.

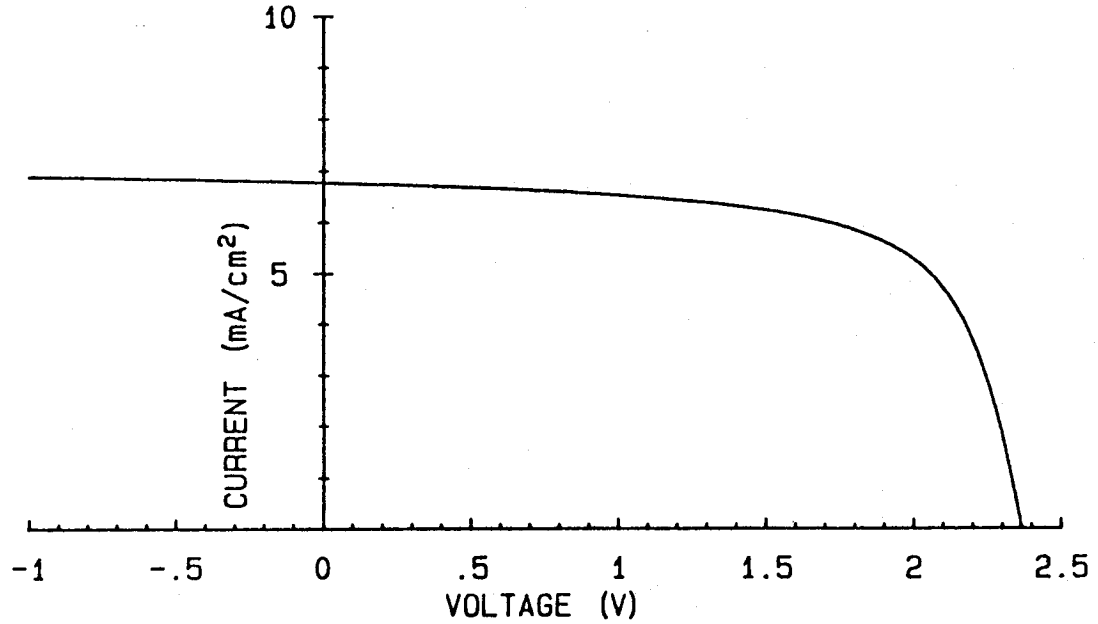

	I_{sc} (mA/cm^2)	V_{oc} (V)	F.F.	η (%)
a-Si/a-Si/a-SiGe cell	6.77	2.36	0.67	10.7

Fig. 7-3-2. Voltage-current and solar cell characteristics of a-Si/a-Si/a-SiGe stacked solar cell.

$\left\{ \begin{array}{ll} I_{sc}: \text{Short circuit current} & V_{oc}: \text{Open circuit voltage} \\ \text{F.F.}: \text{Fill factor} & \eta : \text{Conversion efficiency} \end{array} \right\}$

7-3-2. a-Si/a-Si/a-SiGe stacked solar cell with high stability and high efficiency

To improve the light-induced degradation in a-Si/a-Si/a-SiGe stacked cells, The light-induced degradation in the stacked cells which have i-layers with various thicknesses was analyzed by using the new measuring method of individual I-V characteristics of component cells, [5] as mentioned in sub-section 3-4-2. Moreover, the characteristics of component cells after light exposure were predicted by using the function, [11-13] which was described in section 4-3. And the optimum i-layer thicknesses of component cells have been designed taking account of the balance of the currents after light exposure to obtain high stability.

The light-induced degradation characteristics of the a-Si/a-Si/a-SiGe stacked solar cell under AM 1.5, 100 mW/cm^2 light and maximum output condition are shown in Fig. 7-3-3. [5] The characteristics of the stacked solar cell before and after 550 hours' exposure to AM 1.5, 100 mW/cm^2 light are shown in Table 7-3-1. As a result, an initial conversion efficiency of 10.0% and a degradation ratio of 10% in the first year have been obtained. The degradation ratio in the first year was estimated from the efficiency after 550 hours' exposure to AM 1.5, 100 mW/cm^2 light by using the new accelerated test method, [11-13] which was stated in section 4-5.

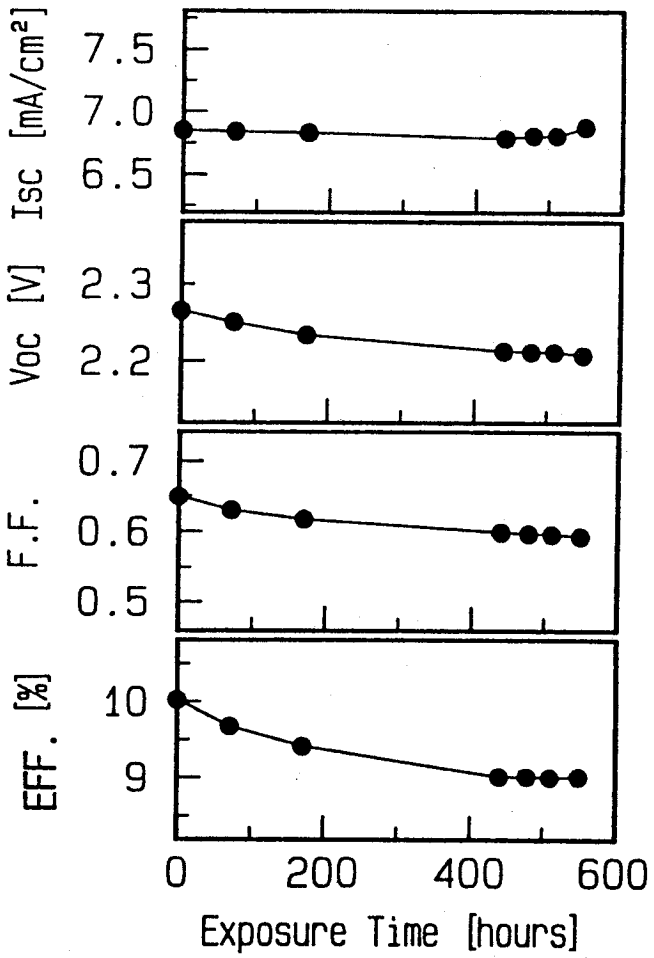

Fig. 7-3-3. Light-induced degradation characteristics of a-Si/a-Si/a-SiGe stacked solar cell under AM 1.5, 100 mW/cm^2 light and maximum output

Table 7-3-1. Characteristics of a-Si/a-Si/a-SiGe stacked solar cell before and after 550 hours' exposure to AM 1.5, 100 mW/cm^2 light under maximum output condition.

(I_{sc}: Short circuit current V_{oc}: Open circuit voltage
F.F.: Fill factor η : Conversion efficiency)

	I_{sc} (mA/cm^2)	V_{oc} (V)	F.F.	η (%)
Before light exposure	6.85	2.27	0.65	10.0
After light exposure	6.88	2.21	0.59	9.0

7-4. Characteristics of a-SiC/a-Si/a-SiGe stacked solar cells

7-4-1. a-SiC/a-Si/a-SiGe stacked solar cell with high initial efficiency

Multi-bandgap stacked solar cells, in which component solar cells with different optical bandgap materials are stacked in the order of decreasing optical bandgap from the light incident side, is expected to obtain high efficiency and high stability, [3] as mentioned in section 7-2. Therefore, a-SiC/a-Si/a-SiGe stacked solar cells were developed.[1-4]

The cell structure and bandgap profile of a-SiC/a-Si/a-SiGe stacked solar cells are shown in Figs. 7-4-1 (a) and (b) respectively. The cell size is 1 cm × 1 cm. The bandgap profiling was applied to the a-SiC top cell and the a-SiGe bottom cell, [1-4] and minimum bandgap distance from the p-layer in the a-SiGe bottom cell is 40 nm, [4] as described in section 5-6. The substrate is a ZnO / silver / textured SnO_2 / glass, which was stated in section 6-4, and MgF_2 / Indium Tin Oxide (ITO) double anti-reflection coating (ARC) was used, as mentioned in section 6-5.

As a result, an initial efficiency of 11.0 % (I_{sc} = 6.81 mA/cm^2, V_{oc} = 2.39 V, and F.F. = 0.68) has been obtained, as shown in Fig. 7-4-2.[2-4]

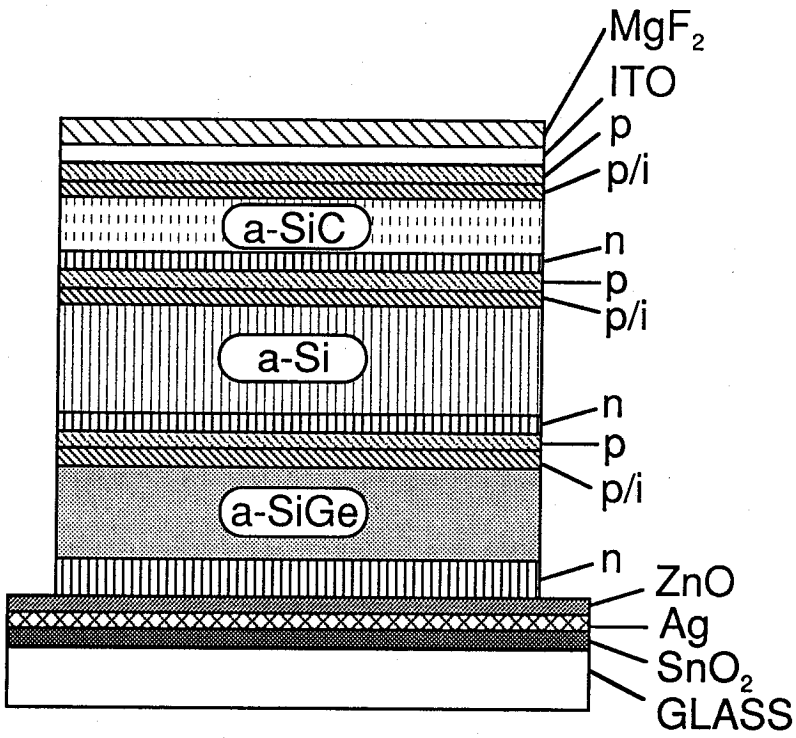

(a) Cell structure

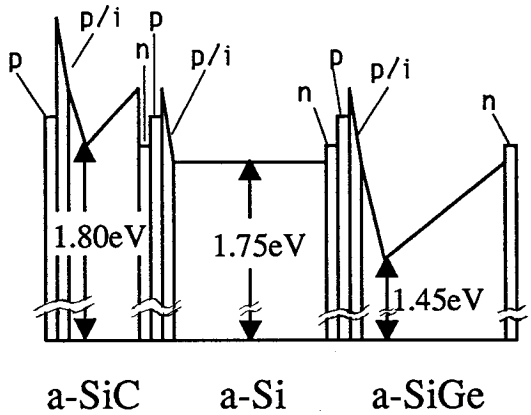

(b) Bandgap profile

Fig. 7-4-1. Cell structure (a) and bandgap profile (b) of a-SiC/a-Si/a-SiGe stacked solar cell.

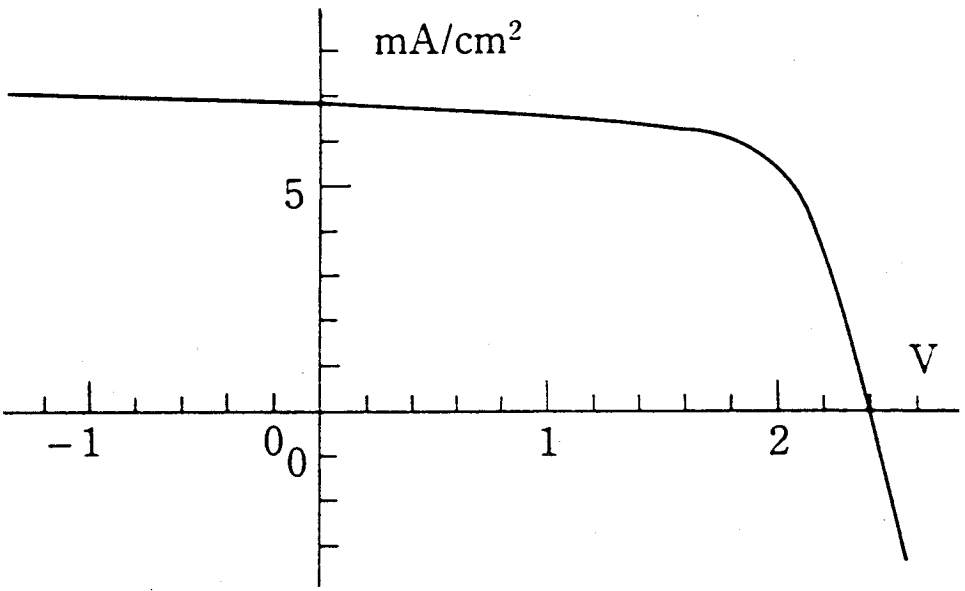

	I_{sc} (mA/cm²)	V_{oc} (V)	F.F.	η (%)
a-SiC/a-Si/a-SiGe cell	6.81	2.39	0.68	11.0

Fig. 7-4-2. Voltage-current and solar cell characteristics of a-SiC/a-Si/a-SiGe stacked solar cell.

[I_{sc}: Short circuit current V_{oc}: Open circuit voltage
F.F.: Fill factor η : Conversion efficiency]

7-4-2. a-SiC/a-Si/a-SiGe stacked solar cell with high stability and high efficiency

To improve the light-induced degradation in a-SiC/a-Si/a-SiGe stacked cells, the light-induced degradation in the stacked cells which have i-layers with various thicknesses was analyzed by using the new measuring method of individual I-V characteristics of component cells, [5] as mentioned in sub-section 3-4-2. And the optimum i-layer thicknesses of component cells have been designed taking account of the balance of the currents after light exposure to obtain high stability. In addition, the minimum bandgap in the a-SiGe bottom cell was positioned at 10 nm from the p-layer to improve the stability, [4] as described in sub-section 5-6-2. The light-induced degradation characteristics of the a-SiC/a-Si/a-SiGe stacked solar cells under AM 1.5, 100 mW/cm^2 light and maximum output condition are shown in Fig. 7-4-3. The light-induced degradation of the stacked solar cells, which is designed to obtain high stability, is decreased as compared with the stacked solar cell which is designed to obtain high initial efficiency and minimum bandgap distance from the p-layer is 40 nm. The characteristics of the stacked solar cell with high stability before and after 550 hours' exposure to AM 1.5, 100 mW/cm^2 light were shown in Table 7-4-1. As a result, an initial conversion efficiency of 10.7 % and a light-induced degradation ratio of 14 % in the first year was obtained. [4] The degradation ratio in the first year was estimated from the efficiency after 550 hours' exposure to AM 1.5, 100 mW/cm^2 light at maximum output power condition using the new accelerated test method of light-induced degradation, [10-12] which was stated in section 4-5.

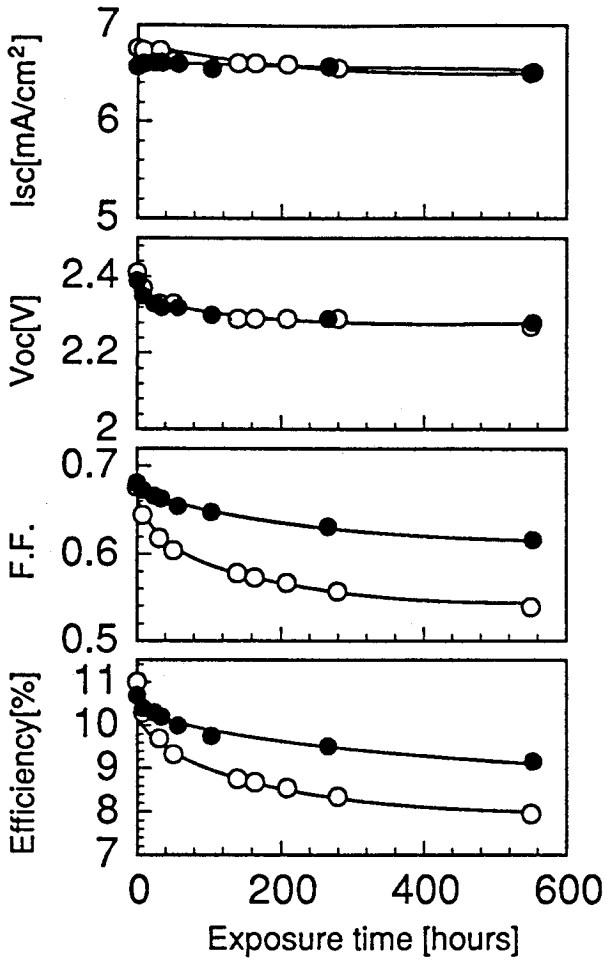

Fig. 7-4-3. Light-induced degradation characteristics of a-SiC/a-Si/a-SiGe stacked solar cells, which are designed to obtain high initial efficiency (○) and high stability (●), under AM 1.5, 100 mW/cm^2 light and maximum output condition.

Table 7-4-1. Characteristics of a-SiC/a-Si/a-SiGe stacked solar cell which is designed to obtain high stability before and after 550 hours' exposure to AM 1.5, 100 mW/cm^2 light under maximum output condition.

[I_{sc}: Short circuit current V_{oc}: Open circuit voltage
F.F.: Fill factor η : Conversion efficiency]

	I_{sc} (mA/cm^2)	V_{oc} (V)	F.F.	η (%)
Before light exposure	6.57	2.39	0.68	10.7
After light exposure	6.51	2.28	0.62	9.2

7-5. Summary

By using the technologies as mentioned in the previous chapters, a-Si/a-Si/a-SiGe stacked solar cells and a-SiC/a-Si/a-SiGe multi-bandgap stacked solar cells were developed to obtain high stability and high conversion efficiency. The results from this development are as follows.

(1) It is shown by the experimental and theoretical data that the multi-bandgap three-stacked solar cell is expected to be one of the most promising cell structures with high efficiency and high stability.

(2) At the a-Si/a-Si/a-SiGe stacked solar cells, an initial efficiency of 10.7 % (I_{sc} = 6.77 mA/cm^2, V_{oc}= 2.36 V, and F.F. = 0.67) has been obtained. Moreover, designing to obtain high stability, an initial conversion efficiency of 10.0 % and degradation ratio of 10 % in the first year have been obtained.

(3) At the a-SiC/a-Si/a-SiGe stacked solar cells, an initial efficiency of 11.0 % (I_{sc} = 6.81 mA/cm^2, V_{oc}= 2.39 V, and F.F. = 0.68) has been obtained. Moreover, designing to obtain high stability, an initial conversion efficiency of 10.7 % and degradation ratio of 14 % in the first year have been obtained.

These characteristics of the multi-bandgap a-Si alloy stacked solar cells are shown in Table 7-5-1.

Table 7-5-1. Characteristics of the multi-bandgap a-Si alloy stacked solar cells with high efficiency and high stability.

Cell Structure	Initial Efficiency (%)	Degradation ratio in the first year (%/Y)	References
a-Si/a-Si/a-SiGe	10.7	—	5
	10.0	10	5
a-SiC/a-Si/a-SiGe	11.0	—	2 - 4
	10.7	14	4

REFERENCES

1) Y. Nakata, H. Sannomiya, S. Moriuchi, A. Yokota, Y. Inoue, M. Itoh and H. Itoh: Mat. Res. Soc. Symp. Proc., Vol. 192 (1990) 15.

2) H. Sannomiya, S. Moriuchi, Y. Inoue, K. Nomoto, A. Yokota, M. Itoh, Y. Nakata and T. Tsuji: Tech. Digest of 5th Int. Photovol. Sci. Engi. Conf., Kyoto (1990) 387.

3) Y. Nakata, H. Sannomiya, S. Moriuchi, Y. Inoue, K. Nomoto, A. Yokota, M. Itoh and T. Tsuji: OPTOELECTRONICS - Devices and Technologies , Vol. 5, No. 2, (1990) 209.

4) Y. Nakata (Editors: Y. Sakurai, K. Suzuki, T. Masumoto, K. Shirae, Y. Hamakawa): PROGRESS IN AMORPHOUS MATERIALS - Science and Technology - (Elsevier Science Publishers B. V., Amsterdam, to be published in 1992) sub-section 4.5.4.

5) S. Moriuchi, Y. Inoue, H. Sannomiya, A. Yokota, M. Itoh, Y. Nakata and H. Itoh: Proc. 21st IEEE Photovol. Spec. Conf., Florida (1990) 1449.

6) S. Tsuda, N. Nakamura, Y. Nakashima, H. Tarui, H. Nishiwaki, M. Ohnishi, and Y. Kuwano, Jpn. J. Appl. Phys., 21, Suppl. 21-2 (1982) 251.

7) R. S. Crandall, RCA Rev., 42 (1981) 441.

8) K. Nomoto, Y. Takeda, S. Moriuchi, H. Sannomiya, T. Okuno, A. Yokota, M. Kaneiwa, M. Itoh, Y. Yamamoto, Y. Nakata and T. Inoguchi: Tech. Digest of 4th Int. Photovol. Sci. Engi. Conf., Sydney (1989) 85.

9) M. Kaneiwa, K. Nomoto, M. Itoh, Y. Yamamoto, Y. Nakata and T. Inoguchi: Tech. Digest of 4th Int. Photovol. Sci. Engi. Conf., Sydney (1989) 673.

10) Y. Nakata and T. Inoguchi: OPTOELECTRONICS - Devices and Technologies,Vol. 4, No. 1, (1989) 75.

11) A. Yokota, H. Sannomiya, S. Moriuchi, Y. Inoue, M. Itoh, Y. Nakata and T. Tsuji: Tech. Digest of 5th Int. Photovol. Sci. Engi. Conf., Kyoto (1990) 637.

12) Y. Nakata, A. Yokota, H. Sannomiya, S. Moriuchi, Y. Inoue, K. Nomoto, M. Itoh and T. Tsuji: Mat. Res. Soc. Symp. Proc., Vol. 219 (1991) 433.

13) Y. Nakata, A. Yokota, H. Sannomiya, S. Moriuchi, Y. Inoue, K. Nomoto, M. Itoh and T. Tsuji: Jpn. J. Appl. Phys., Vol. 31, Part 1, No. 2 (1992) (in press)

VIII. CONCLUSIONS

A series of systematic studies has been carried out on multi-bandgap amorphous silicon (a-Si) alloy stacked solar cells to increase stability. An important key issue for practical power uses of a-Si solar cells is improvement of stability for light-induced degradation as well as conversion efficiency. This key issue has been approached from three directions of material, analytical, and device technologies. The main results obtained in this thesis work are enumerated as follows:

(1) It has been clarified that there is the optimum hydrogen dilution ratio of 10～30 to obtain a-SiC:H films with higher photo-conductivity and higher electron and hole mobilities. By applying these high quality a-SiC:H films to p/i interface layers, the conversion efficiencies of the a-Si:H solar cells are improved. The high quality a-SiC:H films also were applied to the photovoltaic active layer in order to use them as a component solar cell at the light incident side in the multi-bandgap solar cell. The a-SiC:H cells with higher open circuit voltage than a-Si:H cell have been obtained.

(2) As a result of improvement of film quality, the a-Si alloy materials, namely a-SiGe:H, a-Si:H and a-SiC:H, having a photo-conductivity of more than 10^{-5} S/cm were obtained for a wide range of optical bandgap, from 1.39 eV to 2.0 eV. Therefore, these materials with high quality allow us to apply the bandgap control technologies to the multi-bandgap stacked solar cell, the bandgap profiling and so on in order to improve the solar cell characteristics.

(3) On the bases of the methods for measuring spectral photo-response, a new method for measuring individual full current - voltage (I-V) characteristics of component cells in stacked cell has been proposed, by fitting theoretical I-V characteristic to experimental data of output currents that are calculated from spectral photo-response.

(4) Using above new method, the light-induced degradation of each component cell in a-Si alloy stacked solar cells has been demonstrated, and it was shown that the new method is very useful to analyze the light-induced degradation of each component cell and to design the stacked cells with high stability.

(5) It is clarified that the light-induced degradation characteristics of the conversion efficiency of a-Si alloy single-junction solar cells under the condition of the various light intensities and bias voltages can be described by a function as follows:

$$\eta(t) / \eta_0 = f(N_c^{\gamma} R_r^{\beta} t)$$

where N_c is the ratio of the exposure light intensity to 1 sun, R_r is the ratio of recombined carriers in the cell to photo-generated carriers, γ and β are characteristic constants. The result also indicates that the light-induced degradation characteristics of a-Si alloy solar cells, which contain a-Si alloy component cells in stacked solar cells, under the condition of the arbitrary light intensities and bias voltages can be predicted from a series of light-induced degradation data under some light intensities and bias voltages.

(6) Using above analytical formula, a new accelerated test method of light-induced degradation of a-Si alloy solar cells has been proposed by using solar simulator indoor measurement instead of natural sunlight outdoor testing. The validity of the new accelerated test method has been confirmed experimentally.

(7) The physical mechanism of the bandgap profiling on the solar cell characteristics has been clarified. The largest effect is the profile of the photo-generated carriers. The bandgap profiling is effective to optimize the collection of photo-generated electrons and holes.

(8) On the basis of the physical mechanism of the bandgap profiling on the solar cell characteristics, the bandgap profiles of the a-SiC:H cells and the a-SiGe:H cells were designed to apply them to the multi-bandgap a-Si alloy staked solar cells. As a result, the component cells with the high efficiency and the high stability have been obtained.

(9) Using the S.S. / Ag / Ag / ZnO reflector, the short circuit current of the a-SiGe cell with bandgap profile under the red light is increased by 33% as compared with that of the cell with single silver rear reflector.

(10) Using the glass / textured SnO_2 / Ag / ZnO substrate, the short circuit current of the a-SiGe cell with bandgap profile under the red light is increased by 4 % furthermore as compared with that of the cell with the S.S. / Ag / Ag / ZnO substrate.

(11) Using the MgF_2 / Indium Tin Oxide (ITO) double anti-reflection coating (ARC), the short circuit current of the a-SiGe cell with bandgap profiling under the AM 1, 100 mW/cm^2 light is increased by 3 % as compared with that of the cell with ITO single ARC.

(12) By using the technologies as mentioned above, at the a-Si/a-Si/a-SiGe stacked solar cells, an initial efficiency of 10.7 % (I_{sc} = 6.77 mA/cm^2, V_{oc}= 2.36 V, and F.F. = 0.67) has been obtained. Moreover, designing to obtain high stability, an initial conversion efficiency of 10.0 % and degradation ratio of 10 % in the first year have been obtained.

(13) By using the technologies as mentioned above, at the a-SiC/a-Si/a-SiGe stacked solar cells, an initial efficiency of 11.0 % (I_{sc} = 6.81 mA/cm^2, V_{oc}= 2.39 V, and F.F. = 0.68) has been obtained. Moreover, designing to obtain high stability, an initial conversion efficiency of 10.7 % and degradation ratio of 14 % in the first year have been obtained.

These characteristics of the multi-bandgap a-Si alloy stacked solar cells are summarized as follows:

Cell Structure	Initial Efficiency (%)	Degradation ratio in the first year (%/Y)
a-Si/a-Si/a-SiGe	10.7	—
	10.0	10
a-SiC/a-Si/a-SiGe	11.0	—
	10.7	14

VITA

Yukihiko NAKATA was born in Katsura, Kyoto, Japan on October 1, 1946. He graduated from Toyonaka Senior High School, Toyonaka, Osaka in March 1965 and entered Kobe University, Kobe in April 1965. He graduated from Kobe University in March 1969 and entered the Graduate School in April of that year. He received his Master of Engineering degree in Applied Physics in March 1971. Since April 1971, he has joined SHARP Corporation as a researcher.